Minimally invasive routes of AAV administration to treat GM1 gangliosidosis

by

Amanda Lea Gross

A dissertation submitted to the Graduate Faculty of
Auburn University
in partial fulfillment of the
requirements for the Degree of
Doctor of Philosophy

Auburn, Alabama
May 2, 2020

Adeno-associated virus, GM1 gangliosidosis, gene therapy, lysosomal storage disease, neurodegeneration

Approved by

Douglas R. Martin, Chair, Professor of Anatomy, Physiology, and Pharmacology
Emily C. Graff, Assistant Professor of Pathobiology
Tatiana I. Samoylova, Research Professor of Pathobiology
Bruce F. Smith, Professor of Pathobiology

Abstract

GM1 gangliosidosis is a lysosomal storage disease caused by a deficiency of lysosomal β-galactosidase (βgal), which results in the accumulation of GM1 ganglioside and fatal neurodegeneration. In the human type II (late infantile / juvenile) disease, GM1 gangliosidosis is a rapidly progressive disease and is fatal by 4 years of age. Outside of supportive and palliative care, no effective treatments exist. The feline model of GM1 closely mimics the human type II disease and provides a vital resource for developing therapeutics and testing safety prior to initiating human studies. After intracranial injection of adeno-associated viral (AAV) gene therapy, GM1 cats show a dramatic increase in length and quality of life. While the efficacy of intracranial AAV treatment is clear, a less invasive option must be considered, especially with the goal of treating children with severe brain disease.

Previous intracranial administration of AAV into GM1 cats utilized bilateral injection of the thalamus and deep cerebellar nuclei (DCN). In order to decrease the invasiveness of the treatment, but maintain efficacy, GM1 cats were injected bilaterally in the thalamus (Thal) and in the left lateral ventricle. The intracerebroventricular (ICV) injection has the added benefit of delivering AAV to the cerebrospinal fluid (CSF), which surrounds the central nervous system (CNS) and could theoretically increase treatment distribution. Additionally, two methods of density gradient purification of AAV vectors, cesium chloride (CsCl) and iodixanol, were studied, to evaluate if there is a clinical difference between the two methods. The Thal+ICV, CsCl GM1 animals survived 14.8 ± 3.6 months and Thal+ICV, iodixanol animals survived 31.4 ± 8.4 months. Compared to untreated GM1 cats, which survive 8.0 ± 0.6 months, there are significant increases in lifespans in both cohorts. However, the Thal+ICV, iodixanol cohort had a significantly longer average lifespan than that of the CsCl group. Similarly, normalization of

most biomarkers was superior in the iodixanol cohort versus the cesium chloride cohort, further supporting the advantages of iodixanol purification.

Furthering the evaluation of less invasive routes of AAV administration, AAV was delivered directly to the CSF through the cisterna magna (CM). The CM is ventral to the cerebellum and requires no brain penetration to access. Two commonly used AAV serotypes, AAV9 and AAVrh10, were evaluated in this study as well, to determine whether one serotype is more beneficial for treatment of neurological disease. Both the AAV9 and AAVrh10 serotypes led to a significant improvement in average lifespan in comparison to untreated GM1 animals, with the AAV9 cohort surviving 13.9 ± 1.8 months and the AAVrh10 cohort surviving 11.3 ± 0.5 months. All animals had a delay, but not halt, of disease progression. There was normalization of myelin integrity in the cerebellum of the AAV9 cohort but not AAVrh10 cohort. In both CM cohorts, there was recovery of βgal activity in the cerebellum and spinal cord but this recovery did not penetrate deep brain structures.

In an attempt to increase systemic and CNS biodistribution of βgal, AAV9 was delivered via an intravenous injection. With IV treatment alone, GM1 cats survived to approximately 3.5 years. The IV-treated animals had minimal clinical symptoms that were corroborated by other in life studies. Additionally, post-mortem analysis showed increased levels of βgal throughout the CNS, including deep brain structures, and into the periphery. All antemortem and postmortem biomarkers were improved compared to untreated GM1 animals and those treated by Thal+ICV or CM injection.

Taken together, these studies show the therapeutic potential of AAV gene therapy for the treatment of GM1 gangliosidosis and indicate that IV gene therapy is the most effective in the feline model.

Acknowledgments

I would like to first thank my advisor and mentor, Dr. Douglas R. Martin, for inviting me into his lab and helping me discover my passion for gene therapy. I cannot express how much being part of your team has meant to me.

I would also like to thank my graduate committee, Dr. Emily C. Graff, Dr. Tatiana I. Samoylova, and Dr. Bruce F. Smith for their guidance through my graduate career. Additionally, I appreciate Dr. Michael E. Greene for his service as my University Reader.

It would be difficult to imagine getting through this program without the love and support of my husband, Richard Gross, or my parents, Lea Ann and Bill Hazi. I cannot thank you enough for always being there for me. My support group of friends should not be ignored either. Your patience and presence in my life has given me so much joy and made this process easier.

I would be amiss if I did not mention the families and patients who suffer with lysosomal storage diseases, like GM1 gangliosidosis. Seeing your faces is what drives me and has given me such a passion to work as hard as I can to further this technology. I carry you in my heart and mind always.

Table of Contents

List of Tables

Literature Review

Chapter 1

Chapter 2

Chapter 3

Chapter 4

List of Figures

Literature Review

Chapter 1

Chapter 2

Chapter 3

List of Abbreviations

AAV	Adeno-associated virus
AST	Aspartate aminotransferase
βgal	β-galactosidase
BBB	Blood brain barrier
CB	Cerebellum
CBA	Chicken β-actin
CNS	Central nervous system
Cr	Creatine
CRS	Clinical rating score
CsCl	Cesium Chloride
CSF	Cerebrospinal fluid
DCN	Deep cerebellar nuclei
FWHM	Full width half max
GA1	GM1 asialo-derivative
GAGs	glycosaminoglycans
Glu	Glutamate
Gln	Glutamine
GPC	Glycerophosphocholine
GM1	GM1 gangliosidosis
HPTLC	High-performance thin-layer chromatography
ICV	Intracerebroventricular
IND	Investigational new drug

INS	Myoinositol
IV	Intravenous
LDH	Lactate dehydrogenase
MPRAGE	Magnetization-Prepared Rapid Gradient Echo
MPS	Mucopolysaccharidosis
MRI	Magnetic resonance imaging
NAA	N-acetylaspartate
NAAG	N-acetylaspartylglutamate
NHP	Nonhuman primates
OCC	Occipital cortex
OCT	Optimal cutting temperature
PC	Parietal cortex
PCh	Phosphocholine
PCr	Phosphocreatine
SVS	Single voxel spectroscopy
TH	Thalamus
TL	Temporal lobe
TSE	Turbo spin echo
VAPOR	Variable pulse power and optimized relaxation delays
Vg	Vector genomes
WPRE	woodchuck hepatitis virus post-transcriptional regulatory element
X-gal	5-bromo-4-chloro-3-indolyl-β-D-galactopyranoside

Literature review

1. Adeno-associated viral therapy

Adeno-associated virus (AAV) was originally discovered as a contaminant of various adenovirus preparations[1, 2], which is where its name is derived. AAV belongs to the genus Dependovirus and *Parvoviridae* family. Similar to other parvoviruses, AAV is dependent on co-infection with a helper virus, such as adenovirus or herpesvirus, to replicate. AAV contains a protein shell surrounding and protecting, a single stranded DNA genome approximately 5 kilobases (kb) in size. The genome is flanked by inverted terminal repeats (ITRs) and consists of three genes, *rep* (replication), *cap* (capsid), *aap* (assembly).

These genes, through different promoters, alternative start sites, and differential splicing, give rise to at least nine different gene products[3]. The *rep* gene encodes for non-structural, regulatory proteins, Rep40, Rep52, Rep68, and Rep78[4, 5]. These proteins are used for site-specific binding, helicase activity, regulation of gene expression, and other regulatory functions. The next gene immediately downstream from the *rep* gene is *cap*. The *cap* gene gives rise to the viral capsid proteins, VP1, VP2, VP3. Together, these proteins give rise to an icosahedral outer shell, approximately 25 nm in size, that protects the viral genome and is actively involved in cell binding and internalization[6, 7]. The viral coat contains approximately 60 protein molecules in a molar ratio of 1:1:10 (VP1:VP2:VP3)[8]. The *aap* gene overlaps the *cap* gene in an alternate reading frame and is thought to provide a scaffolding function for capsid assembly[9, 10]. Flanking both the trans-acting *rep* and *cap* genes are the ITRs, which are 145 nucleotide cis-acting regions that encode palindromic sequences. These regions allow for base pairing between the palindromic regions and lead to the creation of T-shaped hairpin loops. The secondary structure formed by this offers a free hydroxyl group at the 3’ end, which can serve as a primer since the

AAV *rep* gene does not encode a polymerase[11, 12]. Wild type AAV is able to enter lytic cells and establish infection, however it is non-pathogenic in nature and is not known to be associated with any disease[13]. By removing the trans-acting *rep* and *cap* genes from between the cis-acting ITRs, a recombinant AAV can be created. The AAV can contain a genetic cassette with transgenes as large as 4.7 kilobases in length, which are packaged into virions and ready for delivery into specific host cells[14].

AAV binds primary and co-receptors on the cell surface to infect, which causes endocytosis into endosomes[7]. AAV virions undergo a structural change, which enables escape from the endosomes[15]. Following endosomal escape, the AAV virions are either ubiquitinated and targeted for proteasome-mediated degradation or enter the nucleus. In the nucleus, the virions release their single-stranded genomes which is then converted to double-stranded DNA (dsDNA). The dsDNA is then transcribed into mRNA followed by translation to the therapeutic protein[1, 16]. A detailed figure of this process can be found in figure 1.

1.1 AAV serotypes

AAV is able to infect a wide range of tissues due to a large number of capsid serotypes. In 2002, the atomic structure of AAV was revealed as largely consisting of β-barrel motifs interspaced by loops that are able to interact with cellular receptors and antibodies[17]. As previously stated, the AAP protein is vital for capsid assembly. It plays a role in nucleolar localization of the VP proteins in AAV2[3]. However, in 11 other capsid types, localization varies and AAP has even been proven nonessential in AAV4, AAV5, and AAV11[18]. In naturally occurring AAVs, a glycan moiety is utilized for the initial attachment to the cell surface[19]. Some examples of the interacting glycan moieties include N- or O- linked sialic acid moieties for

AAV1, 4, 5, and 6[20-22], heparin sulfate proteoglycans for AAV2, 3, and 6[23], and N-terminal galactose for AAV9[24, 25]. Less is known about post-attachment interactions; however, it is thought that the AAV engages a proteinaceous receptor to mediate cellular entry[19]. In an attempt to increase efficacy, AAVs have been designed and engineered to overcome barriers such as limited tissue tropism for capsids that bind heparin sulfate[26, 27], poor infection of stem cells[28, 29], limited transgene capacity[30, 31], and immune response[32, 33]. A table of select serotypes, natural[16] and designed, and their tropisms can be found in table 1.

1.2 AAV promoters

Modulation of promoters provide another method for optimizing AAV. Many AAV gene therapy platforms exploit a strong ubiquitous promoter to obtain high transgene expression. Two such promoters commonly employed is the cytomegalovirus (CMV) promoter and the chicken β-actin promoter fused with the CMV enhancer (CBA)[34]. Both promoters typically provide long-term, robust expression in all cell types. However they silencing over time can occur, as shown in the hippocampus and striatum in the brain[35, 36]. Various attempts have been made to produce smaller promoters to best optimize the limited genomic carrying capacity of AAV. Truncating the full length (1.6-kb) CBA promoter by using a SV40 intron produces a 800 bp promoter. However, this promoter has poor motor neuron transduction[37]. Using a hybrid intron from the chicken β-actin intron 1 and minute virus of mice (MVM VP) intron to truncate the CBA promoter (CBh), yields a ubiquitous promoter for CNS applications that is 800 bp[37]. Additional methods to optimize promoters for AAV include using shortened tissue specific promoters. Both the human synapsin 1 gene promoter (hSYN, 480 bp) and the murine cytomegalovirus immediate early promoter (mCMV, 527 bp) have shown efficacy in CNS transduction, although

limited primarily to neurons and astrocytes respectively[38]. Promoters have also been developed to target oligodendrocytes[39, 40], as well as many other cells throughout the body. The combination of AAV serotype and promoter can enhance delivery of a transgene either ubiquitously or cell specifically.

1.3 Production

Originally for AAV production, *rep* and *cap* were expressed in a separate plasmid that was co-transfected with a plasmid containing the AAV genome flanked by the wild type ITRs. Since a helper virus is needed for AAV production, the transfected cells were directly infected with wild type adenovirus[11]. This co-infection raises contamination and safety concerns and therefore new approaches were developed. Current methods use three plasmids containing the necessary helper genes and transgene of interest co-transfected into 293T cells (Figure 2)[7, 41]. The 293T cell line expresses the simian virus 40 (SV40) large T antigen, which supports AAV replication and assembly[42, 43]. The transgene plasmid has a total packaging capacity of approximately 5 kb which needs to include the ITR-flanked expression cassette containing a promoter, the transgene, and a poly-adenylation signal. The helper plasmid contains the E1, E2, E3, and VA genes from adenovirus and contribute to genome replication. Finally, the capsid (or pAAV-RC) plasmid contains the *rep* and *cap* genes, which regulate replication and capsid assembly, respectively[44].

Conventionally, AAV is manufactured in adherent cells, however with the increased demand other methodologies have been explored. Adherent cell culture requires media containing serum, which could pose a contamination risk, as well as being very labor intensive. Additionally, a typical good manufacturing practice (GMP) production of AAV for a clinical

setting requires more than 100 customized “cellstacks” and often results in a yield less that 1E15 vg[45]. Adapting 293T cells to suspension culture in specially formulated serum-free media removes the need for serum in the media and provides an easily scalable production process[46]. Suspension cultured 293T cells utilize the same triple transfection process as adherent cells but are able to produce approximately 1E14 vg/L in 48 hours[47]. Further development and investigation into culture conditions, cell density, and optimized purification methods indicate that these systems could produce even greater quantities[48].

A recombinant baculovirus, derived from the *Autographa californica* nuclear polyhedrosis virus, has been adapted for production of AAV. Termed the baculovirs production system (BV), Sf9 insect cells are used for large scale production of AAV[49] and allows for the use of bioreactor systems to produce sufficient quantities of AAV for pre-clinical studies in a single production[50]. SfF9 cells lines have been developed containing integrated copies of AAV *rep* and *cap*, to simply the system further[51]. The BV system is less commonly used in research settings, possibly due to the need to modify the AAV plasmids for expression in the insect cells[52], but several biopharmaceutical companies have adapted this platform for production for large-scale production of AAV[48].

1.3.1 Purification

Harvesting AAV from production culture requires cell lysis. In small-scale productions, three cycles of freezing at -80°C and thawing at 37°C are used for cell lysis. In large-scale, such as commercial manufacturing, cells are lysed using microfluidization, crossflow filtration, or osmotic shock to rapidly decrease the pressure[53]. In both small-scale and large-scale production, cell lysis causes the release of large amounts of host cell DNA and RNA, in addition to

nonencapsulated DNA. Additionally, AAV is harvested from culture media using polyethylene glycol 8000 (PEG 8000) precipitation to collect both empty and full capsids. The DNA and RNA are digested, typically with Benzonase[54], to remove unwanted nucleic acids as well as decrease the viscosity of the cell lysate and prevent aggregation which would complicate further purification steps. There are several methods of downstream AAV purification including density gradients, affinity chromatography, and ion-exchange chromatography[55-58] (Table 2).

1.3.1.1 Density gradients

The most commonly used density gradients for purification of AAV are cesium chloride (CsCl) and iodixanol. Layers of varying concentrations of either CsCl or iodixanol are used to separate the AAV preparation from cell debris and other contaminates through ultracentrifugation.

CsCl is a salt that forms a continuous density gradient under ultracentrifugation[59]. CsCl gradients work by separating the AAV particles from contaminants based on their buoyancies[53]. Purifying AAV with CsCl is a multistep process that includes cell lysis, precipitation of proteins and DNA, ultracentrifugation, dialysis, and concentration, which make it a multi-day process. The dialysis step of CsCl is vitally important because of the toxic nature of CsCl. With each additional step, there is an opportunity for loss of the AAV product, which leads to inconsistent results between production lots.

Iodixanol has been used as an alternative to CsCl for AAV purification. Iodixanol purification of AAV is less time consuming, requiring only cell lysis, ultracentrifugation, and concentration, which enables the protocol to be completed in one day. Additionally, iodixanol is much less toxic in comparison to CsCl. Iodixanol has been shown to prevent aggregation of

AAV particles, which can increase infectivity[60]. With reduced processing steps, there is also an increase in AAV recovery, with approximately 50% AAV recovery after purification in comparison to the 10-12% from CsCl centrifugation[53].

Although either method of ultracentrifugation is rather straightforward, and produces yields of highly pure AAV, there are limitations preventing use in large-scale AAV manufacturing. The primary drawback is the limited capacity of ultracentrifuges, which would require large preparations to be split into different purification batches. This results in variable quality even within the same AAV preparation, especially using the CsCl method.

1.3.1.2 Chromatography

Various methods of column chromatography have been used to purify AAV, including ion exchange, affinity, gel filtration, and hydrophobic interaction[53]. Acquisition of high yield and purity AAV using chromatography requires a series of optimized steps sometimes including ultracentrifugation. Additionally, many chromatographic elution buffers are not suitable for *in vivo* use, therefore AAV preparations require additional purification steps.

Ion-exchange chromatography purification is based on the net charge of the proteins on the exterior of the AAV capsid[53]. This purification method has been used for AAV2, AAV4, and AAV5 capsids[61-63]. For the first step, the capsid binds to a cation-exchange resin in a neutral pH, followed by running the preparation on a second column at a lower pH (pH 5.5) to promote removal of cellular contaminants and helper Ad, if used[61]. Additionally, columns with different charge bases can be used sequentially, such as a cation-exchange column followed by an anion-exchange column, to purify AAV preparations with different capsids based on the expected contaminants and their relative charges[64].

Affinity chromatography utilizes reversible interactions between the AAV capsid and ligands or receptors bound to a chromatographic matrix to separate viral particles from DNA and protein contaminants[53]. Heparan sulfate proteoglycans mediate AAV2 cellular entry[23] and are utilized for affinity chromatography. This method produces AAV of comparable purity to that of ion-exchange chromatography[65]. However, AAV2 is not unique in binding heparin, and therefore additional purification steps are needed to ensure removal of other heparin binding particles.

1.4 Uses in gene therapy

There are two U.S. Food and Drug Administration approved AAV gene therapies. First, AAV2 was approved to treat *RPE65*-related blindness (Leber's congenital amaurosis) through an intraretinal injection[66]. Following that, AAV9 has been approved for the treatment of spinal muscular atrophy through a systemic injection[67]. Intramuscular delivery of an AAV1 encoding for lipoprotein lipase has been approved for use in Europe[68].

Currently, there are 205 clinical trials[69] and innumerable preclinical studies utilizing AAV gene therapy. These studies range from metabolic disorders, such as Pompe disease[70, 71], to chronic degenerative diseases, such as Alzheimer's disease and Parkinson's disease[72].

2. GM1 gangliosidosis

GM1 gangliosidosis is a lysosomal storage disease (LSD) caused by mutations in the *GLB1* gene, which encodes lysosomal β-galactosidase (βgal; EC 3.2.1.23). βgal is synthesized as a 85-kDa precursor that undergoes posttranslational modification to form the mature 65 kDa lysosomal enzyme[73]. The mature βgal hydrolyzes the terminal β-galactosyl residues from GM1

ganglioside, converting it into GM2 ganglioside[74]. βgal operates in complex with neuraminidase and protective protein /cathepsin A (PPCA). As a whole, the incidence rate of LSDs, which make up approximately 50 inherited disorders, is about 1 in 5000[75]. The incidence of GM1 gangliosidosis is estimated to be around 1 in 100,000 to 200,000 live births[76].

GLB 1 is located on the short arm of chromosome 3 and contains 16 exons and gives rise to two alternatively spliced mRNAs[77]. The 2.5 kB transcript encodes lysosomal βgal and the 2.0 kB transcript (which lacks exons 3, 4 and 6) encodes an elastin binding protein[78, 79]. To date, there have been over 130 mutations identified in patients with GM1[80].

2.1 Clinical manifestations

There are 3 clinical classifications of GM1: type I (infantile), type 2 (late infantile/juvenile), and type 3 (adult/chronic)[77, 81]. The severity of each type often correlates with the amount of residual activity maintained by the mutant βgal[82]. While the three forms of GM1 differ in their severity, there are numerous overlapping symptoms.

The type I form has an onset between birth and 6 months of age and is associated with progressive hypotonia, severe central nervous system degeneration, and a rapid time course with death between 1 and 4 years of age. Type II GM, has a later onset of between 7 months and 3 years in age, delay in motor and cognitive development, and slower progression. Type III disease has a later onset of between 10 and 30 years of age[77] and has the slowest progression of the three types.

In GM1, there is an accumulation of GM1 ganglioside in the CNS as well as accumulation of glycosaminoglycans and oligosaccharides in peripheral tissues (Figure 3), which leads to clinical manifestations. Neuronal death and demyelination in tandem with astrogliosis and

microgliosis are seen in regions with high neuronal GM1 accumulation[77]. Mechanisms such as neuronal apoptosis, endoplasmic reticulum stress[83, 84], and disruption of neuronal-oligodendroglial interactions[85] have been implicated in the pathogenesis of GM1.

2.2 Animal models

There are several animal models of GM1, which enable the study of potential therapies. Naturally occurring GM1 mutations have been recorded in cats, dogs, calves, and sheep[77]. Several mouse models of GM1 have been created. Initially, the mouse models were created by inserting the exogenous neomycin resistance gene into the *GLB1* locus using embryonic stem cell gene targeting[86, 87]. Hahn et al.[86] inserted the targeting cassette into exon 6 to disrupt *glb1* and Matsuda et al.[87] inserted the cassette into exon 15. More recently, CRISPR-Cas9 (clustered regularly interspaced short palindromic repeats-Cas9) gene editing has been used to create murine models of GM1 and Morquio B by targeting exon 8[88]. While murine models are an invaluable resource for studying disease progression and therapeutic development, they do not faithfully recapitulate the human disease. In addition, their short lifespans[89], small body and brain weights, and lack of cerebral complexity make translation to human studies more difficult.

The feline GM1 model was first reported in the 1970s and has been studied extensively. This naturally occurring model is caused by a G to C substitution at position 1448 of the open reading frame, causing an arginine to proline substitution at amino acid 483[90]. The feline mutation is homologous to known human mutations[91-94]. The feline GM1 model faithfully recapitulates type II GM1 disease, with similar phenotypes, lipid storage, and ganglioside metabolism[95-97]. Additionally, the feline brain is approximately 50 times larger than the murine brain and more closely resembles the human brain in complexity, architecture and structure[98].

2.3 Treatment (to date)

There is no FDA approved treatment for GM1 gangliosidosis. Studies have been conducted using numerous methods including chaperones, enzyme replacement therapy (ERT), substrate reduction, stem cell transplantation, and gene therapy.

2.3.1 Chaperones

Small molecule chaperones can be used to stabilize mutant enzymes in their correct conformation as a therapy[99]. A synthetic galactose derivative, *N*-octyl-4-epi-β-valien-amine (NOEV), is able to bind mutant βgal intracellularly and forms a complex which stabilized and transport it lysosomes where it dissociates, leaving behind a stable, functional enzyme[100]. In murine models of GM1 gangliosidosis, NOEV has shown efficacy in arresting neurological progression and prolonging life[101, 102]. NOEV and a complementary chaperone MTD118, a bicyclic 1-deoxygalactonjirimycin derivative, have been shown to cross the blood brain barrier[103]. Though efficacious in the mouse model, pharmacokinetic analysis of these chaperones showed rapid absorption in the intestines with renal excretion following oral administration[104], which could require significant optimization to maintain necessary levels in the CNS for adequate treatment of GM1.

2.3.2 Enzyme replacement therapy

Enzyme replacement therapy (ERT) is a treatment where patients with LSDs received weekly to bimonthly infusions of purified enzymes. ERTs have shown great clinical success in patients with non-neurological enzyme deficits; however, results are limited in neuropathic diseases due to the blood brain barrier. Recently, intracerebroventricular (ICV) administration of

recombinant human βgal (rhβgal) has shown promise in treating GM1 mice[105]. Following 8 weekly doses of ICV delivered rhβgal, mice showed reduced levels of brain ganglioside storage as well as reversal of secondary neuropathy[105]. Delivery of ERT to the CNS can pose challenges, with repeated dosing being necessary. For ERTs that cannot cross the blood brain barrier, intraparenchymal injection is necessary, which would require an ICV device for delivery. ICV drug delivery devices numerous complications, with 33% of which are non-infectious and 27% are infectious complications[106]. Development of alternative delivery systems, such as polymersomes[107] and other nanoparticles[108] could help decrease invasiveness and possibly increase efficacy of ERT.

2.3.3 Substrate reduction

Substrate reduction therapy (SRT) uses a small, orally available, molecule to inhibit the first step in glycosphingolipid biosynthesis[109]. The imino sugars *N*-butyldeoxynojirimycin (NB-DNJ, miglustat) and *N*-butyldeoxygalactonojirimycin (NB-DGJ) inhibit glucosylceramide[110], which is the first step in glycosphingolipid biosynthesis. Both sugars improved function in *βgal-/-* mice, though NB-DNJ exasperated gastrointestinal tract dysfunction it was shown to have the best overall functional improvement[110]. NB-DNJ was administered orally to 3 patients, two juvenile and one adult onset, in an off-label study. All three patients showed gradual improvement during treatment[111]. NB-DNJ, or miglustat, is being investigated in a clinical trial in conjunction with a ketogenic diet (https://clinicaltrials.gov/ Identifier NCT02030015).

2.3.4 Bone marrow transplantation

Bone marrow transplant (BMT) replaces bone marrow that has been damaged or destroyed. For treatment of GM1 gangliosidosis, the bone marrow is ablated and donor marrow is transplanted in hopes to repopulate with cell able to produce βgal. In a canine model of GM1, BMT was performed at 81 days of age to study early intervention. The BMT failed to increase CNS βgal or slow neurological progression[112]. Shield et al demonstrated a similar lack of efficacy in preventing neurological decline after BMT in a human patient[113].

2.3.5 Gene therapy

There have been numerous studies developing treatments for GM1, most recently using AAV. Both murine and feline models have shown recovery of βgal activity throughout the CNS after injection of AAV into the brain parenchyma and CSF[114-116]. Additionally, the feline model has shown marked improvement in quality and length of life as well as normalization of disease biomarkers after injection into the thalamus and deep cerebellar nuclei[114].

There are two current clinical trials evaluating therapies solely for GM1, both of which utilize AAV gene therapy. The first study is utilizing AAV9 for intravenous delivery has begun enrollment and administering treatments (https://clinicaltrials.gov/ Identifier NCT03952637). The other study evaluates CSF delivery, through the cisterna magna, of AAVrh10 and is anticipated to start in April of 2020 (https://clinicaltrials.gov/ Identifier NCT04273269). The other study involves unrelated umbilical cord blood transfusion[117].

Tables and Figures

Table 1. AAV tropisms

AAV serotype	Tissue tropism
AAV1	Muscle, CNS, Heart
AAV2	Liver, CNS, Muscle
AAV2.7m8+	Eye (retina)[118]
AAV3	Muscle, Stem cells
AAV4	Eye, CNS
AAV5	CNS, Lung, eye
AAV6	Muscle, CNS, Heart, Lung
AAV7	Muscle, CNS
AAV8	Liver, Muscle, Pancreas, CNS
AAVrh8	Retina, CNS
AAV9	Every tissue
AAV10	Muscle
AAVrh10	CNS
AAV12	Nasal
AAV-PHP.B+	CNS[119]*

* Restricted primarily to C57/BL6 mice, +Indicates engineered capsid

Table adapted from (31).

Table 2. Methods of AAV purification

Type	Steps	Purity	Scalability
CsCl UC	2-3	90-98%	No
Iodixanol UC	1	>95%	No
AVB sepharose IEC	1	>90%	Yes
Heparin AC	1	>90%	Yes
Heparin AC	2	>99%	Yes

UC – Ultracentrifugation, IEC – Ion-exchange chromatography, AC – Affinity Chromatography

Adapted from (120)

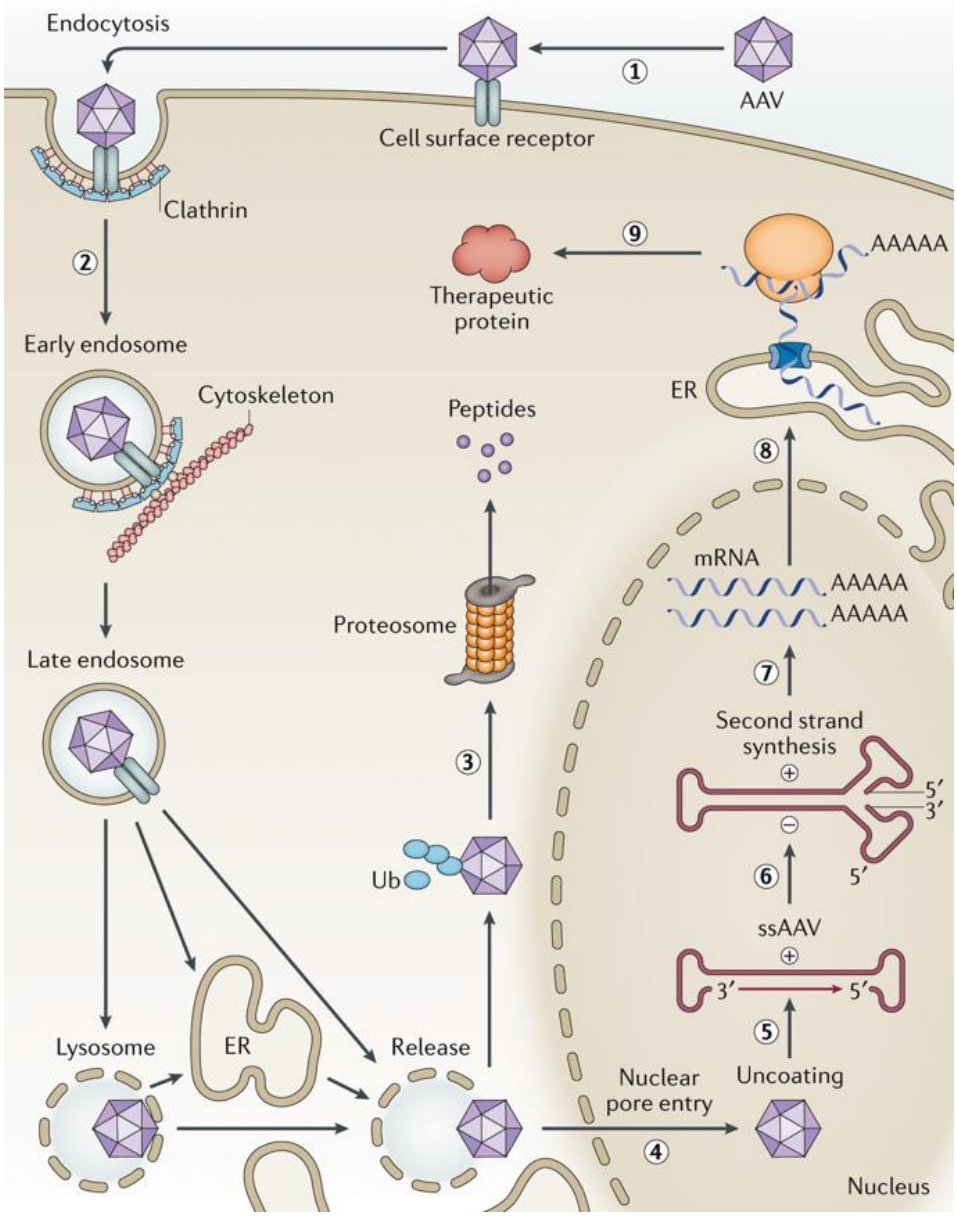

Figure 1. AAV transduction. AAV binds to surface receptors (step 1) and enters the cell via endocytosis (step 2). Following endosomal escape, the AAV virions are either ubiquitinated (step 3) or enter the nucleus (step 4). The AAV virions are then uncoated and the single-stranded genome is released (step 5). The genome is then converted into double-stranded DNA (step 6), which is then transcribed to mRNA (step 7). This mRNA is then translated in the endoplasmic reticulum (ER, step 8), which leads to the production of the therapeutic protein (step 9). Figure from (16).

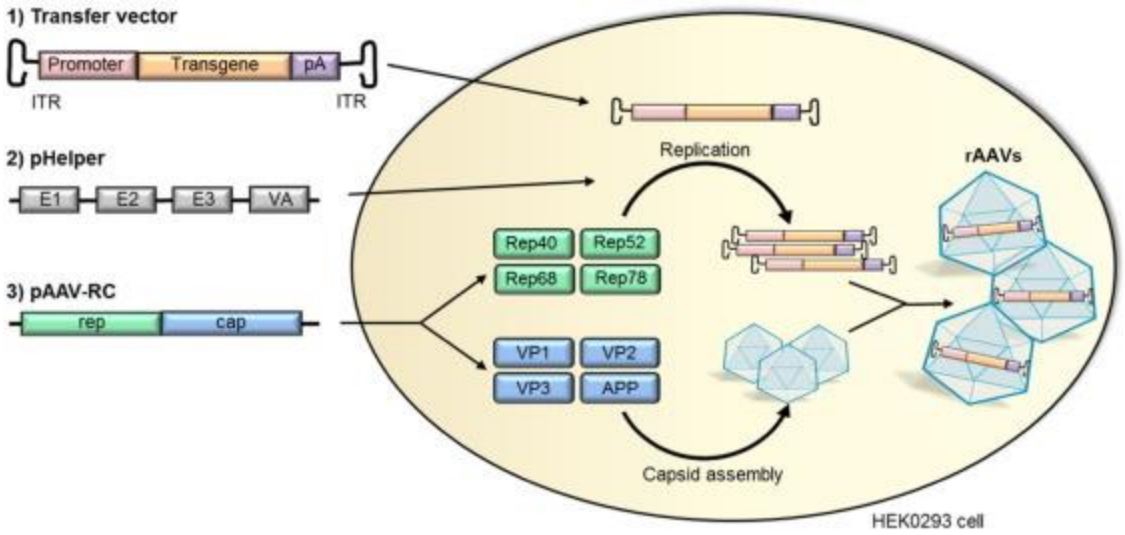

Figure 2. AAV production process. The triple transfection method of AAV production utilizes a transgene plasmid (Transfer vector, 1), a helper plasmid (pHelper, 2), and a plasmid containing the *rep* and *cap* genes (pAAV-RC, 3). The combination of these plasmids in 293T cells leads to virus formation and release. Figure from (41).

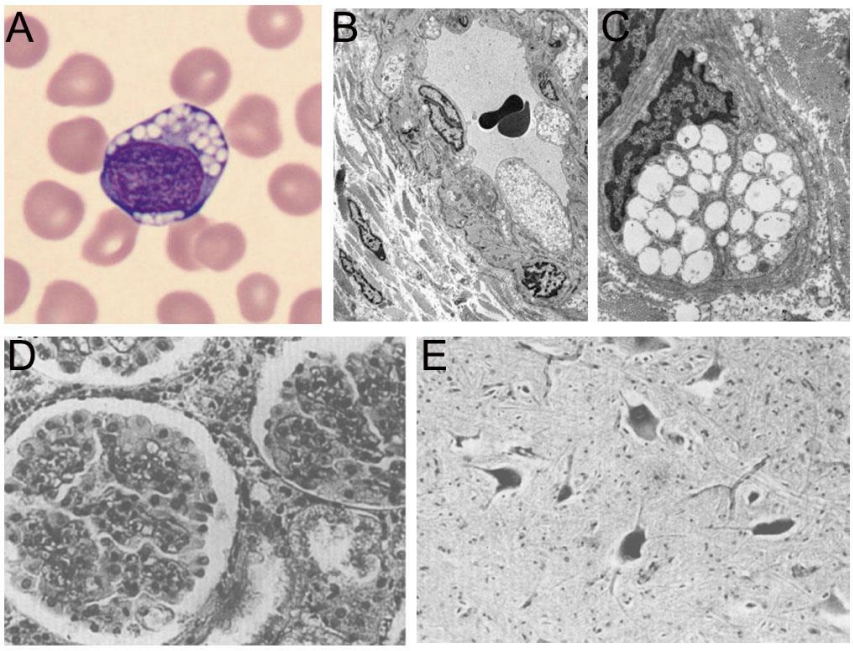

Figure 3. Storage lesions in GM1 gangliosidosis. (A) Lymphocyte swollen with large vacuoles[77]. Electron micrographs of a capillary[77] (B), Schwann cell[77] (C), Kidney[121] (D) showing extensive vacuolization. (E) Cortical neurons swollen with storage material[121].

Chapter 1

Therapeutic response of AAV in feline GM1 gangliosidosis after intracranial and intra-CSF injection

Amanda L. Gross[1, 2], Kalajan Lopez Mercado[1], Bryan Murdock[1], Heather L Gray-Edwards[1*], Ana Rita Batista[3, 4], Miguel Sena-Esteves[3, 4], Douglas R Martin[1, 2]

[1] Scott-Ritchey Research Center, [2] Department of Anatomy, Physiology, & Pharmacology, College of Veterinary Medicine, Auburn University, Auburn, Alabama, USA

[3]Department of Neurology, [4]Horae Gene Therapy Center, University of Massachusetts Medical School, Worcester, Massachusetts, USA

* Current address: Department of Radiology, University of Massachusetts Medical School, Worcester, MA 01605 USA.

Abstract

Adeno-associated viral (AAV) gene therapy has shown immense efficacy in treating cats with GM1 gangliosidosis, a fatal neurodegenerative disease, after intracranial injection of the thalamus and deep cerebellar nucleus. However, with concerns about translation to the human disease, where the majority of patients are children with symptomatic neurological disease, less invasive routes of administration need to be evaluated. Additionally, two different methods of AAV purification were evaluated to determine if there would be a differential efficacy. This study utilized an AAVrh8 vector expressing a cDNA for feline β-galactosidase (βgal), the deficient enzyme in GM1 gangliosidosis, purified either by cesium chloride (CsCl) or iodixanol density gradient centrifugation. GM1 cats were treated through bilateral thalamic injection and an intra-cerebrospinal fluid injection of the left lateral ventricle. There was a significant improvement in length and quality of life in all treated animals, with the CsCl cohort living to 1.8 times longer than untreated animals and the iodixanol cohort living significantly longer than both the untreated (2.3 times longer) and CsCl cohort (2.1 times longer). Magnetic resonance imaging (MRI) evaluation of brain architecture and spectroscopy (MRS) evaluation of brain metabolites showed similar results with a delay in neurodegeneration. Though the treated animals lived longer, their disease progression was not completely halted, and by endpoint some of these markers were the same if not worse than untreated GM1 animals. Postmortem analysis revealed recovery of βgal activity across the central nervous system, with the iodixanol cohort expressing at or above normal levels in the thalamus and across the spinal cord. The CsCl cohort only showed normal levels in the thalamus and caudal portion of the spinal cord. This data supports the use of less invasive AAV delivery methods to treat GM1 gangliosidosis as well as an increased efficacy of iodixanol purified AAV vector over CsCl purified vectors.

Introduction

The fatal lysosomal storage disease, GM1 gangliosidosis, is caused by a deficiency of β-galactosidase (βgal, EC 3.2.1.23). Lack of βgal, which hydrolyzes the terminal galactose residues from numerous molecules, results in intracellular storage of GM1 ganglioside and leads to profound neurodegeneration and death[74]. GM1 ganglioside storage occurs throughout the central nervous system (CNS), particularly in neurons[122]. The ganglioside storage is accompanied by various features of neurodegeneration, including microgliosis, demyelination, and astrogliosis[122, 123]. βgal deficiency extends outside of the CNS as well, causing peripheral disease manifestations[124]. Due to this severe CNS and peripheral disease, an effective treatment must not only reach the CNS in its entirety, it must also have the ability to treat the peripheral organs.

The feline GM1 closely models human type II (late-infantile/juvenile) disease, with similar amounts of enzymatic deficiency, GM1 storage levels, CNS and peripheral organ pathology[95-97]. Additionally, well characterized brain biomarkers, measured via MRS, and biomarkers from body fluids, give the GM1 cats many advantages over murine models when studying potential therapeutics[125]. Previously, the feline GM1 model has been used to show efficacy of adeno-associated viral (AAV) gene therapy after bilateral injection into the thalamus and deep cerebellar nuclei [114, 126]. While the treatment showed a marked improvement in length and quality of life, the risk of intracranial surgery in patients that have severe, pre-existing neurological disease must be addressed[127]. Additionally, it has been shown that there are high levels of transduction immediately surrounding the injection locations, but variable results outside of those regions[98, 128, 129]. Therefore, a treatment that can distribute AAV throughout the CNS and periphery might produce enhanced results. Cerebrospinal fluid (CSF) is constantly produced and flows throughout the CNS before reaching reabsorption points[130, 131]. Injection of

an AAV9 preparation spiked with an MR contrast agent into the CSF through various injection locations shows distribution around the brain and spinal cord[132].

AAV preparations must be purified from cell debris and other contaminants prior to use. Two common AAV purification methods are cesium chloride (CsCl) and iodixanol density gradients[55]. Though both of these methods are widely used, there are limited reports characterizing AAV purified by either method and comparing efficacy[55, 60, 133]. Thus, in attempt to evaluate a less invasive AAV administration route and directly compare AAV purification, the current study injected GM1 cats with an AAVrh8 vector, purified by either CsCl or iodixanol, bilaterally in the thalamus and in the left lateral ventricle.

Results

Clinical Data

In attempt to decrease invasiveness of previously successful AAV treatment of GM1[114], six GM1 affected animals were injected bilaterally in the thalamus and in the left lateral ventricle (intracerebroventricular, ICV) with an AAVrh8 vector encoding feline βgal. Three cats received AAV that had been purified using iodixanol and the other three received AAV purified via CsCl. Animals were treated at 2.8 ± 0.2 months of age (Table 1) and followed until they reached humane endpoint. Untreated GM1 animals have a substantially shorter lifespan when compared to normal cats, living only 8.0 ± 0.6 months versus the normal average of 12 to 15 years. Both treated cohorts had significantly longer lifespans than untreated animals (Figure 1A). The iodixanol treated cohort also survived significantly longer (31.4 ± 8.4 months) than the CsCl cohort (14.8 ± 3.6 months).

In addition to longevity, animals were assessed ever two weeks for neurological progression. Neurological symptoms are tracked using a 10 point clinical rating score (CRS), which is detailed in the materials and methods section. Untreated GM1 animals rapidily progress through disease symptoms, such as hindlimb weakness (4.8 ± 0.5 months), wide stance (5.4 ± 0.3 months), ataxia (5.7 ± 0.3 months), instability (6.3 ± 0.5 months), and the inability to walk (7.3 ± 0.4 months). Body tremors and spastic legs are additional markers of neurological decline and occur at 3.8 ± 0.3 months of age and 6.0 ± 0.7 months of age, respectivily. By approximately 8 ± 0.6 months of age, untreated animals were unable to stand, which was considered humane endpoint. Both treatment cohorts showed a delay in disease progression (Figure 1B), paricular in motility. While there was a delay in symptom onset, neither treatment group displayed a halt in disease progression. As a whole, the CsCl cohort only showed a mild delay in symptom development, with one cat plateauing for several months prior to developing mobility symptoms. The iodixanol cohort showed a slower disease progression with the majority of symptoms being acquired later than the CsCl cohort. One animal in the iodixanol cohort plateaued prior to mobility issues, but with body tremors, and maintained this status for approximately 25 months. Though not assessed in the CRS, two cats from each cohort developed seizures, which are a part of the natural history of GM1 gangliosidosis that occurs beyond the humane endpoint and are well managed with medication.

Magnetic Resonance Imaging

Magnetic resonance imaging (MRI) is a powerful, noninvasive, tool to evaluate brain architecture. Ultra-high field (7 Tesla) T2 weighted MRI was used to assess brain architecture in untreated animals at endpoint and in treated animals at a midpoint in disease progression and at endpoint (Figure 2). In normal animals, white matter is hypointense relative to gray matter, due

to the increased lipid content within the myelin of the white matter. In untreated GM1 animals, the white and gray matter become isointense (the same degree of darkness) in both the cerebral cortex and in the cerebellum, due to demyelination of the white matter and increase GM1 storage in the gray matter. Additionally, brain atrophy is indicated by an increase in CSF, as shown by the bright white fluid around the brain and in the ventricles. At 18.0 ± 4.7 months of age, the iodixanol cohort maintained the hypointensity of white matter to gray matter in the cerebral cortex and the cerebellum, indicating delay in neurodegeneration. Furthermore, there were minimal increases in CSF accumulation. However, in the longest living cat in the iodixanol cohort at endpoint (43.2 months of age), only the dorsal region of the cerebrum showed maintenance of gray and white matter intensity (Supplemental Figure 1). Additionally, there was an increase in CSF accumulation around the brain and in the ventricles. The CsCl treated cohort showed similar maintenance of brain architecture, however there was a greater accumulation of CSF at 14.2 ± 2.7 months of age.

Magnetic Resonance Spectroscopy

MR spectroscopy (MRS) supports the presence of delayed neurodegeneration shown in survival and MRI. Glycerophosphocholine (GPC) and phosphocholine (PCh) increase with demyelination due to their role in membrane synthesis and degradation[134]. In the parietal cortex (PC), thalamus (TH), temporal lobe (TL), occipital cortex (OCC), and cerebellum (CB) there was an increase in GPC+PCh in untreated GM1 animals as the disease progressed (Figure 3A). In the iodixanol cohort, there was a trend to normalization at 18.0 ± 4.7 months of age. The CsCl cohort showed significantly elevated levels of GPC+PCh compared to age-matched normal animals in the occipital cortex and cerebellum at 14.2 ± 2.7 months of age, with a trend of elevation above normal and the iodixanol cohort in the PC and TL.

Myoinositol (INS), a marker of gliosis[135], was increased significantly in untreated GM1 animals cerebellum at humane endpoint (Figure 3B) compared to normal. Both the treated cohorts had increases compared to normal in INS in some but not all voxels at their respective time points. Interestingly, the iodixanol cohort had a significant increase in INS compared to untreated animals, in the thalamus at the designated time point.

N-acetyl aspartate alone (NAA), and with N-acetyl aspartyl glutamate (NAA+NAAG) neuronal markers[136], decreased significantly with disease progression in the untreated GM1 animals in the cerebellum (NAA: Figure 3C, NAA+NAAG: Figure 3D). There was no improvement in either cohort in the cerebellum.

Creatine and phosphocreatine (CR+PCR), a marker of metabolism[137], had no marked change in untreated GM1 animals, however there were elevated levels in the cerebellum that increased with disease progression (Figure 3E). The iodixanol cohort showed similar results as the untreated cohort except in the thalamus, where there was a significant increase in CR+PCR in comparison to both the normal and untreated animal. The CsCl cohort showed a significant increase in the temporal lobe and the cerebellum over that of the untreated cohort.

Glutamate, a neurotransmitter[138], and its precursor glutamine (Glu+Gln), was unchanged in the untreated GM1 animals (Figure 3F). There were significantly decreased levels of Glu+Gln in the cerebellum for both cohorts, as well as in the temporal lobe and occipital cortex for the CsCl group.

CSF Biomarkers

Aspartate aminotransferase (AST), a transaminase enzyme that catalyzes the conversion of aspartate and alpha-ketoglutarate to glutamate and oxaloacetate[139], and lactate dehydrogenase (LDH), an enzyme that catalyzes the conversion of lactate to pyruvate[140], are commonly used to

evaluate hepatocellular damage and necrosis in peripheral blood. They do not readily cross the blood brain barrier, therefore in the CSF increased AST and LDH indicate CNS cell damage. Untreated GM1 animals have significantly increased activity of both AST and LDH (Figure 4). AST levels are partially normalized in the iodixanol treated cohort, even at endpoint. While LDH levels are significantly lower than untreated GM1 animals, they remain higher than normal. For both AST and LDH, the CsCl cohort showed significantly increased levels compared to normal and significantly lower levels compared to untreated GM1 animals at humane endpoint.

Bgal biodistribution

Treatment with AAVrh8 via Thal+ICV injection resulted in treated animals having increased βgal activity throughout the CNS (Figure 5). In the brain (Figure 5B), the iodixanol cohort had the highest recovery of βgal in the thalamus (Blocks D and E) and the regions surrounding it, with a range of 0.5-1.5-fold normal activity. The CsCl cohort showed significant increases in βgal in the thalamus and part of the frontal cortex (Block B), with a range of 0.1 – 1.1-fold normal activity across the brain. In the spinal cord (Figure 5D), the iodixanol cohort had an average βgal activity at or above normal levels throughout the spinal cord, with a range of 1.0 – 2.5-fold normal activity. The average βgal activity reached at or above normal levels only in the mid lumbar region (block O) for the CsCl cohort, with a range of 0.4 – 3.0-fold normal activity throughout the spinal cord. Overall, the iodixanol cohort had a greater recovery of βgal throughout the CNS versus animals treated with CsCl purified AAV.

Comparison of vectors

In attempt to identify the cause for the disparity between the two treatment cohorts, the preparations were studied using transmission electron microscopy (TEM, Figure 6) to determine the ratio of empty to full capsids. The CsCl preparation had an average of 20.6% empty capsids

(Figure 6A). The iodixanol preparation had significantly more empty capsids than the CsCl cohort, with 37.2% of total particles being empty (Figure 6B).

The particles were also measured on a ZS Ultra zetasizer for size, particle concentration, and zeta potential (Table 2). The iodixanol-isolated virions are larger than the CsCl virions, with diameters of 49.2 ± 3.2 and 30.8 ± 0.13 nm respectively. Purification using iodixanol produced a higher concentration of particles (7.58E13 vg/mL) in comparison to the CsCl purification (4.82E12 vg/mL). Zeta potential is a measurement of the electrostatic or charge repulsion/attraction between particles[141]. Zeta potential can affect how particles interact with cell membranes. There was only a minor difference in zeta potential between the purification methods (CsCl virions, -3.77 ± 0.515 mV; iodixanol virions, -9.71 ± 1.72 mV).

Discussion

This study demonstrated the potential of an AAVrh8 vector for treatment of neurological diseases. When administered via injection bilaterally into the thalamus and into the left lateral ventricle, animals treated with either CsCl or iodixanol purified virus showed a significant increase in lifespan. Additionally, there was a delay in neurological disease progression after treatment. Although Thal+ICV treatment did significantly improve length and quality of life in GM1 cats, the results were not as robust as bilateral AAV injection in the thalamus and deep cerebellar nuclei[114]. Although 2/3 of the cats in each cohort developed seizures, seizures have been documented in feline GM1 cats treated via Thal+DCN injection[114], as well as in late stage untreated animals[96, 142] and are well controled with medication. Seizures are also documented in late stage GM1 human patients[143-145].

Amelioration of the severity and rate of neurological deterioration was confirmed by MRI and MRS. By both measures, the cerebellum was the most severely affected region of the brain

from untreated GM1 cats. The neurological deficits in all treated animals, such as tremors, ataxia, and instability, are typical of cerebellar dysfunction[146]. The significant abnormalities of several cerebellar metabolites, including NAA, NAA+NAAG, and Glu+Gln, highlight the worsening cerebellar disease in GM1 cats treated by injection of the thalamus and lateral ventricle. At the time the MRS was collected, the iodixanol and CsCl cohorts were 2.3 times and 1.8 times older, respectively, than the lifespan of untreated GM1 animals. The significant loss of NAA ± NAAG, is indicative of not only loss of neuron integrity and health[136], but also of synaptic plasticity[147]. NAAG modulates glutamate release[147], therefore decreased levels of NAAG correspond with decreases in Glu+Gln. The continued loss of these metabolites in the cerebellum indicates that there is ongoing neuronal damage that was not seen in the Thal+DCN treated cats[114]. The trend towards normalization, especially in the iodixanol cohort, in the majority of metabolites in particular regions of the brain shows there is promise to the Thal+ICV administration route.

There were increased levels of βgal throughout the central nervous system of both treatment cohorts, as reported in other models[148-150]. In both cohorts, the region of highest βgal recovery in the brain was the thalamus, which was the injection site. Thalamic βgal levels were an average of 1.1-fold normal in the CsCl cohort and 1.6-fold normal in the iodixanol cohort. There was abatement of the super-physiological transduction of the area immediately surrounding the injection site, unlike previous studies[151-153]. As hypothesized, the ICV injection allowed the CSF to carry the AAV throughout the CNS and allow for spinal cord delivery. The iodixanol cohort had at or above normal levels of βgal throughout the spinal cord.

Comparison of empty to full capsids between the two AAV preparations revealed that the iodixanol cohort had a significantly larger empty capsid population that the CsCl preparation.

Although counterintuitive, the iodixanol cohort also had the most clinical success. It has been proposed that empty capsids can enhance therapeutic efficacy of AAV preparations by acting as decoys for the immune system[154, 155]. AAV neutralizing antibodies would bind to empty capsids as easily and readily as full capsids thereby potentially more full capsids to transduce cells[156]. Alternatively, the elevated number of empty capsids in the iodixanol preparation may play no role in the preparations efficacy.

The physicochemical properties of particles, such as their shape, size, and charge, can affect cellular uptake. AAV is internalized into cells through endocytosis after binding surface receptors[7]. A difference in charge could affect the internalization of AAV and what cellular compartments it will enter once inside the cell. Though minimal, there is a difference in charge between the two preparations. It has been shown that more negatively charged particles are take up more readily by mammalian cells[157]. Since both of the preparations were in a saline solution, which has been shown to be non-conducive to zeta potential measurements, the zeta potential of these preparations should be evaluated in a neutral solution. Additionally, CsCl has been shown to cause virus inactivation through virus aggregation, which is something iodixanol has been shown to prevent[53].

Taken together these data indicate that AAV preparations purified in iodixanol hold an advantage over those purified in CsCl. Due to the preliminary nature of these results further investigation should be conducted. Additionally, Thal+ICV administration of AAV does delay disease progression in GM1 cats, proving that AAV is a viable option for treatment.

Materials and Methods

Vector production

A single AAV preparation was produced using triple transfection of 293T cells with a helper plasmid (Fd6)[158], a plasmid expressing the AAVrh8 capsid, and the plasmid containing the feline βgal expression unit[114]. To limit variations, the preparation was split after harvesting and purified using either a CsCl continuous gradient or an iodixanol density gradient.

Animals and injection procedure

All animal procedures were approved by the Auburn University Institutional Animal Care and Use Committee (IACUC). Treatment groups are detailed in Table 1 for this study. GM1 cats were treated with AAV with bilateral injection of the thalami and in the left lateral ventricle for a total dose of 7.5E11 vg. Animals were fully anesthetized for the injection procedure which was induced with ketamine (10 mg/kg) and dexmedetomidine (0.04 mg/kg) through and intravenous catheter and maintained with isofluorane (0.5 – 1.5%) in oxygen via an endotracheal tube. Cats were positioned sternally for injection using a Horsely-Clark stereotaxic apparatus (David Kopf Instruments, Tujunga, CA, USA) and injected bilaterally in the thalamus and in the left lateral ventricle. Equal volumes and concentrations of iodixanol and CsCl-purified vector were used for injection.

Every two weeks animals were assessed for neurological disease symptoms using a 10 point clinical rating score. Starting with a score of ten, one point was subtracted for each symptom acquired: hind limb weakness, wide base stance, ataxia, instability, inability to walk more than a few steps, tremors, spastic limbs, and the ability to stand but not walk.

MRI/MRS

MRI and MRS data was collected as previously described[125, 159] using a 7T MAGNETOM scanner (Siemens Healthcare, Erlangen, Germany). Normal and untreated animals were scanned at 2, 4, 6, and 8 months of age as well as between 2 – 4 years for normal animals.

Treated animals were measured at approximately 12 months of age and then at humane endpoint. MRI data was analyzed with EFilm 3.2 software (Merge Healthcare, Chicago, IL, USA) and MRS data was processed with LC model and internal water scaling (http://s-provencher.com/lcmodel.shtml). Results were divided by age-matched normal values to determine the fold normal of each MRS metabolite.

Lysosomal enzyme activity

At necropsy, the brain was divided into 6 mm coronal blocks with the right hemisphere, portions of the spinal cord, and select peripheral tissues preserved in optimal cutting temperature (OCT) medium. All other tissues were flash frozen in liquid nitrogen and stored at -80°C or were formalin fixed. Frozen sections were collected, homogenized, and assayed for βgal activity as previously described[114]. Specific activity is expressed as nmol 4 MU/mg protein/h and each result was divided by the average normal value to calculate fold normal activity.

CSF biomarker analysis

Animals were sedated and placed under general anesthesia as previously described for CSF collection. CSF was collected via the cerebromedullary cistern and samples underwent at least one freeze-thaw cycle prior to being analyzed for biomarkers. Aspartate aminotransferase (AST) and lactate dehydrogenase (LDH) were analyzed on a Cobas C311 chemistry analyzer (Roche Hitachi, Basel, Switzerland & Tokyo, Japan).

AAV particle analysis

Transmission electron microscopy analysis of AAV was adapted from a protocol previously published[160]. Briefly, both virus preparations were diluted to 3.8E12 vg/mL in 1X PBS. A carbon film 200 mesh copper grid (Electron Microscopy Sciences, Hatfield, PA, USA) was placed on a 20µL drop of diluted AAV and incubated for 5 minutes. The grids were then

washed on 20µL drops of 1X PBS three times for a few seconds each. The girds were stained by placing the grid on a 20µL of 2% uranyl acetate for 1 minute, followed washing on a drop of ddH_2O. The grids were allowed to air-dry before being imaged in a Zeiss EM 10 Transmission Electron Microscope (Zeiss, Oberkochen, Germany). For particle assessment, particle size, concentration, and zeta potential were measured on a Malvern Zetasizer Ultra (Malvern instruments, Ltd., Worcestershire, UK).

Statistics

Statistical analyses were completed in Prism (Graphpad, La Jolla, CA, USA). Brown-Forsythe and Welch one-way ANOVA tests were used to compare all groups (normal, untreated GM1, CsCl, and iodixanol).

Tables and Figures

Table 1. Treatment groups

Group	Cat	Gender	Treatment Age (months)	Necropsy age (months)	CRS at necropsy
CsCl	9-1819	M	2.8	12.5	0.5*
	8-1836	F	2.6	19.9	0.5*
	8-1912	F	2.7	12.1	1.0
Mean ± s.d.			**2.7 ± 0.1**	**14.8 ± 3.6**	**0.7 ± 0.2**
Iodixanol	8-1822	M	2.7	25.3	1.0*
	8-1824	F	2.7	43.3	1.5*
	9-1844	M	3.2	25.6	2.0
Mean ± s.d.			**2.9 ± 0.2**	**31.4 ± 8.4**	**1.5 ± 0.4**

* Denotes cat had seizure activity, well-controlled with medication

Table 2. AAV Characteristics

	Size	**Concentration**	**Zeta Potential**
	d.nm	vg/mL	mV
CsCl	30.8 ± 0.13	4.82E+12	-3.77 ± 0.515
Iodixanol	49.2 ± 3.2	7.58E+13	-9.7 1± 1.72

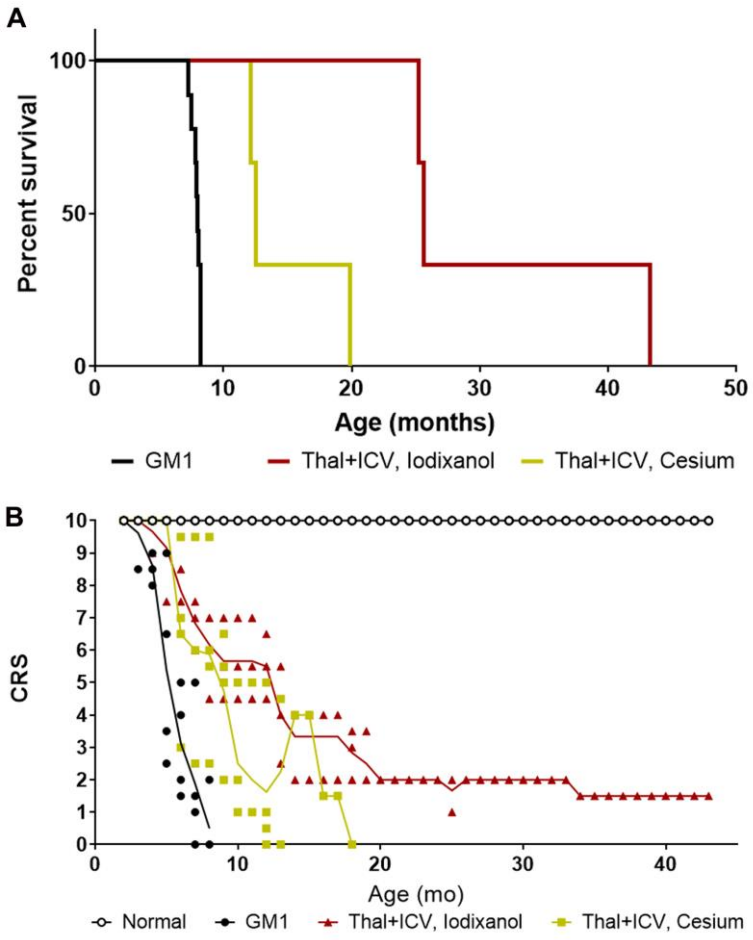

Figure 1. Clinical outcomes after Thal+ICV AAV treatment. A. Kaplan-Meier curve showing siginificantly increased survival in both Thal+ICV cohorts (Iodixanol p=0.0089, CsCl p= 0.0089). Untreated GM1 animals survive 8.0 ± 0.6 months, but after treatment Iodixanol animals survived significantly longer (31.4 ± 8.4 months) than the CsCl cohort (14.8 ± 3.6 months, p=0.025). B. Both treatment cohorts show a delay in disease progression in comparison to untreated GM1 animals. Point represent individual animal measurements and the trend line indicates the average clinical rating score (CRS) at any given time for the cohort. The trend line for the CsCl cohort is for one animal after 15 months of age, which accounts for the apparent increase in CRS score.

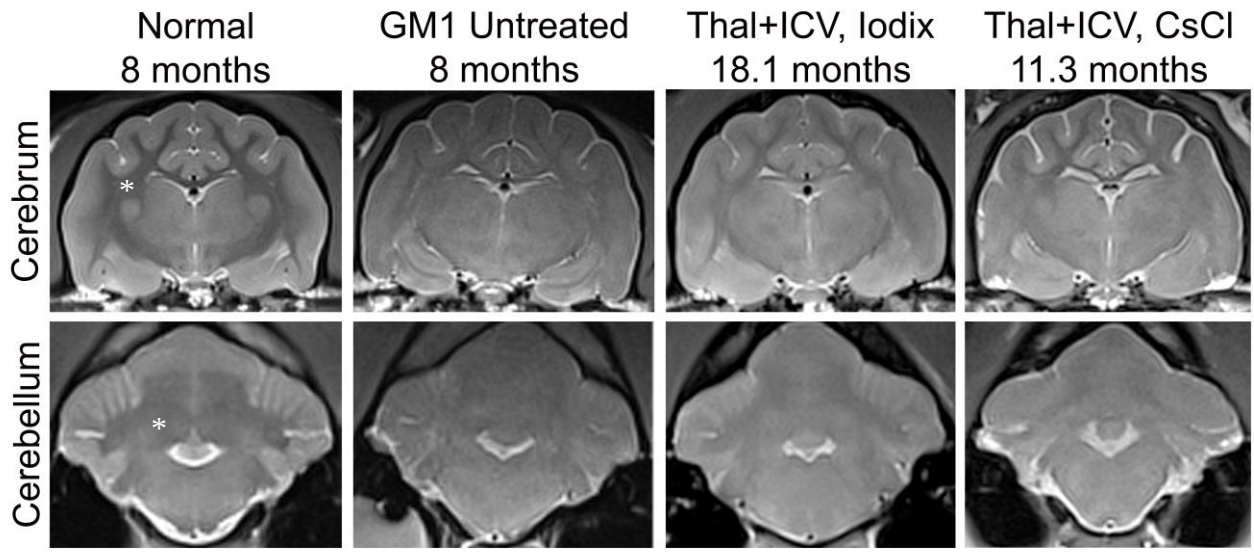

Figure 2. Normalization of brain architecture after AAV treatment. Brain architecture was evaluted using T2-weighed images from a 7T MRI. Cerebrum images were taken at the level of the thalamus and the cerebullar images are taken at the level of the deep cerebellar nuclei. In normal animals, white matter (asterisks) is hypointense to (darker than) gray matter. Untreated GM1 animals show an isointensitiy of white and gray matter at 8 months of age, indicative of both myelin loss and storage accumulation. Both the Iodixanol and CsCl groups showed a normalization in gray and white matter intensities. Addititionally, CSF accumulation (bright white) around the brain was normal in the Iodixanol group but was increased in the CsCl group. Shown are representative images from animals in each cohort.

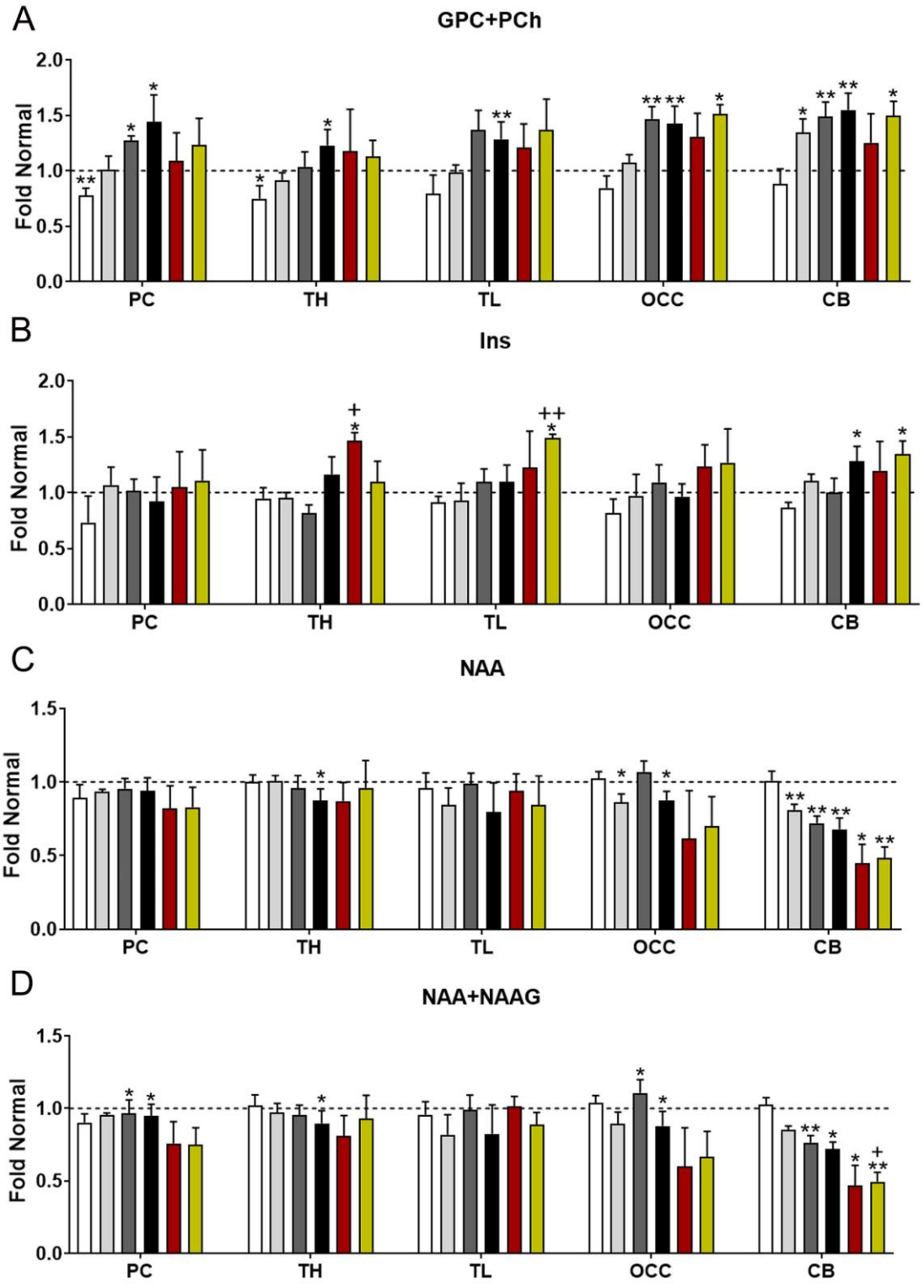
A
GPC+PCh
Fold Normal
2.0
1.5
1.0
0.5
0.0
PC
TH
TL
OCC
CB
B
Ins
C
NAA
D
NAA+NAAG

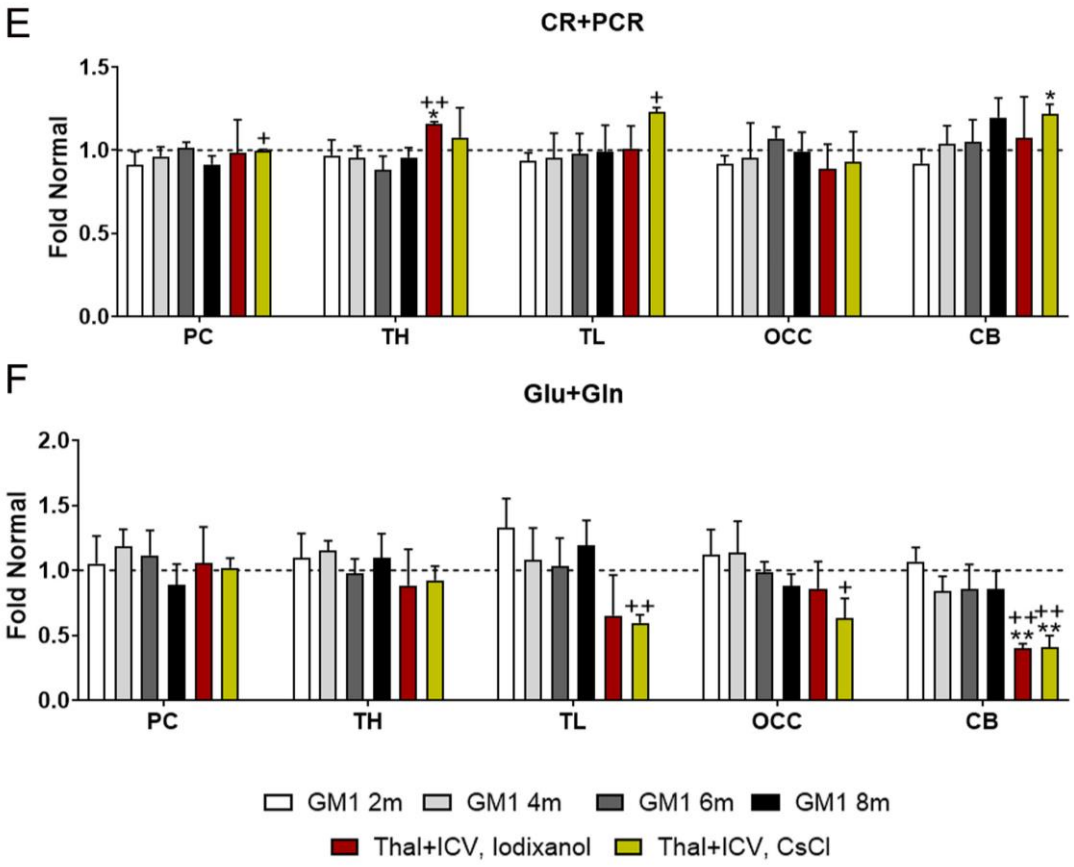

Figure 3. Analysis of brain metabolites. Brain metabolites were measured via MRS in 5 voxels across the brain: parietal cortex (PC), thalamus (TH), temporal lobe (TL), occipital cortex (OCC), and cerebellum (CB). Glycerophosphocholine and phosphocholine (GPC+PCh, A), Myinositol (INS, B), N-Acetyl aspartate (NAA, C), NAA and N-acetyl aspartyl glutamate (NAA+NAAG, D), creatine and phosphocreatine (CR+PCR, E), and glutamate and its precusor glutamine (Glu+Gln, F) were measured longitudinally (every 2 months) in untreated GM1 animals and at 18.0 ± 4.7 months in the iodixanol cohort or 14.2 ± 2.7 months in the CsCl groups. * $p<0.05$ and ** $p<0.005$ versus age-matched normal and + $p<0.05$ versus age-matched untreated GM1 animals.

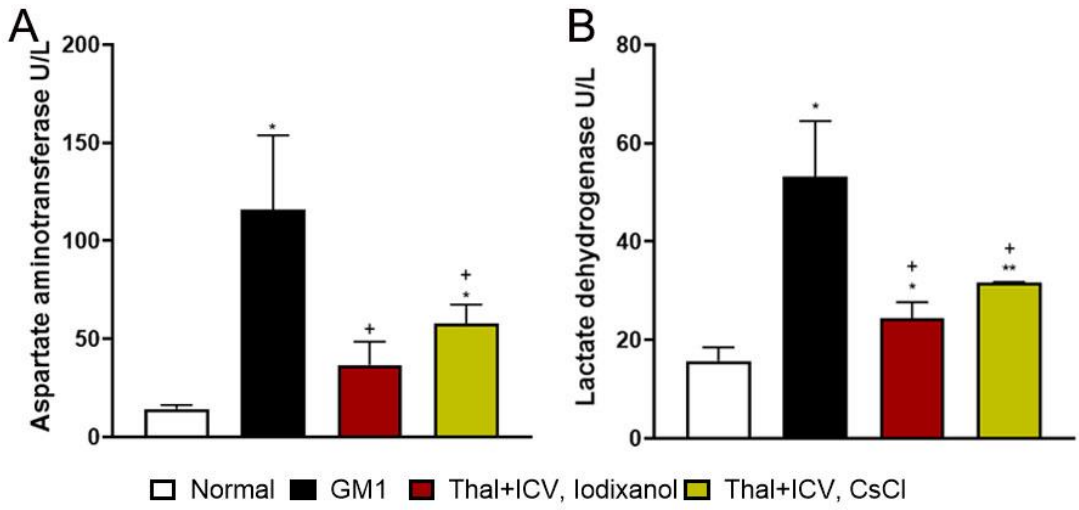

Figure 4. CSF markers of neurodegeneration. Average apsartate aminotransferase (AST, A) and lactate dehydrogenase (LDH, B) levels in normal, untreated GM1, and both treated cohorts at humane endpoint. Error bars indicate standard deviation. * $p<0.05$ and ** $p<0.005$ versus normal and + $p<0.05$ versus untreated GM1 animals.

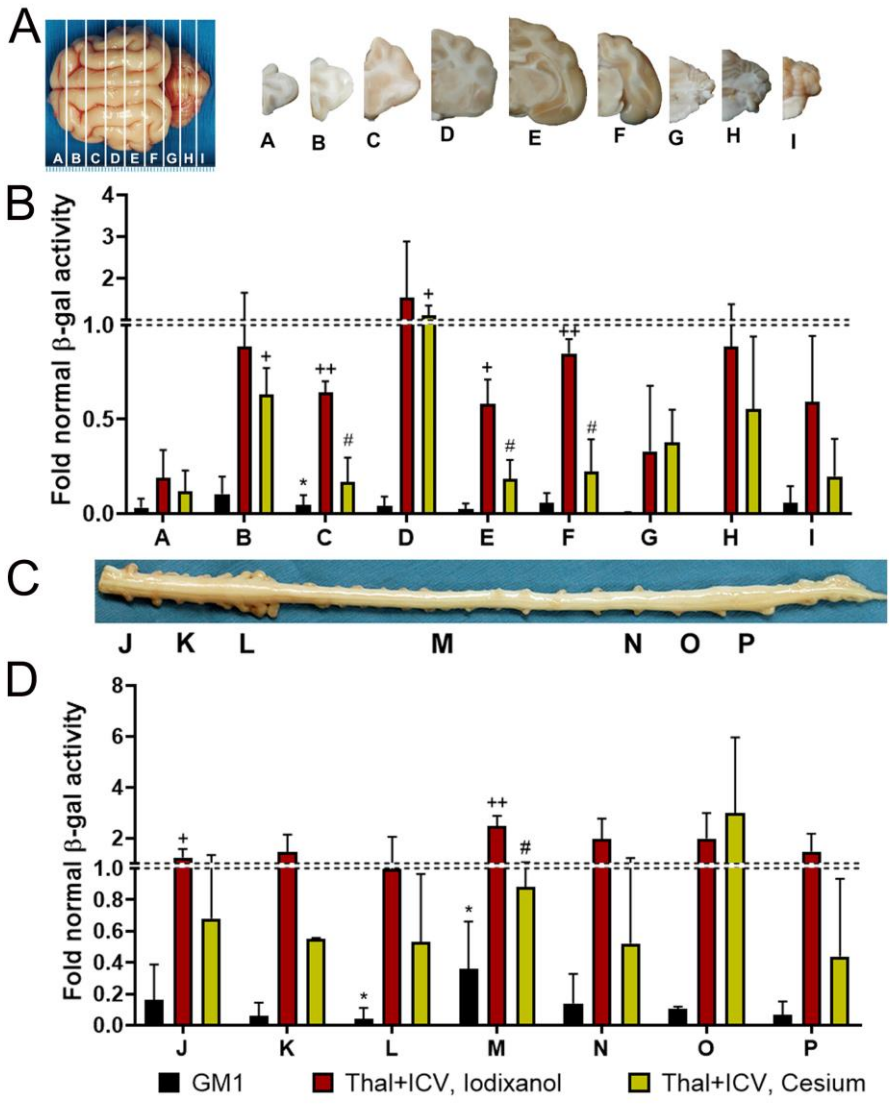

Figure 5. Increased βgal activity following AAV treatment. Gross images of the feline brain after sectioning into 6mm blockes that were used in anaylsis. B. Average βgal activity from btain homogentates from each section, which were determined usising a fluorogenic substrate. C. Gross image of the feline spinal cord with sections studied denoted by letters. D. Average βgal activity, after assaying with flourogenic substrate, in each spinal cord segment homogenate. Dahsed hortizonal line indicated normal level of βgal * $p<0.05$ versus normal, + $p<0.05$ and $p<0.005$ versus untreated GM1 animal, and # $p<0.05$ versus Iodixanol cohort.

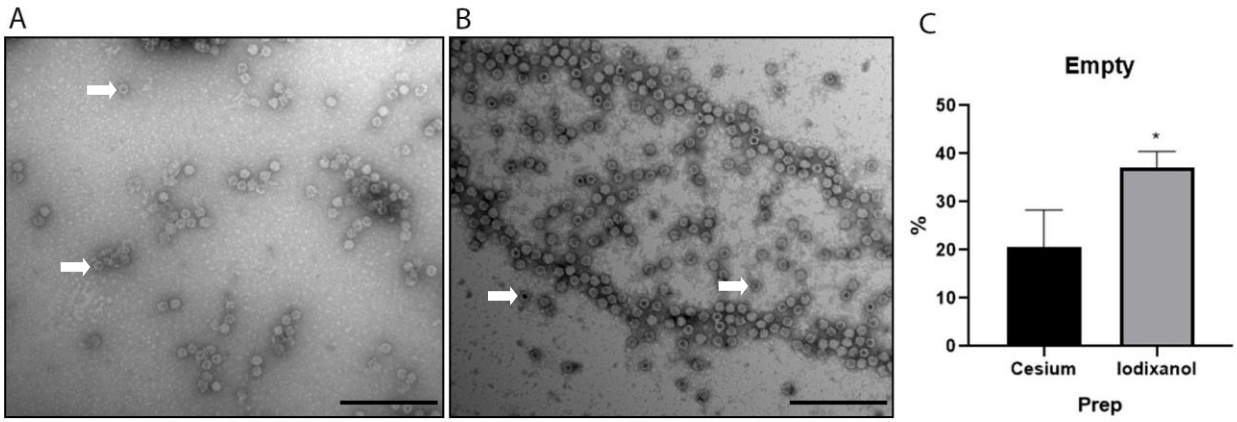

Figure 6. Ratio of empty to full AAV capsids Transmission electron microscopy (TEM) of CsCl (A) and Iodixanol (B) virus preparations. White arrows indicate empty capsids. Scale bars represent 250nm. C. Average percentage of empty capsids for each preparation determined from 3 separate images. Error bars represent standard deviation. * $p<0.05$ versus cesium.

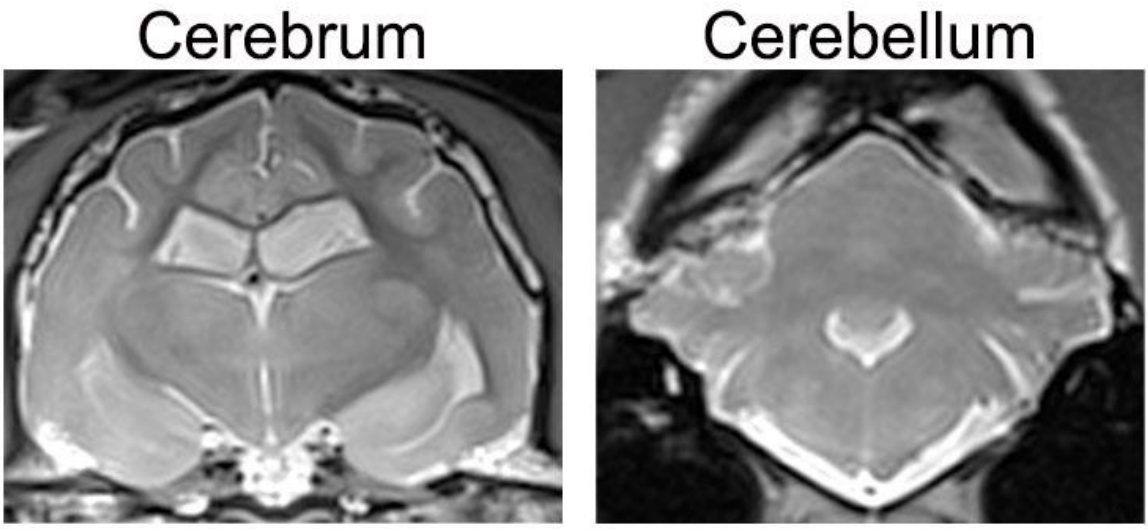

Supplemental Figure 1. MRI of Thal+ICV, Iodixanol cat at endpoint. MRI imaging showing an endpoint GM1 cat after treatment with iodixanol purified AAVrh8 (43.2 months of age).

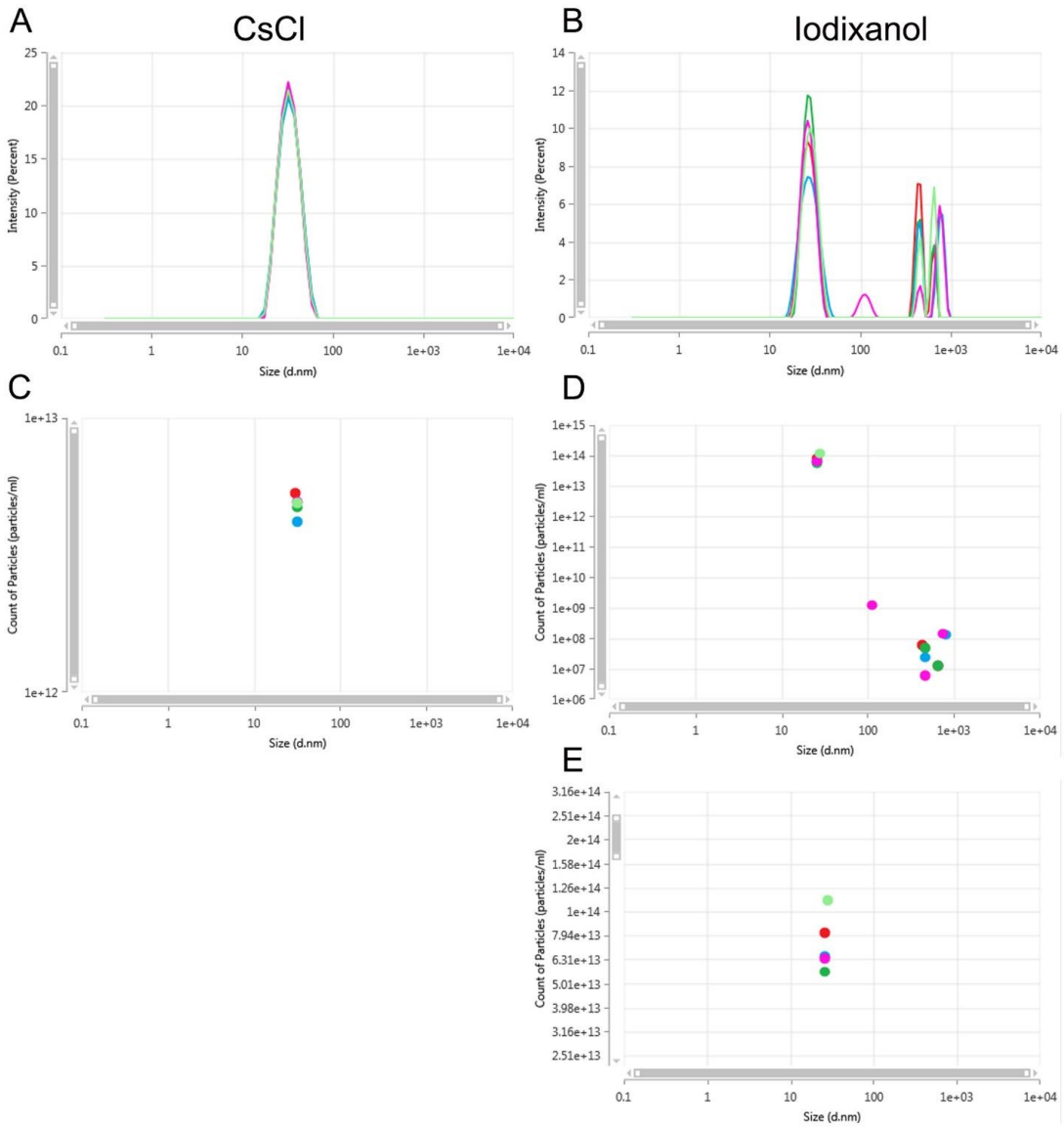

Supplemental Figure 2. Detailed AAV measurements. Depictions of the five measurements done for size (Cesium A, Iodixanol B) and concentration (Cesium C, Iodixanol D). The x-axis for the size measurement (intensity percent) describes how much light is scattered by the particles in different size bins. The subpopulation that resides in the 42 nm size range of the iodixanol preparation, which is likely the actual AAV, is highlighted in panel E for concentration.

Chapter 2

Evaluation of AAV serotype after intra-CSF injection for treatment of feline GM1 gangliosidosis

Amanda L Gross[1, 2], Heather L Gray-Edwards[1*], Miguel Sena-Esteves[3, 4], Douglas R Martin[1, 2]

[1] Scott-Ritchey Research Center, [2] Department of Anatomy, Physiology, & Pharmacology, College of Veterinary Medicine, Auburn University, Auburn, Alabama, USA

[3]Department of Neurology, [4]Horae Gene Therapy Center, University of Massachusetts Medical School, Worcester, Massachusetts, USA

* Current address: Department of Radiology, University of Massachusetts Medical School, Worcester, MA 01605 USA.

Abstract

GM1 gangliosidosis is a fatal neurodegenerative disease caused by a deficiency of lysosomal β-galactosidase (βgal). GM1 animals are effective models for studying gene therapy since the therapeutic vector, through restoration of enzymatic activity, can also act as a reporter construct. Cerebrospinal fluid (CSF) administration of adeno-associated viral (AAV) therapy is hypothesized to be an effective method for treating neurodegenerative diseases. In this study, we evaluated two serotypes (AAV9 and AAVrh10) using CSF delivery via the cisterna magna (CM). All treatment cohorts received 1.5e13 vector genomes/kg body weight at 2.3 ± 0.3 months of age. Untreated GM1 animals survived 8.0 ± 0.6 months while treated animals lived significantly longer. The AAV9 cohort (N=3) survived 13.9 ± 1.8 months and the AAVrh10 cohort (N=2) survived 11.3 ± 0.5 months. Clinical assessments included neurological exams, CSF biomarkers, and 7T magnetic resonance imaging (MRI) and spectroscopy (MRS). Postmortem analysis included βgal distribution. Neurological abnormalities, which in untreated GM1 animals lead to an inability to stand by 8 months of age, were delayed but not halted in both CM treated cohorts and all animals became blind as their disease progressed. CSF activity of aspartate aminotransferase (AST) and lactate dehydrogenase (LDH), biomarkers of central nervous system damage were both reduced in all treatment cohorts. MRI revealed delayed progression of neurodegeneration after treatment with either serotype, supporting the findings from clinical and neurological exams. MRS biomarkers showed limited correction in the AAVrh10 cohort and more widespread correction in the cerebellum of the AAV9 cohort. βgal activity was restored in the cerebellum and spinal cord but did not penetrate deep brain structures (such as thalamus). All cohorts had some degree of βgal restoration in the heart, liver, and

skeletal muscle. This study demonstrates clear efficacy of AAV to treat a severe, fatal neurologic disease after a minimally invasive injection.

Introduction

Diseases that affect the central nervous system (CNS) are immensely difficult to treat. This is due mainly to the blood brain barrier (BBB), a biological barrier made up of capillary endothelial cells, protoplasmic astrocytes, pericytes, a basement membrane and neurons, which prevent large molecules from entering the CNS. The BBB functions as a partition between the brain and the circulating blood[161]. Due to this difficulty, it has been hypothesized that direct treatment of the cerebrospinal fluid (CSF), the fluid that surrounds the brain and spinal cord, will enable treatment of these diseases. The use of adeno-associated viral (AAV) gene therapy for this treatment has been evaluated using numerous capsids, including AAV9 [132, 148, 162, 163], AAV2.5[148], AAVrh10[163], AAV2[163], AAV8[163], AAV5[163], AAV6[163]. However, these studies were conducted in mouse models and in nonhuman primates (NHP). While mouse models are a useful resource for evaluating human disease progression and possible therapeutics, they are not reliable in mimicking human disease. Their short lifespan prevents long term evaluation[89] and they have a significantly less complex brain than humans. NHPs are used extensively for toxicity studies, but there are few disease models that can be produced in NHPs. Additionally, NHPs have further limitations, including difficulties in procurement, increased ethical considerations, and significantly higher husbandry costs[164].

The GM1 gangliosidosis feline model closes resembles the human type II (late infantile/ juvenile) disease phenotype[95, 97]. GM1 gangliosidosis (GM1) is caused by a mutation of the *GLB1* gene, which encodes lysosomal β-galactosidase (βgal, EC 3.2.1.23) and results in a fatal neurodegenerative disease[81]. Bgal degrades GM1 ganglioside, which accumulates in lysosomes when βgal is deficient[74]. There are murine models of GM1[86, 87, 165], however their disease progression doesn't always mimic the human disease as closely as the feline model.

Additionally, the cat brain is 50x larger than their murine counterparts and has a closer brain to body weight ratio to humans. Also, the feline brain more closely resembles the architecture and organization of the human brain[98]. In addition to being therapeutic for GM1 models, βgal can be used as a reporter construct to chart distribution of enzyme activity, reinforcing the usefulness of the feline GM1 model.

The GM1 feline model has previously been used to evaluate distribution and therapeutic effect after bilateral injection of AAV into the thalamus and deep cerebellar nuclei (DCN)[114]. This treatment showed a significant improvement in length and quality of life with minimal neurological decline. While effective, intracranial surgery poses significant risk to patients, especially those who already have a severe neurological condition. For this reason, CSF delivery was evaluated in this study.

The AAV serotypes AAV9 and AAVrh10 were selected because they are among the few serotypes currently under evaluation in human clinical trials, and also based on their cell affinities. AAV9, which was isolated from human tissues, has been shown to transduce neurons and glial cells throughout the CNS through a variety of administration routes[162, 166, 167]. The AAVrh10 serotype, which was isolated from rhesus monkeys, has shown tropisms to sensory nerves[163], as well as for neurons and glial cells[168]. These CNS tropisms make them ideal candidates for comparison in a CSF based delivery study for the treatment of GM1.

Results

Clinical Data

The goal of this study was to directly compare the efficacy of two AAV serotypes, AAVrh10 and AAV9, to correct neurological and biochemical symptoms of cats with GM1 after

a single intra-cerebrospinal fluid (CSF) injection. GM1 cats were injected with the identical AAV backbone (expressing feline β-galactosidase) encapsulated by either AAVrh10 (N=2) or AAV9 (N=3, Table 1). Untreated GM1 cats typically survive 8.0 ± 0.6 months while both treatments significantly increased GM1 animal lifespan (Figure 1A). The AAVrh10 cohort survived 11.3 ± 0.5 months and the AAV9 cohort survived 13.9 ± 1.8 months, increasing lifespan to 1.4 ± 0.1 and 1.7 ± 0.2 times that of untreated animals, respectively. Survival increases after AAV treatment were statistically significant (AAVrh10, p=0.0405; AAV9, p=0.0136). There was no significant difference between the average lifespan of each treatment cohort (though animal numbers per cohort were relatively low).

Neurological symptoms were evaluated every two weeks using a 10-point clinical rating score (CRS), which is detailed in the materials and methods section. Cisterna magna injection of AAV delayed, but did not halt, disease progression (Figure 1B). Untreated GM1 animals typically develop hind limb weakness around 4.8 ± 0.5 months, which was significantly delayed to 6.3 ± 0.1 months in the AAVrh10 cohort and 7.5 ± 1 months in the AAV9 cohort. Averaging the age of symptom onset for all symptoms, the AAVrh10 cohort had a 2.8 ± 1.7 month delay in symptom onset and the AAV9 cohort had a 2.7 ± 1.9 month delay. The AAV9 cohort did not have as severe disease progression as AAVrh10 cohort, with an average CRS at necropsy of 3.7 ± 2.1 and 0.5 ± 0.5, respectively. Additionally, all treated animals became blind, which is not included in the clinical rating score, and resulted in euthanasia for some animals due to concerns on quality of life.

MRI/MRS

Ultra-high field (7 Tesla) T2 weight magnetic resonance imaging (MRI) can be used to track brain architecture during disease progression. By 8.8 months of age, the AAVrh10 cohort

had maintained normal brain architecture in some regions of the cerebral cortex (parietal and frontal lobes), but other regions revealed isointensity of the gray and white matter (temporal lobe and cerebellum). Other areas had inverted intensities of gray and white matter, particularly in the gyri on the lateral surface of the brain and in the hippocampal region (Figure 2E). Additionally, there was an increase in CSF surrounding the brain, and in the ventricles, indicating cerebral atrophy. By endpoint, the AAVrh10 cohort had further cortical neurodegeneration and atrophy (Figure 2G). Significant neurodegeneration was apparent throughout the cerebellum of the AAVrh10 cohort as early as 8.8 months (Figure 2F), as indicated by the isointensity of the region, which persisted through endpoint (Figure 2H). At 8.8 months, the AAV9 cohort had also maintained cerebral architecture and only a moderate increase in CSF (Figure 2I). By endpoint, there was an increase in brain atrophy as well as further neurodegeneration (Figure 2K). Similar to disease progression in the cerebral cortex, the AAV9 cohort had a slower rate of neurodegeneration in the cerebellum, with some normal brain architecture at 8.8 months (Figure 2J), which progressed continuously to humane endpoint (Figure 2L). The neurodegenerative changes in the MRI's are indicative of demyelination of the white matter, causing it to appear lighter (more hyperintense) than normal, and increased GM1 storage in the gray matter, indicated by a darker (more hypointense) than normal appearance.

Magnetic resonance spectroscopy was used to evaluate metabolites across 6 voxels in the brain: parietal cortex, thalamus, corona radiata temporal lobe, occipital cortex, and the cerebellum. Glycerophosphocholine and phosphocholine (GPC+PCh, Figure 3A) is a metabolite that increased with the loss of myelin integrity. GPC+PCh increases with age in untreated GM1 cats in most voxels. The AAVrh10 cohort only demonstrated decreased levels of GPC+PCh in the cerebellum at both 8.8 months and endpoint in comparison to age-matched untreated animals.

Similarly, the AAV9 cohort was significantly lower than 8-month untreated GM1 animals in the cerebellum and maintained a lower GPC+PCh through humane endpoint.

Myoinositol (INS), a marker of gliosis, is elevated in several voxels by humane endpoint in the untreated GM1 animals (Figure 3B). INS remained elevated in the AAVrh10 group at all timepoints. The AAV9 cohort had lower INS levels than the AAVrh10 cohort at 8.8 months in all voxels. By endpoint, the INS levels for the cohort AAV9 cohort were elevated above normal and untreated animals in all voxels.

N-acetylaspartylglutamate (NAAG), a metabolite whose signal overlaps with its precursor N-acetylaspartate (NAA), modulates glutamate release[169]. Due to their overlapping peaks, both the NAAG (Figure 3C) and the NAA+NAAG (Figure 3 D) graphs show similar results. In both the NAA and NAA+NAAG graphs, at endpoint, untreated GM1 animals are below normal levels in all voxels studied. The levels of NAA and NAA+NAAG were below normal and untreated levels by endpoint in all voxels besides the temporal lobe for both cohorts.

Creatine and phosphocreatine, markers of cell metabolism, was relatively normal in untreated animals, however both treated cohorts had elevated levels at 8.8 months and endpoint in the temporal lobe and cerebellum (Figure 3E). In addition, there were elevated levels in endpoint treated animals in the thalamus for both cohorts. The neurotransmitter glutamate, with its precursor glutamine (Glu+Gln), showed no clear trend for either untreated GM1 or treated animals (Figure 3F).

CSF biomarkers

Aspartate aminotransferase (AST) and lactate dehydrogenase (LDH) are enzymes present in almost all cells across the body. When measured in CSF, they are indicative of central nervous system cell damage. Both AST and LDH were significantly elevated in untreated GM1 animals

compared to normal (Figure 4), with AST 9.0 ± 2.0-fold normal and LDH 3.9 ± 0.8-fold normal. The AAV9 cohort showed the most normalization for both biomarkers, with AST 3.3 ± 0.5-fold normal (p=0.0059 versus GM1) and LDH 2.0 ± 0.3-fold normal (p=0.0284 versus GM1). The AAVrh10 cohort had normalized AST values (4.4 ± 0.5-fold normal, p=0.0323 versus GM1) but not LDH (2.6 ± 0.1-fold normal, p=0.1811 versus GM1).

β-galactosidase biodistribution and activity

Biodistribution and activity of βgal was assessed qualitatively using an x-gal staining solution (at an acidic pH), which forms a blue precipitate when cleaved (Figure 5). There is βgal activity in the cerebellum and spinal cord of all treated animals. However, the activity is primarily limited to surfaces readily exposed to CSF, particularly the cisterna magna region. There was little activity detected in the cerebrum and none in deep brain tissues, such as the thalamus and DCN. Quantitative analysis of tissue homogenates using a standard fluorogenic substrate confirmed the staining results. There was limited βgal activity in the cerebrum of both treatment cohorts, with 0.21 to 0.56-fold activity for the AAVrh10 cohort and 0.27 to 0.60-fold normal activity in the AAV9 cohort (Figure 6A). The highest activity in the cerebral cortex was detected in the homogenates from the most caudal region, the occipital cortex. There was increased βgal activity in the cerebellum, with 0.38 to 0.70 fold-normal activity in the AAVrh10 cohort and 0.51 to 1.0-fold normal in the AAV9 cohort. In the spinal cord, βgal activity ranged from 0.29 to 0.97-fold normal in the AAVrh10 cohort and 0.45 to 1.47-fold normal in the AAV9 cohort (Figure 6B).

While GM1 gangliosidosis is primarily a neurodegenerative disease, peripheral manifestations can be debilitating in human and feline patients. For this reason, it is imperative to not only assess treatment efficacy in the CNS, but also in the periphery. There was an increase

in βgal activity in the adrenal gland, sciatic nerve, heart, skeletal muscle, and liver for both treatment cohorts (Figure 6C). Activity in these regions ranged from 0.18 to 2.8-fold normal activity for the AAVrh10 cohort and 0.18 to 2.5-fold normal for the AAV9 cohort.

Discussion

The blood brain barrier is an immense challenge to overcome for treatment of CNS diseases. In attempt to bypass this blockade, intra-CSF delivery of AAV via the cisterna magna was explored. The surface of the central nervous system is constantly bathed in CSF, which is turned over approximately every 4 to 5 hours[170]. CSF freely flows between the lateral ventricles, the third ventricle, the fourth ventricle and the subarachnoid space, where is surrounds the brain and spinal cord. At all points during this flow, CSF is absorbed into the bloodstream. AAV injection into this CSF flow should enable CNS treatment as well as peripheral treatment for diseases.

Numerous studies have demonstrated the efficacy and safety of AAV gene therapy, including two U.S. Food & Drug Administration approved therapies. These treatments utilize AAV2 for retinal injection[66] and AAV9 for systemic injection[67]. No CSF-targeted gene therapy is yet approved for human use, but several candidates are in clinical trials. In the current study, administration of AAV solely via the CSF, using either AAVrh10 or AAV9, showed a significant increase in lifespan and quality of life of GM1 cats. Treated GM1 animals showed up to a 3 month delay in symptom onset, which clearly correlated with MRI and MRS findings. In previous studies with GM1 cats, AAV1 and AAVrh8 have been shown to have dramatic effect in long-term correction of disease progression after intracranial injection[114, 125]. In those studies, profound therapeutic benefit was achieved by injection of the thalamus and cerebellum, with

survival routinely >5 times longer than that of untreated GM1 cats. The dramatic difference in survival between GM1 cats treated by intracranial (>5-fold increase) versus CM injection (1.7-fold increase) may be explained by several factors. Though the vector backbone was very similar in both studies, previous experiments used AAV1 or AAVrh8 capsids for direct intracranial injection, while the current study used AAV9 or AAVrh10 for CM injections. The decision to use AAV9 or AAVrh10 for the current study was a practical one motivated by the common use of those serotypes in recent clinical trials. When the previous intracranial studies began, AAV9 and AAVrh10 were very early in development. Nevertheless, several reports and our own unpublished data strongly suggest that only minor differences in transduction or biodistribution exist among the 4 serotypes tested. Likewise, dosing is not likely to be a primary reason for the difference in efficacy, since CM-treated cats received ~3 times as much vector as those treated by injection of the thalamus and DCN. The likely reason for enhanced efficacy in cats treated by thalamic and cerebellar injection is the clear superiority in treating deep brain structures. The thalamus and DCN both centers of neural interconnectivity. The thalamus receives and processes sensory information and the majority of cerebellar output passes through the DCN. Neurodegeneration of these areas, which occurs without proper treatment, leads to debilitating neurological decline. The CM treatment did not reach these deep brain structures and the CM-treated animals exhibited a dramatically worse neurological decline in comparison to the Thal+DCN-treated animals.

When directly comparing AAV9 to AAVrh10 in this model, there are slight, though real, differences in the clinical and physiological outcomes of the two cohorts. Looking initially at the in-life measures, such as survival, CRS, MRI, and MRS, there was an increase in length and quality of life in the AAV9 cohort over the AAVrh10 cohort. In attempt to further quantify

differences between animals treated with AAVrh10 and AAV9, a third animal was added to the AAVrh10 cohort and will be evaluated under the same conditions as those already discussed. The main concern, which ultimately led to euthanasia of the final two AAV9 animals, was with quality of life due to blindness. In humans there is a decrease in quality of life with blindness[171], but not to the level seen in research cats. While normal cats may exhibit little to no decrease in quality of life, the same cannot be said for animals with neurological deficits. Due to their ataxia and hind end weakness, these animals exhibit signs of increased distress and disorientation, clear markers of a decreased quality of life. The levels of AST and LDH, which are biomarkers of cellular health[139, 140], were more moderately reduced in the AAVrh10 cohort than in the AAV9 cohort. Looking at the post-mortem βgal recovery, AAV9 resulted in moderately more βgal activity than that of the AAVrh10 cohort. Taken together, this data suggests that AAV9 is a better candidate for treating GM1 in this model.

Though improved over untreated GM1 animals, the CM treatment did not reach deep brain structures, such as the DCN, thalamus, and striatum[115, 172-174] that have shown efficacy when treated directly. It is estimated that each brain neuron is within a few microns of a capillary[175]. Combining this knowledge, with the demonstrated improvement in efficacy of AAV9, and the knowledge that AAV9 can cross the blood-brain barrier[176-178], it would be advantageous to investigate the potential of AAV9 gene therapy for intravenous delivery.

Materials and Methods

Animals and treatment

An AAV backbone expressing feline βgal with a CBA promoter was packaged with either AAVrh10 or AAV9 capsid. The vectors were produced using the triple transfection method and purified on an iodixanol density gradient.

Treatment groups and animal information are detailed in Table 1. All animal procedures were approved by the Auburn University Institutional Animal Care and Use Committee. GM1 cats were treated with either an AAV9 or an AAVrh10 virus at approximately 2.3 months of age at the total dose of 1.5E13 vector genomes/kg body weight. Animals were fully anesthetized using a combination of intravenous dexmedetomidine (0.04 mg/kg) and ketamine (10 mg/kg) and maintained using isoflurane. Location of the cistern manga was confirmed using ultrasound and injection was completed over several minutes.

Every two weeks animals were evaluated for neurological decline using a 10 point clinical rating score. One point was subtracted from a normal score of 10 for each symptom acquired: tremors, spastic limbs, hind limb weakness, wide based stance, ataxia, instability, inability to walk more than a few steps, and the ability to stand but not walk. Animals were followed until they reached humane endpoint, defined as the inability to stand, or until concerns over quality of life lead to earlier euthanasia.

After euthanasia, the brain was divided into 6mm coronal blocks with the left hemisphere being split between formalin fixation and flash frozen and stored at -80°C. The right hemisphere was preserved in optimal cutting temperature (OCT) medium. The spinal cord was divided into seven regions: rostral cervical, mid cervical, cervical intumescences, mid thoracic, thoracolumbar, mid lumbar, lumbar intumescence. These seven regions were formalin fixed, preserved in OCT, and flash frozen and stored at -80°C. Peripheral tissues were formalin fixed and flash frozen and stored at -80°C, with select tissues stored in OCT.

MRI/MRS

Animals were fully anesthetized as previous described during MRI/MRS collection. MRI and MRS data were acquired on a 7 Tesla MAGNETOM scanner (Siemens Healthcare, Erlangen, Germany). A 32-channel head coil (Nova Medical, Boston, MA) was used for all scans. Anatomical coronal images were acquired using 3D MPRAGE (Magnetization-PRepared RApid Gradient Echo) with 0.5mm isotropic resolution and TR/TE of 1910/2.5ms, followed by 2D axial T2 turbo spin echo (TSE) images with TR/TE of 5450/12ms and a resolution of (0.25x0.25x1) mm. Single voxel spectroscopy (SVS) was then acquired using a PRESS (Point Resolved Spectroscopy) sequence optimized for 7T with TE/TR = 30/5000 ms, 64 averages and a Variable Pulse power and Optimized Relaxation Delays (VAPOR) water suppression. Shimming was performed using FASTESTMAP followed by manual shimming if needed. The resulting full width half max (FWHM) of unsuppressed water was typically 16Hz. Optimization of RF pulse amplitudes and of the water suppression scheme was performed prior to acquiring each spectrum. The unsuppressed water signal was obtained and used for eddy current correction and for quantification of metabolites. Using high resolution 3D MRI images, voxels were positioned in the thalamus (7x6x8mm), parietal cortex (7x6x8mm) and cerebellum (7x7x8mm). MRI data were analyzed with EFilm 3.2 software (Merge Healthcare, Chicago). MRS data were processed with LC model and internal water scaling (http://www.s-provencher.com/pages/lcmodel.shtml).

Biomarker Analysis

CSF was collected from the cisterna magna and blood from the jugular vein. Animals were sedated using dexmedetomidine for CSF collection and as needed for blood collection. CSF samples were analyzed for aspartate aminotransferase (AST) and lactate dehydrogenase (LDH)

concentration using a Cobas C311 chemistry analyzer (Roche Hitachi, Basel, Switzerland & Tokyo, Japan).

Enzyme Activity

Lysosomal enzymes were isolated from CNS tissues with 3-6 sections (40 µM) cut from coronal blocks stored in OCT. For peripheral tissues, 50-70 mg was taken from the flash frozen samples. Tissues were homogenized manually in 500 µL of 50 mM citrate phosphate buffer, pH 4.4 (50 mM citric acid, 50 mM Na_2HPO_4, 10 mM NaCl) containing 0.1% Trition X-100 and 0.05% BSA, followed by two freeze-thaw cycles in liquid nitrogen and centrifugation at 15,700 x g for 5 minutes at 4°C. The activity of β-galactosidase was measured using a synthetic fluorogenic substrate as previously described[179]. CSF samples were analyzed for βgal activity using 30µL of sample and 10µL of substrate followed by incubated at 37°C for one hour. Specific activity was expressed as nmol 4MU cleaved/mg protein/hour after normalization to protein concentration determined by Lowry method.

Distribution of βgal activity was determined via histochemical staining as previously described[114].

Statistics

Statistical analyses were performed using Prism (Graphpad, La Jolla, CA USA) and Microsoft Excel (Microsoft, Redman, WA USA). Brown-Forsythe and Welch one-way ANOVA tests were used to compare all groups for statistical significance. For MRS, only spectra with Cramér-Rao minimum variance bounds of <30 were included in the analyses.

Figures and Tables

Table 1. Treatment groups and clinical data of GM1 cats with AAV intra-CSF delivery

Group	Cat	Gender	Treatment age (months)	Treatment weight (kg)	Necropsy age (months)	CRS at necropsy
GM1+AAVrh10 CM	9-1963	M	2.6	0.8	11.8	0.0
	9-1979	M	2.1	0.7	10.8	1.0
	Mean ± s.d.		**2.4 ± 0.3**	**0.8 ± 0.0**	**11.3 ± 0.5**	**0.5 ± 0.5**
GM1+AAV9 CM	9-1966	F	2.6	1.0	15.1	4.0*
	9-1974	F	2.2	1.0	15.3	6.0*
	9-1981	F	1.9	0.7	11.2	1.0
	Mean ± s.d.		**2.2 ± 0.3**	**0.9 ± 0.1**	**13.9 ± 1.9**	**3.7 ± 2.1**

*animal necropsied due to disorientation and distress due to blindness coupled with ataxia and hind end weakness

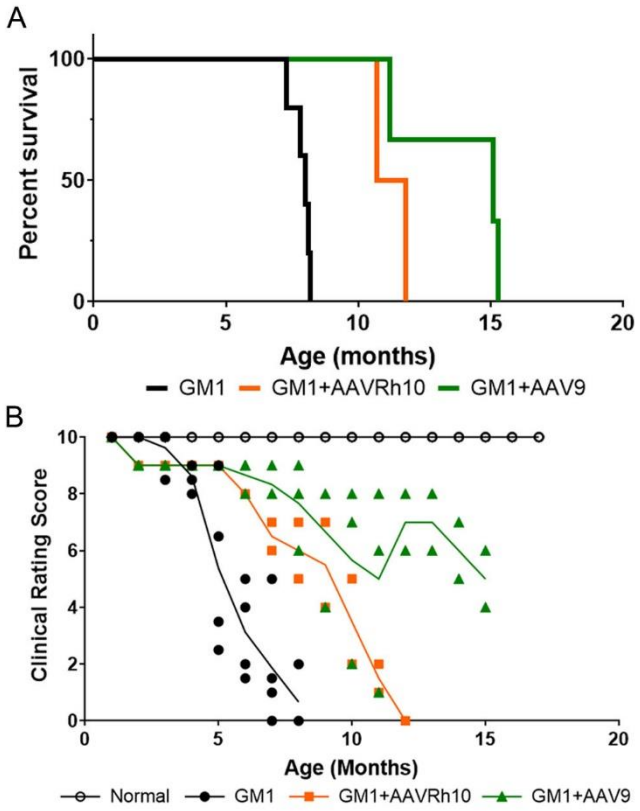

Figure 1. Clinical outcomes. A. Kaplan-Meier curve showing survival of cohorts. Untreated GM1 animals (black line) survived 8.0 ± 0.6 months, the AAVrh10 cohort survived 11.3 ± 0.5 months (p= 0.0405), and the AAV9 cohort survived 13.9 ± 1.8 months (p= 0.0136). There was no statistical difference between treatment groups (p= 0.2072). B. Animals are assessed using a 10-point clinical rating scale. Untreated GM1 animals show a rapid decline in clinical rating score, with endpoint reached at approximately 8 months of age. Both the AAVrh10 (orange) and AAV9 (green) cohorts had a delay in disease progression.

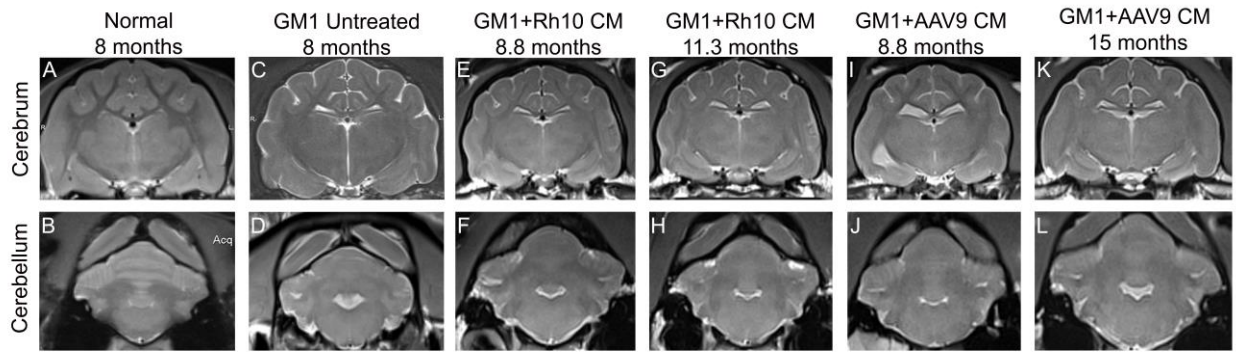

Figure 2. Magnetic resonance imaging. Compared to normal cat cerebrum (A) and cerebellum (B), GM1 cats have isointense gray and white matter with atrophy, indicated by the CSF around the brain (CSF) in both the cerebrum (C) and cerebellum (D). At 8.8 months, in the AAVrh10 cerebrum (E) and cerebellum (F) there is evidence of delay of disease progression with the gray and white matter maintaining their appropriate intensities and minimal CSF accumulation. The AAV9 cohort at 8.8 months (I and J) showed an even great maintenance of normal architecture. By endpoint, both the AAVrh10 (11.3 months, G and H) and the AAV9 (15 months, K and L) show further signs of neurodegeneration and increased atrophy. All images are T2 weighted from a 7T scanner. Cerebrum images were taken at the thalamus and cerebellar images at the level of the deep cerebellar nuclei.

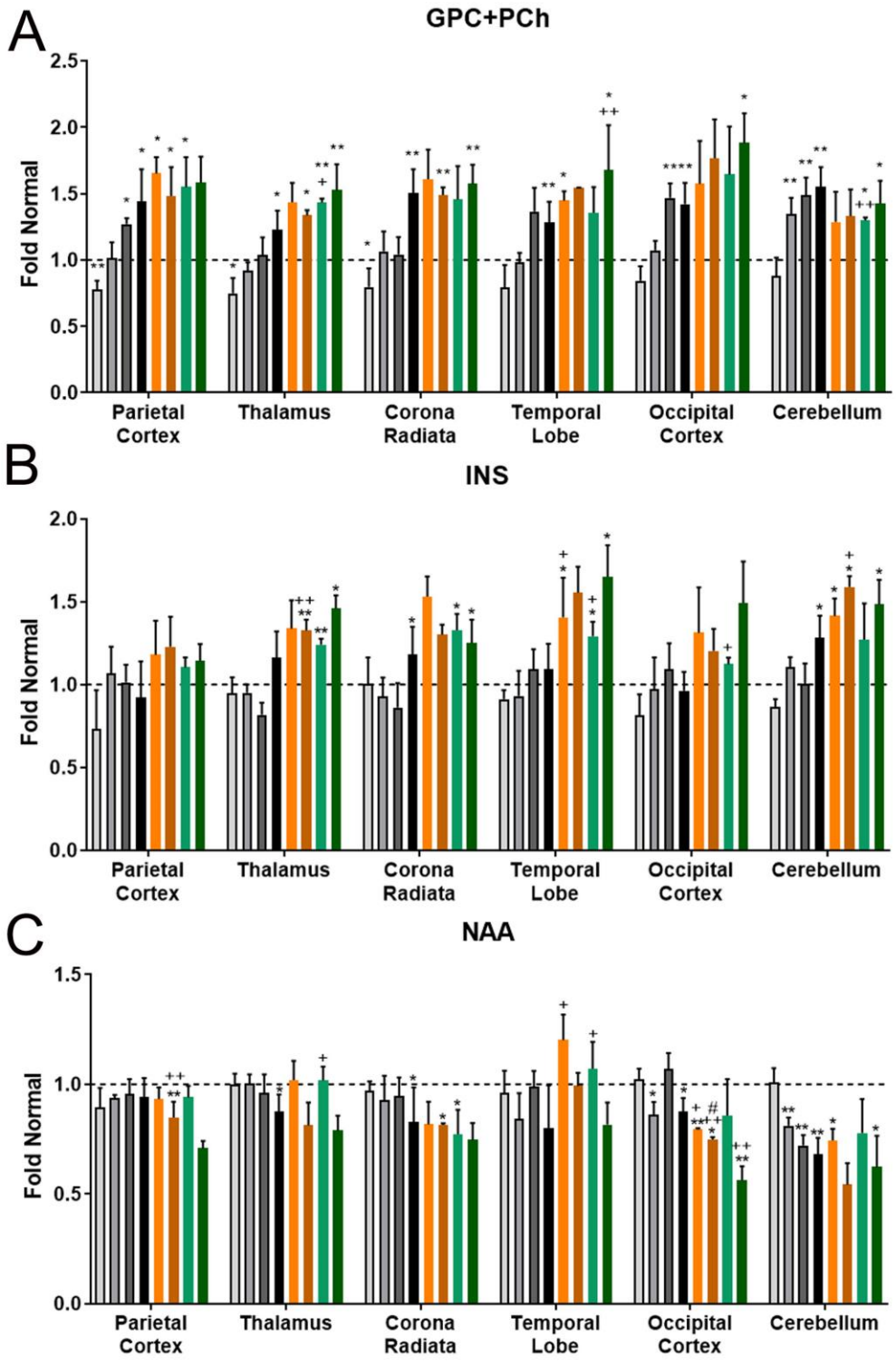
A
GPC+PCh
Fold Normal
2.5
2.0
1.5
1.0
0.5
0.0
Parietal Cortex
Thalamus
Corona Radiata
Temporal Lobe
Occipital Cortex
Cerebellum
B
INS
Fold Normal
2.0
1.5
1.0
0.5
0.0
Parietal Cortex
Thalamus
Corona Radiata
Temporal Lobe
Occipital Cortex
Cerebellum
C
NAA
Fold Normal
1.5
1.0
0.5
0.0
Parietal Cortex
Thalamus
Corona Radiata
Temporal Lobe
Occipital Cortex
Cerebellum

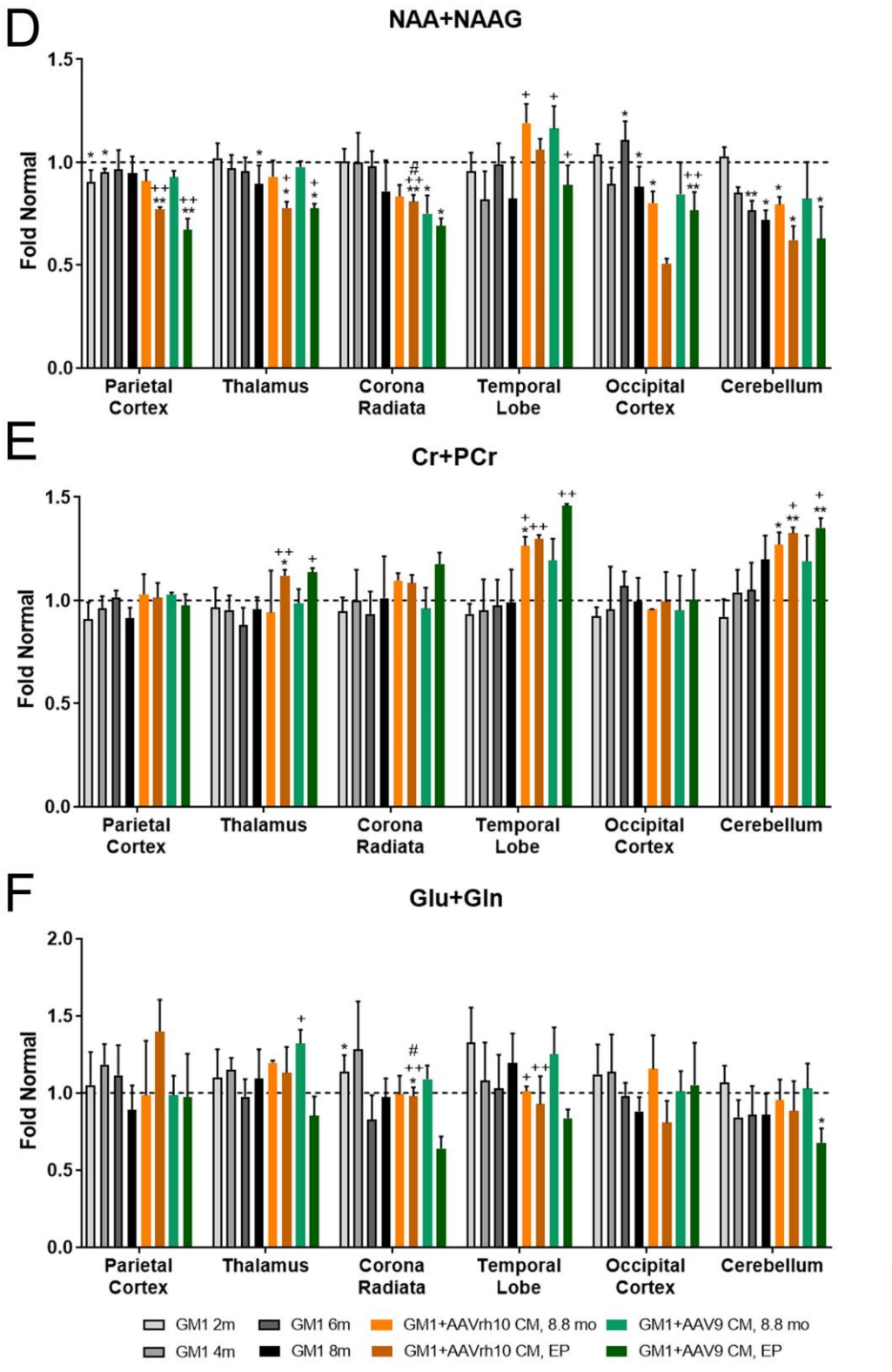

Figure 3. Magnetic resonance spectroscopy. Glycerophosphocholine and phosphocholine (GPC+PCh, A), myoinositol (INS, B), N-acetyl aspartate (NAA, C), N-acetyl aspartate and N-

acetyl aspartyl glutamate (NAA+NAAG, D), creatine and phosphocreatine (Cr+PCr, E), and glutamate and glutamine (Glu+Gln, F) were measured in six voxels across the brain. Scans were completed at 2, 4, 6, and 8 months in normal and GM1 animals and all treated animals were scanned at 8.8 months and at endpoint. Measurements are standardized to the appropriate age matched normal animal and are represented as fold normal ± S.D. *$p \leq 0.05$ and **$p \leq 0.005$ versus age-matched normal, +$p \leq 0.05$ and ++$p \leq 0.005$ versus untreated GM1, and #$p \leq 0.05$ versus AAV9 cohort.

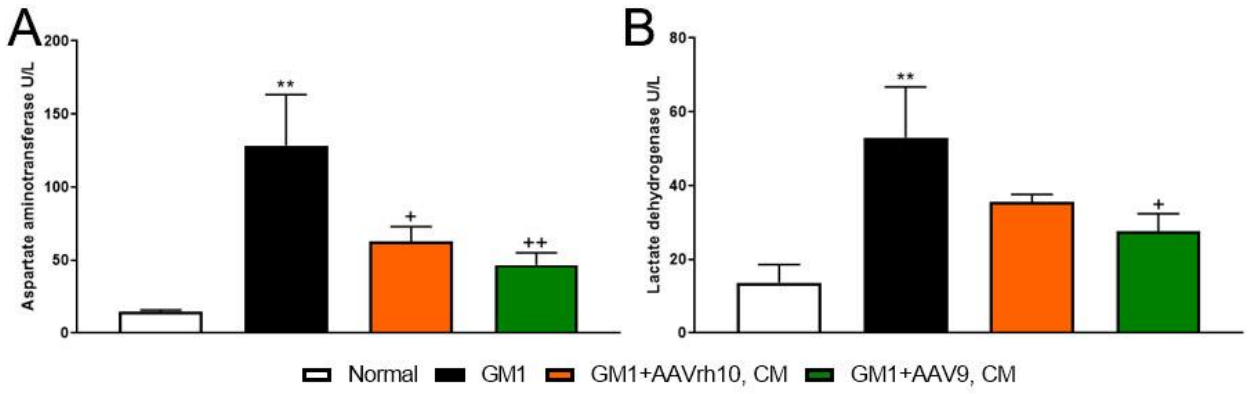

Figure 4. CSF biomarkers. Aspartate aminotransferase (AST,A) and lactate dehydrogenase (LDH, B) levels in the CSF of normal, GM1 untreated, and both treated cohorts. *p≤0.05 and **p≤0.005 versus normal, +p≤0.05 and ++p≤0.005 versus untreated GM1 animals.

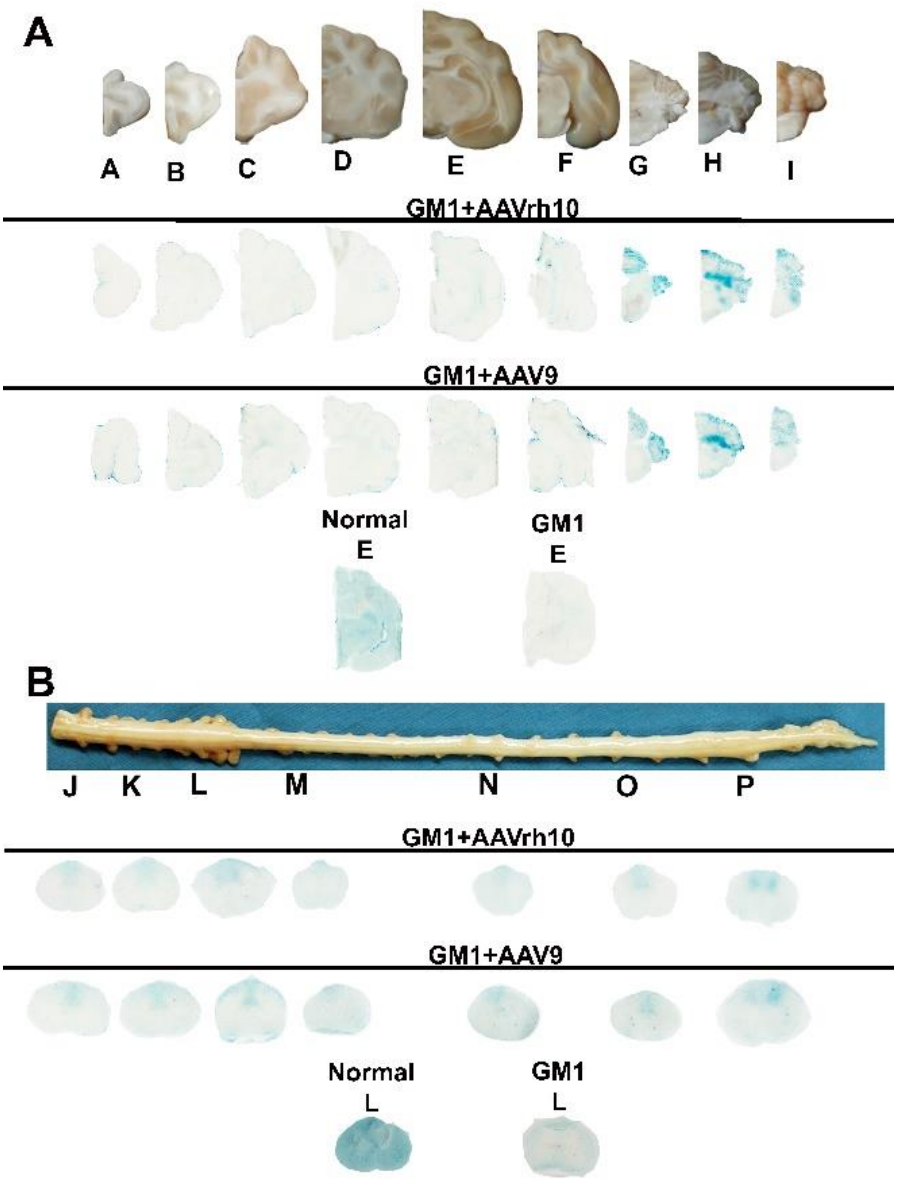

Figure 5. βgal biodistribution. A. Across the top are gross images of the right hemisphere of each brain block used to assess βgal distribution, from frontal lobe (A) to caudal cerebellum (I). Below are representative images for each treatment group, as well as normal and untreated endpoint animals. B. Regions of the spinal cord that were used to assess βgal distribution in normal, treated, and untreated GM1 animals. The blue stain indicates active βgal.

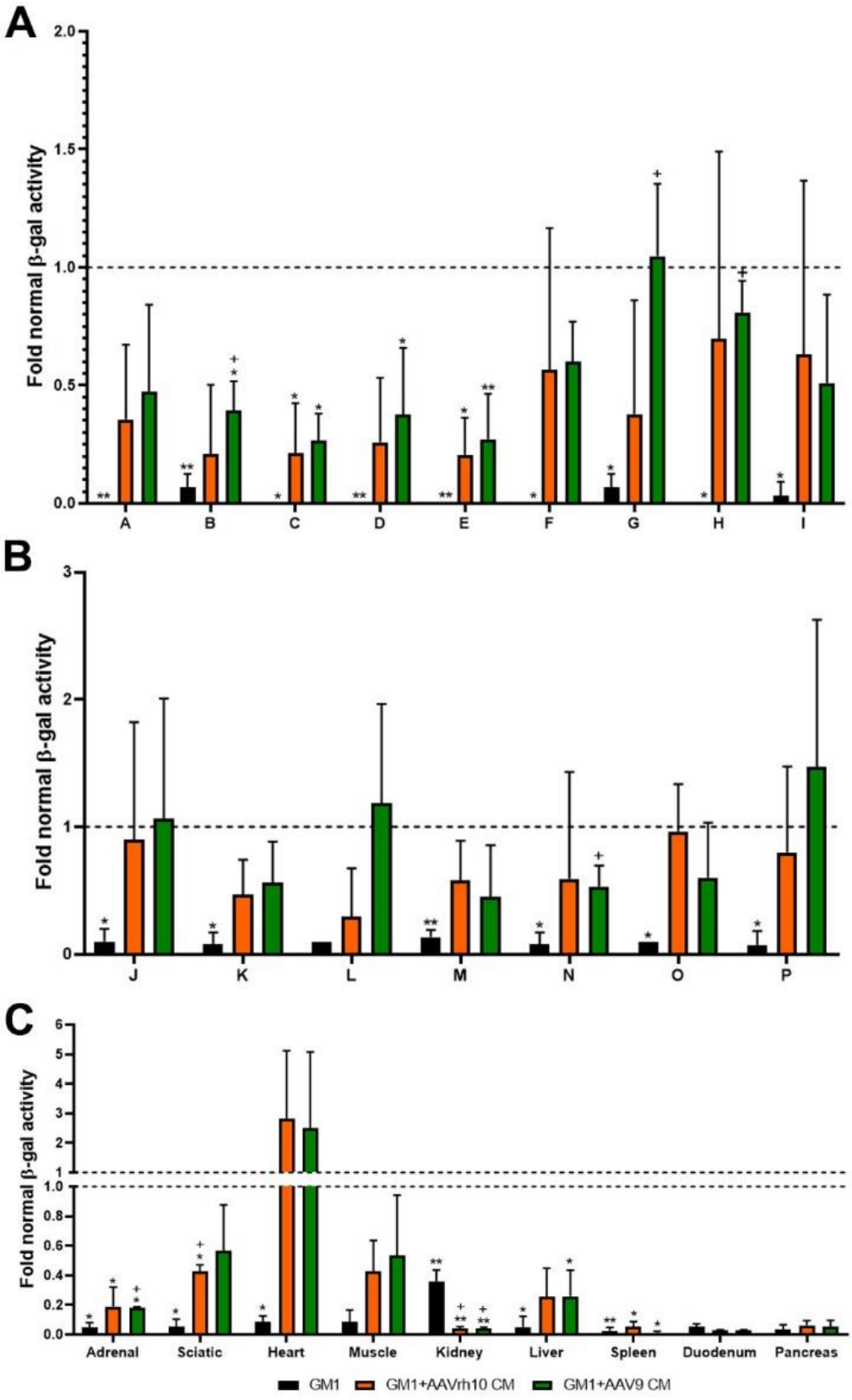
A
Fold normal β-gal activity
2.0
1.5
1.0
0.5
0.0
A
B
C
D
E
F
G
H
I
B
Fold normal β-gal activity
3
2
1
0
J
K
L
M
N
O
P
C
Fold normal β-gal activity
6
5
4
3
2
1
1.0
0.8
0.6
0.4
0.2
0.0
Adrenal
Sciatic
Heart
Muscle
Kidney
Liver
Spleen
Duodenum
Pancreas
GM1
GM1+AAVrh10 CM
GM1+AAV9 CM

Figure 6. βgal Activity. Activity of βgal was assessed in homogenates from brain (A), spinal cord (B), and select peripheral tissues (C). Data is represented as mean fold normal with error bars representing standard deviation. The dashed horizontal line indicates normal activity. *$p \leq 0.05$, **$p \leq 0.005$ versus normal, +≤ 0.05, ++$p \leq 0.005$ versus untreated GM1 animals.

Chapter 3

Intravenous delivery of AAV gene therapy in feline gangliosidosis

Amanda L. Gross[1,2], Heather L. Gray-Edwards[1]*, Cassie N. Bebout[1], Nathan L. Ta[3], Kayly Nielsen[1], Brandon L. Brunson[2], Ana Rita Batista[4,5], Stacy Maitland[4,5], Thomas N. Seyfried[3], Miguel Sena-Esteves[4,5], Douglas R. Martin[1,2]

[1] Scott-Ritchey Research Center, College of Veterinary Medicine, Auburn University, Auburn, AL 36849 USA.

[2] Department of Anatomy, Physiology, and Pharmacology, College of Veterinary Medicine, Auburn University, Auburn, AL 36849 USA.

[3] Biology Department, Boston College, Chestnut Hill, MA 02467

[4] Department of Neurology, University of Massachusetts Medical School, Worcester, MA 01605 USA.

[5] Horae Gene Therapy Center, University of Massachusetts Medical School, Worcester, MA 01605 USA.

* Current address: Department of Radiology, University of Massachusetts Medical School, Worcester, MA 01605 USA.

Abstract

GM1 gangliosidosis is a fatal neurodegenerative disease caused by a deficiency of lysosomal β-galactosidase. In its most severe form, GM1 gangliosidosis causes death by 4 years of age, and no effective treatments exist. Previous work has shown that injection of the brain parenchyma with an adeno-associated viral vector provides pronounced therapeutic benefit in a feline GM1 model. To develop a less invasive treatment for the brain and increase systemic biodistribution, intravenous injection of AAV9 was evaluated. GM1 animals were injected with 1.5e13 vg/kg body weight at approximately 1 month of age via a catheter in the cephalic vein. Untreated GM1 animals survived 8.0 ± 0.6 months while intravenous treatment increased survival to approximately 3.5 years with substantial improvements in quality of life and neurologic function. MRI and MR spectroscopy showed normalization in treated animals, which was supported by postmortem histological evaluation. β-galactosidase activity was increased throughout the CNS, reaching normal levels in the CSF, cerebellum, and spinal cord. Peripheral tissues such as heart, skeletal muscle, and sciatic nerve also had normal β-galactosidase activity in treated GM1 cats. Additionally, there was significant reduction of ganglioside accumulation in the CNS in both short and long term cohorts. This data supports the promise of intravenous gene therapy as an alternative for intracranial injection and as a safe, effective treatment for GM1 gangliosidosis.

Introduction

GM1 gangliosidosis is a progressive neurodegenerative disease caused by a mutation of the GLB1 gene, resulting in a deficiency of β-galactosidase (βgal, EC 3.2.1.23)[81]. GM1 is a lysosomal storage disease, which as a group, represent over 50 distinct diseases[180]. βgal is utilized in the lysosome to break down GM1 ganglioside and therefore a deficiency in βgal results in accumulation of GM1 ganglioside[74]. GM1, which can occur at any stage of life, is divided into three types based on age of onset: type I (infantile), type II (late infantile / juvenile), and type III (adult/chronic)[77, 81]. The most common forms of GM1 are infantile and juvenile, which have a more rapid disease progression than the adult onset. All forms of GM1 are characterized primarily by debilitating and progressive neurological disease, though accumulation of substrates with terminal galactose moieties occurs throughout the body[121]. Outside of palliative and supportive care, there is no effective therapy for GM1.

Animal models are useful and necessary for evaluating candidate therapeutics prior to initializing clinical trials. Murine[87, 165, 181] and feline[95] models of GM1 both exist and have been well characterized. The feline GM1 disease model closely resembles the type II phenotype in human patients[96, 97]. While mouse models provide an invaluable resource for studying disease progression and treatment, they do not always mimic the human clinical disease phenotype. Additionally, their limited lifespans prevent long term studies[89]. Feline brains are 50x larger than murine brains and more closely resemble the architecture and organization of the human brain[98]. Previously, both models showed recovery of βgal activity throughout the CNS after injection of adeno-associated viral (AAV) vectors into the brain parenchyma and cerebrospinal fluid (CSF)[115, 116, 182]. Widespread CNS distribution of enzyme via intraparenchymal injection is dependent on treating highly interconnected brain structures like the deep cerebellar nuclei

(DCN)[172], thalamus[115], and striatum[173, 174]. In the feline model of GM1, bilateral injection of AAV into the thalamus and DCN showed a marked improvement in quality of life, with minimal neurological symptoms and vastly increased lifespans[182]. While the intraparenchymal injections were successful, the risk of serious adverse events due to intracranial surgery, volume and administration rate are concerns that must be addressed for human patients[127]. Though invasive, brain parenchyma injections were the only way to treat the CNS effectively until the advent of a method to circumvent the blood-brain barrier (BBB).

AAV9, as well as other AAV serotypes, cross the BBB and transduce neurons and glial cells throughout the CNS after systemic injection[176, 177, 183]. Systemic delivery of AAV also leads to high transduction of peripheral tissues, which is expected to benefit the global enzyme deficiency and storage accumulation in GM1. Administration of AAV9 intravenously in GM1 mice restored enzymatic activity and extended survival significantly [184]. Broad transduction of numerous cell and tissue types is not restricted to mice. For example, intravenous (IV) injection of an AAV9-GFP construct in nonhuman primates led to the transduction of neurons, glial cells, and motor neurons in the spinal cord, as well as skeletal muscles and peripheral organs[185, 186]. Thus, with the goal of developing a minimally invasive treatment, and the promise of AAV in numerous species, the current study injected GM1 cats intravenously with AAV9 gene therapy as a test of scale-up and potential efficacy in human clinical trials.

Results

Clinical data

The objective of this study was to determine the efficacy of an AAV9 vector expressing feline βgal in correcting neurological and biochemical symptoms of cats with GM1 after a single

intravenous injection. Six animals were injected at approximately 1.3 months of age (Table 1). They were divided into two cohorts; the short-term group was necropsied at 5.1 ± 0.1 months of age (16-weeks post treatment) and the long-term group was followed to humane endpoint. Neurological symptoms were tracked with a 10 point clinical rating score (CRS), detailed in the material and methods section. Untreated animals progress through disease symptoms, which include hind limb weakness, ataxia, and body tremors, to humane endpoint at approximately 8 months of age. In the short-term cohort, 3 of the 4 animals had no clinical symptoms by the pre-determined endpoint at approximately 5 months of age. One short-term animal had hind limb weakness, the first sign of clinical disease (Table 1). In comparison, untreated GM1 cats at approximately 5 months of age exhibit hind limb weakness, wide stance, ataxia, and overt body tremors. Both animals in the long-term cohort exhibited a mild hind limb weakness and slight wide based stance from approximately 3 months of age until euthanasia at 42.1 ± 1.8 months of age (Figure 1A). Long-term animals were humanely euthanized due to weight loss or related symptoms such as pancreatitis, rather than the typical neurological endpoint of this model. The long-term cohort lived an average of 5.3 ± 0.23 times longer than untreated GM1 animals (Figure 1B).

MRI/MRS

Brain architecture was evaluated using an ultra-high field (7 Tesla) T2 weighted MRI (Figure 2A). In untreated GM1 animals at or near humane endpoint, the gray and white matter were isointense (of the same degree of darkness), due to demyelination in the white matter and increased GM1 storage in gray matter in both the cerebral cortex and cerebellum. Additionally, there was an increase in CSF surrounding the brain and within the ventricles due to cortical atrophy. Sixteen weeks after IV injection of GM1 cats (5 months of age), white matter remained

hypointense to gray matter, as in normal cats, in both the cerebral cortex and cerebellum. There was a minor increase in CSF (brain atrophy) in the short-term cohort. Two years post IV injection, the gray-white matter boundaries of GM1 cats maintained a normal appearance.

MR spectroscopy of the parietal cortex, thalamus, corona radiata, temporal lobe, occipital cortex, and cerebellum corroborated the MRI images showing demyelination[187] in untreated GM1 animals. Commonly used as indicators of demyelination, glycerophosphocholine (GPC) and phosphocholine (PCh) increase with cell turnover due to their role in membrane synthesis and degradation[134]. In all voxels of untreated GM1 animals, GPC+PCh increased with disease progression (Figure 2B). IV treatment decreased the levels of GPC+PCh in both the short-term and long-term cohorts. Significant normalization of GPC+PCh levels in treated GM1 animals was apparent in the corona radiata, occipital cortex, and cerebellum of the long-term animals and solely in the cerebellum of short-term animals. Mean levels of GPC+PCh in all treated cats were untreated levels cats in almost every voxel.

Additional metabolites studied included myoinositol (glial marker[135]), N-acetyl aspartate with N-acetyl aspartyl glutamate (neuronal marker[136]), creatine with phosphocreatine (metabolism markers[137]), and glutamate with its precursor glutamine (neurotransmitter[138]) (Supplemental figure 1, A-D). By humane endpoint in untreated GM1 cats, myoinositol in the thalamus, corona radiate, and cerebellum was significantly elevated (supplemental figure 1A). Treatment normalized myoinositol in these regions. Creatine with phosphocreatine were also elevated in endpoint GM1 animals (supplemental figure 1C). IV gene therapy normalized both metabolites in the cerebellum in short-term and long-term cohorts. N-acetyl aspartate and N-acetyl aspartyl glutamate (supplemental figure 1B) demonstrated a significant decrease with age

in the cerebellum, which was partially normalized after treatment. No clear trend existed for glutamate with glutamine (supplemental figure 1D).

Biodistribution

Intravenous injection of AAV9 produced a broadly distributed increase of βgal activity throughout the entire central nervous system of cats in short-term and long-term cohorts (Figure 3). βgal activity was widely distributed through the brain (blocks A-I), including the thalamus and cerebellum, as shown by X-gal staining (Figure 3A). Normal or above normal enzyme activity was measured in the cerebellum (blocks H and I) of the long-term cohort. βgal activity in the brain of the long-term cohort ranged from 0.4-2.8 fold normal and in the short-term cohort ranged from 0.2-0.8 fold normal (Figure 3C). Similarly, βgal activity was present throughout the entire spinal cords of all treated animals and primarily localized in the gray matter (Figure 3B). βgal levels in the spinal cord ranged from 7.1 – 26.0 fold above normal in the long-term cohort and 1.2 – 1.6 fold above normal in the short-term cohort (Figure 3D). Although variability existed in both cohorts, all animals had similar changes in enzyme activity. Additionally, the high standard deviation in the short-term treatment group can be attributed to two animals having a lower overall activity, although relative βgal distribution was similar among all animals in the cohort.

Vector was well distributed throughout the brain in both the short-term and long-term cohorts (supplemental figure 2A). Similar levels of vector genomes were detected in each brain section within each cohort. AAV also was detected in the spinal cord at similar levels in both cohorts (supplemental figure 2B). In peripheral tissues of short-term cohort animals, the highest levels of vector were measured in heart, which had 4 times as much vector as liver and 41 times as much vector as spleen. In the long-term cohort animals, there was 6 times as much vector in

the heart as the liver and 16 times as much vector in the spleen (supplemental figure 2C). In comparison with the brain section having the highest vector content, the heart had 122 times more vector in the short- term cohort and 27 times as much vector in the long-term cohort. Additionally, relative to the spinal cord block with the highest vector content, there was 94 times more vector in the heart of the short-term cohort and 108 times more vector in the heart of the long-term cohort.

Ganglioside Content

GM1 ganglioside was measured in the parietal cortex, temporal lobe, thalamus, cerebellum, brainstem, and cervical intumescence of normal, treated, and untreated GM1 animals (Figure 4). Ganglioside levels in untreated GM1 cats were significantly elevated in all regions, ranging from 2.4 to 3.2 times normal. Sixteen weeks after treatment, mean GM1 ganglioside levels were reduced, with significant decreases to near-normal levels in the cerebellum and cervical intumescence of the spinal cord. The long-term cohort had significant decreases in GM1 ganglioside in all regions, with normalized levels in the parietal cortex, thalamus and cerebellum.

CSF Biomarkers

βgal activity in the CSF was elevated above untreated animals in both cohorts of treated animals (Figure 5A). βgal levels were 0.4 ± 0.1 fold of normal in the short-term cohort and 8.5 ± 6.4 fold above normal in the long-term cohort. CSF markers of cellular damage correlate with disease progression in GM1[125]. Aspartate aminotransferase (AST, Figure 5B) and lactate dehydrogenase (LDH, Figure 5C) were elevated in untreated GM1 animals. Both AST and LDH were normalized in two animals of the short-term cohort (9-1916 and 9-1933), but not in the other animals (9-1920 and 9-1925). Normalization of AST and LDH levels occurred in the short-

term animals with the highest levels of βgal activity in the CNS (Figure 3). The long-term cohort showed normal levels of AST and LDH approximately two years after treatment.

Histology

Untreated GM1 cats show widespread neurodegeneration in tissue sections. For example, neurons distended with foamy, vacuolated storage are prevalent in the thalamus, cerebellum (Purkinje cells), spinal cord, and numerous other sites of the CNS (Figure 6A). Additionally, no βgal activity is present in the CNS of untreated GM1 animals, as indicated by lack of blue staining with X-gal (pH 4.2-4.5). The short-term cohort showed diffuse, mildly expanded neurons throughout the CNS, with the majority of cells maintaining a near normal appearance. An impressive increase in βgal activity was present throughout the CNS, with particularly intense staining in thalamic neurons and Purkinje cells of the cerebellum. The CNS of the long-term cohort was largely normal in appearance, with limited regions enlarged by storage material, though not to the extent of the untreated animals. Moderate increases in X-gal staining were present throughout the CNS of the long-term animals. In general, areas of increased βgal activity overlapped with normalized histopathology (i.e., decreased storage).

IBA-1, a microglia marker, was increased throughout the brain of untreated GM1 animals, with statistical significance reached in the thalamus, cerebellar folia, deep cerebellar nuclei (DCN), and brainstem (Figure 6B). Both treatment cohorts trended toward normalization throughout the brain, with significance reached in the parietal cortex, cerebellar folia, and DCN of the short-term cohort. GFAP, an astrocyte marker, was elevated in all brain regions in untreated GM1 animals (Figure 6C). In the short-term cohort, there was a significant decrease in GFAP staining compared to untreated GM1 animals in the parietal cortex, thalamus, hippocampus, temporal lobe, occipital cortex, cerebellar folia, and DCN. The long-term cohort

had significantly less GFAP staining in the parietal cortex, cerebellar folia, DCN, and brainstem in comparison to untreated animals. Images of these stains can be found in supplemental Figure 3.

Peripheral Disease

Since storage also occurs outside of the CNS in GM1, it is imperative to also assess the status of peripheral tissues when determining efficacy of treatment. Normal levels of βgal activity were achieved in the sciatic nerve, heart, skeletal muscle, and pituitary gland of both treated cohorts (Figure 7A). In the long-term cohort, βgal activity was normalized in liver, spleen, and adrenal gland. In untreated GM1 cats, hepatocytes were markedly expanded by enlarged, finely vacuolated foamy cytoplasm (Figure 7B). Two cats of the short-term cohort (9-1916, shown, and 9-1933) had normal hepatocyte morphology with no storage, and the other two (9-1920 and 9-1925) had hepatocytes with mild evidence of storage. Liver histology was largely normal in both cats of the long-term treatment group, with only scant numbers of hepatocytes showing slight cytoplasmic vacuoles.

In addition to GM1 ganglioside, glycosaminoglycans (GAGs) are cleaved by βgal and are subsequently excreted in the urine. Untreated GM1 cats have significantly elevated amounts of urinary GAGs [125] (Figure 7C), while GAG levels were significantly normalized in the long-term cohort. The short-term cohort displayed significantly elevated GAG levels, despite their improved phenotype. The reason for increased urinary GAG levels in GM1 cats treated for 16 weeks is yet to be determined.

Discussion

Numerous preclinical and clinical studies have demonstrated the safety and efficacy of AAV gene therapy, and the U.S. Food & Drug Administration recently approved the first AAV vectors to treat *RPE65*-related blindness (Leber's congenital amaurosis)[66] and spinal muscular atrophy[67]. Retinal pathology caused by *RPE65* deficiency is corrected by a direct injection of the approved AAV2 vector and spinal muscular atrophy is corrected by systemic administration of AAV9. Similarly, in previous studies, we showed that direct injection of the brain with AAV1 or AAVrh8 vectors produced profound, long-term correction of GM1 biochemically[114, 125] and clinically. While untreated GM1 cats lived to 8.0 ± 0.6 months of age, those treated by intracranial AAV injection have survived an average of 5.2 years, with two treated cats still alive at ~ 9 years of age. The efficacy of intracranial AAV treatment in the feline GM1 model is clear. Even so, a less invasive method of treating children with severe brain disease is needed.

The efficient, selective blockade that the blood brain barrier poses was a major obstacle to the treatment of CNS disorders by intravascular routes, until certain brain-penetrant AAV variants, such as AAV9, were reported[176-178]. In addition to minimizing invasiveness, intravenous injection of appropriate serotypes uses the extensive vasculature of the brain as a near-global distribution network. For example, each brain neuron is estimated to be within a few microns of a capillary[175], providing a built-in means of treating neurologic disorders through the bloodstream. The current study demonstrated the efficacy of intravenous delivery of AAV9 in a feline model of GM1 gangliosidosis. The widespread CNS deterioration of feline GM1 results in the inability to walk (humane endpoint) at approximately 8 months of age. Systemic infusion of AAV9 encoding feline βgal changed the course of disease progression in all treated animals, which had mild hind limb weakness and a slightly wide based stance but did not progress to

more severe neurological symptoms even at ~3.5 years of age. Clinical efficacy was similar to our previous study of GM1 cats treated intracranially with AAV1 or AAVrh8 vectors[114, 125]. Though intracranial injection led to a mean survival that was 48.6% longer than in the current study, IV-treated cats lived substantially longer than, or equivalent to, 4 of the 10 cats treated intracranially (1.4, 2.1, 3.0 and 3.8 years).

MRI showed degradation of the brain architecture in untreated GM1 animals, similar to what has been previously reported in GM1 cats[125] and human patients[188, 189]. AAV-treated animals maintained normal relative intensities of the gray matter and white matter. Additionally, atrophy in both the short-term and long-term groups was minimal. The normalization of choline metabolites, such as GPC+PCh, is likely to indicate preservation of myelin integrity[134] and agrees with the maintenance of normal white matter appearance on anatomical MRI scans. GPC+PCh levels were normalized in many brain regions of AAV-treated cats, particularly in the corona radiata, occipital cortex, and cerebellum. Additional biomarkers of disease progression, such as AST and LDH levels in the CSF[125] were normalized in the long-term cohort but not in the short-term cohort. While there was large disparity of AST and LDH levels as well as in urine GAG levels in the short-term cohort, it is possible that complete normalization requires longer than the pre-determined 16 week follow-up for this group.

The widespread distribution of βgal activity throughout the CNS was the desired outcome of intravenous delivery, which is now possible due to a new generation of brain penetrating capsids and has advantages compared to other delivery routes. Both CSF and intracranial injections are relatively invasive compared to intravenous delivery. While the CSF circulatory system is reported to be an effective medium for AAV transduction[148-150], delivery of AAV in the CSF often results in transduction of superficial cortical layers only, rather than the whole

tissue[186]. Intra-parenchymal injections can lead to high levels of transduction and gene expression immediately surrounding the injection site[151, 152], which may cause neurotoxicity[153]. Although high levels of βgal activity were noted in the IV treated animals, particularly in the spinal cord, no evidence of toxicity was noted in neurological assessment or histologically. βgal activity was distributed throughout the periphery, an important consideration for whole-body protein deficiencies such as storage diseases and thus another advantage of the intravenous approach.

Another important finding of the current study is the degree of βgal restoration in CNS neurons after systemic delivery of the AAV9 vector. While intravenous delivery of AAV9 beyond the neonatal period is reported to transduce brain glia primarily[177], neurons of the thalamus, cerebellum, and other regions expressed high levels of βgal. Cats were treated at 1.2 – 1.5 months of age, a time at which the blood brain barrier is intact, at least by measuring the quotient of albumin in the CSF versus serum. The albumin quotient (Q_A) is a standard method for determining blood brain barrier integrity[190] and reaches adult levels in cats between 0.9 – 1.4 months of age (unpublished data). Dye exclusion studies in cats suggested that the blood brain barrier is functionally intact well before 1 month of age, at least for trypan blue[191]. It is possible that the blood brain barrier at this age did not exclude small particles such as AAV vectors (~25 nm diameter) and/or that GM1 pathology in affected cats influenced permeability. Nevertheless, systemic delivery of AAV9 in this study effectively treated neurons in deep brain structures such as the thalamus, an advantage over CSF delivery routes published to date.

Though some studies report superior overall transduction of the brain with CSF versus systemic delivery, the intravenous route may produce equivalent or better clinical effect. For example, dogs with mucopolysaccharidosis (MPS) VII were treated with similar doses of AAV9

intravenously or via the cisterna magna. Though CSF delivery produced higher activity of the missing lysosomal enzyme throughout the brain, gait function after systemic treatment was equivalent to, or better than that of CSF delivery[192]. In the current study, treated GM1 animals did not have a normal lifespan but survived 5.2 times longer than untreated cats, with a vastly improved quality of life. In fact, GM1 cats in the long-term cohort had near-normal neuromuscular function as assessed by our clinical rating scale. Their demise ultimately was caused by weight loss. Weight loss may have been due to an intermittent pancreatitis, which may not be related to gangliosidosis because it occurs in normal members of the feline research colony. Weight loss also may have been related to accumulation of GM1 and its related asialo-derivative (GA1) in the digestive tract. GA1 acts as a receptor for various gut bacteria and is suggested to be responsible for the excretion of bacterial flora from the gastrointestinal tract in mice[193]. GA1 is shown to be increased in the brains of GM1 patients[122] as well as in brain, liver, spleen, and kidney of GM1 mice[194]. This increase of GA1 could facilitate the binding of and increased turnover of intestinal bacteria. Additionally, *E. coli* heat labile toxin utilizes GM1 as a receptor on the enterocyte membrane to gain entry into the intestinal epithelia where it results in increased secretion of serotonin resulting in diarrhea[195]. This uptake correspondingly increases with higher levels of GM1[196]. Increased levels of both GM1 and GA1 could disrupt the intestinal microbiota, which has been shown to cause weight loss[197].

In summary, intravenous delivery of AAV9 expressing feline βgal dramatically improved quality and length of life in GM1 cats. βgal distribution was widespread throughout the central nervous system and peripheral organs, reaching normal levels in the cerebellum, spinal cord, heart, liver, spleen, and skeletal muscle. We also observed reduced accumulation of GM1 in the CNS. No indications of treatment toxicity were apparent clinically or histologically. The simple

intravenous injection is substantially less invasive than intracranial or CSF delivery and ultimately will be possible as an outpatient procedure. Taken together, this data supports the use of AAV9 via intravenous delivery for the treatment of GM1 gangliosidosis and these data supported an IND for the first human clinical trial for GM1, which is ongoing (https://clinicaltrials.gov/ Identifier NCT03952637).

Materials and Methods

Vectors

The AAV backbone expressing feline βgal was previously described[114] and contained a hybrid CBA promoter, including the CMV immediate-early enhancer fused to the chicken β-actin promoter[198]. The woodchuck hepatitis virus post-transcriptional regulatory element (WPRE) was included for enhancement of gene expression. The vector was produced by triple transfection of 293T cells with the helper plasmid (Fd6)[158], the plasmid expressing AAV9 capsid (pAR-9)[199], and the plasmid containing the feline βgal expression unit, and purified using an iodixanol density gradient.

Animals and injection procedure

All animal procedures were approved by the Auburn University Institutional Animal Care and Use Committee. Treatment groups for this study are detailed in Table 1. Cats diagnosed with GM1 gangliosidosis were treated with an AAV9 vector expressing feline βgal at a total dose of 1.5E13 vector genomes/kg body weight. Treatment was administered to unsedated animals at 1.3 ± 0.1 months of age and ~0.5 kg body weight via a cephalic vein catheter. Injection rate was 0.3 mL/min. Vector injection was followed by approximately 0.5 mL saline flush.

Animals were clinically assessed every two weeks using a 10 point clinical rating score. One point was subtracted from a normal score of 10 for each acquired symptom: hind limb weakness, wide based stance, ataxia, instability, inability to walk more than a few steps, tremors, spastic limbs, and ability to stand but not walk.

Animals were evaluated for 16 weeks post treatment (short-term) or until humane endpoint (long-term), defined as the inability to stand. The brain was divided into 6mm coronal blocks with the right hemisphere and select peripheral tissues preserved in optimal cutting temperature (OCT) medium. All other tissues were flash frozen in liquid nitrogen and stored at -80°C or were formalin-fixed.

MRI/MRS

Animals were fully anesthetized for MRI using a combination of intravenous ketamine (10 mg/kg) and dexmedetomidine (0.04mg/kg) and anesthesia was maintained using isoflurane. MRI and MRS data were acquired on a 7 Tesla MAGNETOM scanner (Siemens Healthcare, Erlangen, Germany). A 32-channel head coil (Nova Medical, Boston, MA) was used for all scans. Anatomical coronal images were acquired using 3D MPRAGE (Magnetization-PRepared RApid Gradient Echo) with 0.5mm isotropic resolution and TR/TE of 1910/2.5ms, followed by 2D axial T2 turbo spin echo (TSE) images with TR/TE of 5450/12ms and a resolution of (0.25x0.25x1) mm. Single voxel spectroscopy (SVS) was then acquired using a PRESS (Point Resolved Spectroscopy) sequence optimized for 7T with TE/TR = 30/5000 ms, 64 averages and a Variable Pulse power and Optimized Relaxation Delays (VAPOR) water suppression. Shimming was performed using FASTESTMAP followed by manual shimming if needed. The resulting full width half max (FWHM) of unsuppressed water was typically 16Hz. Optimization of RF pulse amplitudes and of the water suppression scheme was performed prior to acquiring

each spectrum. The unsuppressed water signal was obtained and used for eddy current correction and for quantification of metabolites. Using high resolution 3D MRI images, voxels were positioned in the thalamus (7x6x8mm), parietal cortex (7x6x8mm) and cerebellum (7x7x8mm). MRI data were analyzed with EFilm 3.2 software (Merge Healthcare, Chicago). MRS data were processed with LC model and internal water scaling (http://www.s-provencher.com/pages/lcmodel.shtml).

Lysosomal enzyme activity

Lysosomal enzymes were isolated from CNS tissues with 3-6 sections (40 µM) cut from coronal blocks stored in OCT. For peripheral tissues, 50-70 mg was taken from the flash frozen samples. Tissues were homogenized manually in 500 µL of 50 mM citrate phosphate buffer, pH 4.4 (50 mM citric acid, 50 mM Na_2HPO_4, 10 mM NaCl) containing 0.1% Trition X-100 and 0.05% BSA, followed by two freeze-thaw cycles in liquid nitrogen and centrifugation at 15,700 x g for 5 minutes at 4°C. The activity of β-galactosidase was measured using synthetic fluorogenic substrates as previously described[179]. CSF samples were analyzed for βgal activity using 30µL of sample and 10µL of substrate and incubated at 37°C for one hour. Specific activity was expressed as nmol 4MU cleaved/mg protein/hour after normalization to protein concentration determined by Lowry method.

Distribution of βgal activity was determined via histochemical staining as previously described[114].

Ganglioside Content

As described in greater detail previously[200], total lipids were extracted with chloroform (CHCl3) and methanol (MeOH) 1:1 by volume and purified from the lyophilized brain tissue[201-203]. Neutral and acidic lipids were separated using DEAE-Sephadex (A-25; Pharmacia Biotech,

Uppsala, Sweden) column chromatography[204]. The total lipid extract was applied to a DEAE-Sephadex column after suspension in solvent A (CHCl3:CH3OH:dH20, 30:60:8 by volume), which also was used to collect the neutral lipid fraction. Acidic lipids were eluted from the column with CHCl3:CH3OH:0.8 mol/l Na acetate (30:60:8 by volume), dried by rotary evaporation, and then partitioned so that acidic lipids were in the lower organic phase and gangliosides were in the upper aqueous phase[205-207]. The resorcinol assay was used to measure the amount of sialic acid in the ganglioside fraction, which then was further purified with base treatment and desalting. Neutral lipids were dried by rotary evaporation and resuspended in CHCl3:CH3OH (2:1 by volume). Gangliosides were analyzed qualitatively by HPTLC and quantitated as previously described[200, 203]. Total brain ganglioside distribution was normalized to 100% and the percentage distribution was used to calculate sialic acid concentration of individual gangliosides[202].

Biomarker analysis

Cats were sedated using dexmedetomidine (0.04mg/kg) for CSF collection and as needed for blood collection. Blood was collected from the jugular vein and CSF was collected from the cerebellomedullary cistern. CSF Samples underwent one freeze-thaw cycle prior to being analyzed for aspartate aminotransferase (AST) and lactate dehydrogenase (LDH) concentration using a Cobas C311 chemistry analyzer (Roche Hitachi, Basel, Switzerland & Tokyo, Japan).

Histopathology

Paraffin embedded tissue sections (4 μm) were stained with H&E on a Autostainer XL (Leica, Bufflo Grove, IL USA) and with GFAP (undiluted, Dako, Carpinteria, CA, USA) and IBA-1 (1:750 dilution, Biocare Medical, Concord, CA, USA) on a Autostainer Link 48 system (Dako), using an Envison Flex kit (Dako). After staining, the IBA-1 and GFAP slides were

scanned using Leica Scanscope at 40x and analyzed using algorithms developed in house on Visiopharm software (Broomfield, CO, USA).

Urine GAGs

Glycosaminoglycans (GAGs) in the urine were measured as previously described[125] in normal cats, GM1 untreated cats at approximately 8 months of age (humane endpoint), and both cohorts of treated GM1 cats. Data is represented as μg GAG/ mg protein/ dL urine.

Statistics

Statistical analyses were performed using Prism (Graphpad, La Jolla, CA USA) and Microsoft Excel (Microsoft, Redman, WA USA). Brown-Forsythe and Welch one-way ANOVA tests were used to compare all groups for statistical significance. For MRS, only spectra with Cramér-Rao minimum variance bounds of <30 were included in the analyses.

Tables and Figures

Table 1. Intravenous treatment of GM1 cats with AAV9

Group	Cat	Gender	Treatment age (months)	Treatment weight (kg)	Necropsy age (months)	CRS at necropsy
Short term	9-1916	F	1.5	0.5	5.3	10.0
	9-1920	F	1.3	0.4	5.0	10.0
	9-1925	M	1.3	0.5	5.0	10.0
	9-1933	M	1.4	0.6	5.1	9.0
Mean ± s.d.			**1.4 ± 0.1**	**0.5 ± 0.1**	**5.1 ± 0.1**	**9.8 ± 0.4**
Long term	8-1714	M	1.2	0.6	43.9	8.5
	8-1716	F	1.2	0.5	40.3	8.5
Mean ± s.d.			**1.2 ± 0.0**	**0.5 ± 0.0**	**42.1 ± 1.8**	**8.5 ± 0**

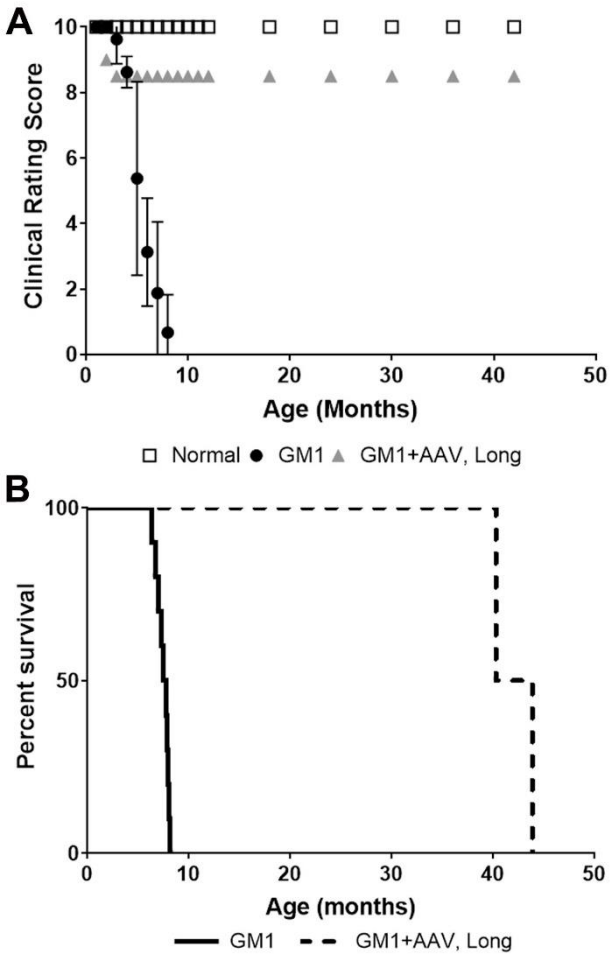

Figure 1. Clinical therapeutic effect. A. Untreated GM1 animals (black, circles) show a rapid drop in clinical rating score, with the lowest scores reached at approximately 8 months of age. The long-term cohort (GM1+AAV, Long; gray, triangles) shows an initial drop in clinical rating score to 8.5, indicating only mild disease progression which remained stable for ~3 years. B. Kaplan Meier curve showing untreated GM1 animals (solid line) survived 8.0 ± 0.6 months, while the long-term cohort (GM1+AAV,Long; dashed line) survived 42.1 ± 1.8 months ($p=0.0215$).

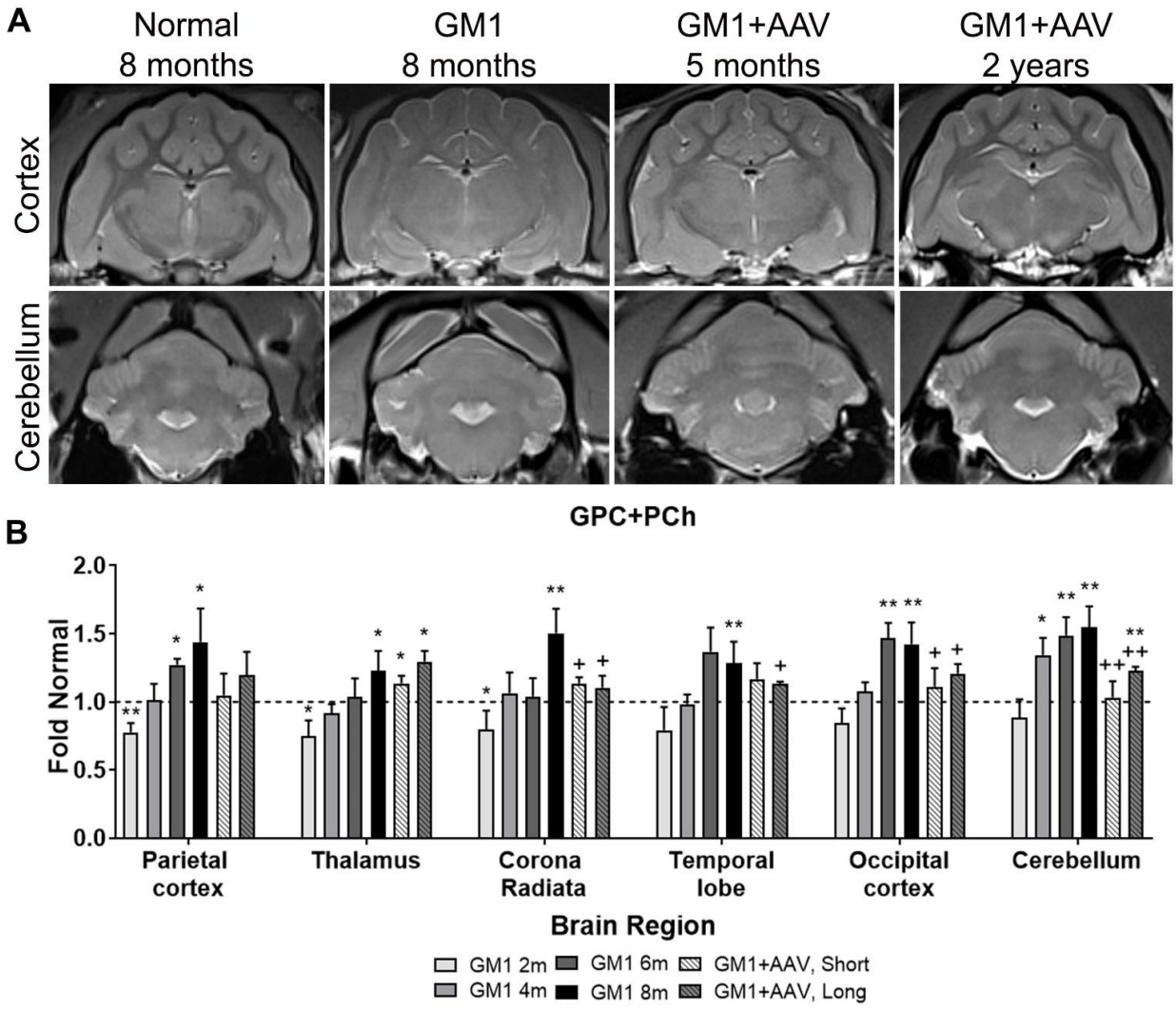

Figure 2. MRI and MRS evaluation of GM1+AAV animals. A. In normal cats, white matter is hypointense to gray matter on T2-weighted images. Untreated GM1 animals have isointense gray and white matter, with atrophy indicated by increased CSF (bright white) around and within the brain. At both time points (5 months and 2 years), treated animals had normalized gray:white matter intensities and minimal changes to CSF levels. B. Glycerophosphocholine and phosphocholine (GPC+PCh) was measured via MRS in 6 voxels: parietal cortex (PC), thalamus (TH), corona radiata (CR), temporal lobe (TL), occipital cortex (OCC), and cerebellum (CB). Scans were performed at 2, 4, 6 and 8 months of age in untreated GM1 cats, 5 months in the

short-term cohort (GM1+AAV, Short), and 2 years in the long-term group (GM1+AAV, Long). Measurements are standardized to the appropriate age-matched normal controls and are represented as fold normal ± S.D. *$p<0.05$ and **$p<0.005$ versus age-matched normal and + $p<0.05$ and ++ $p<0.005$ versus age-matched untreated GM1.

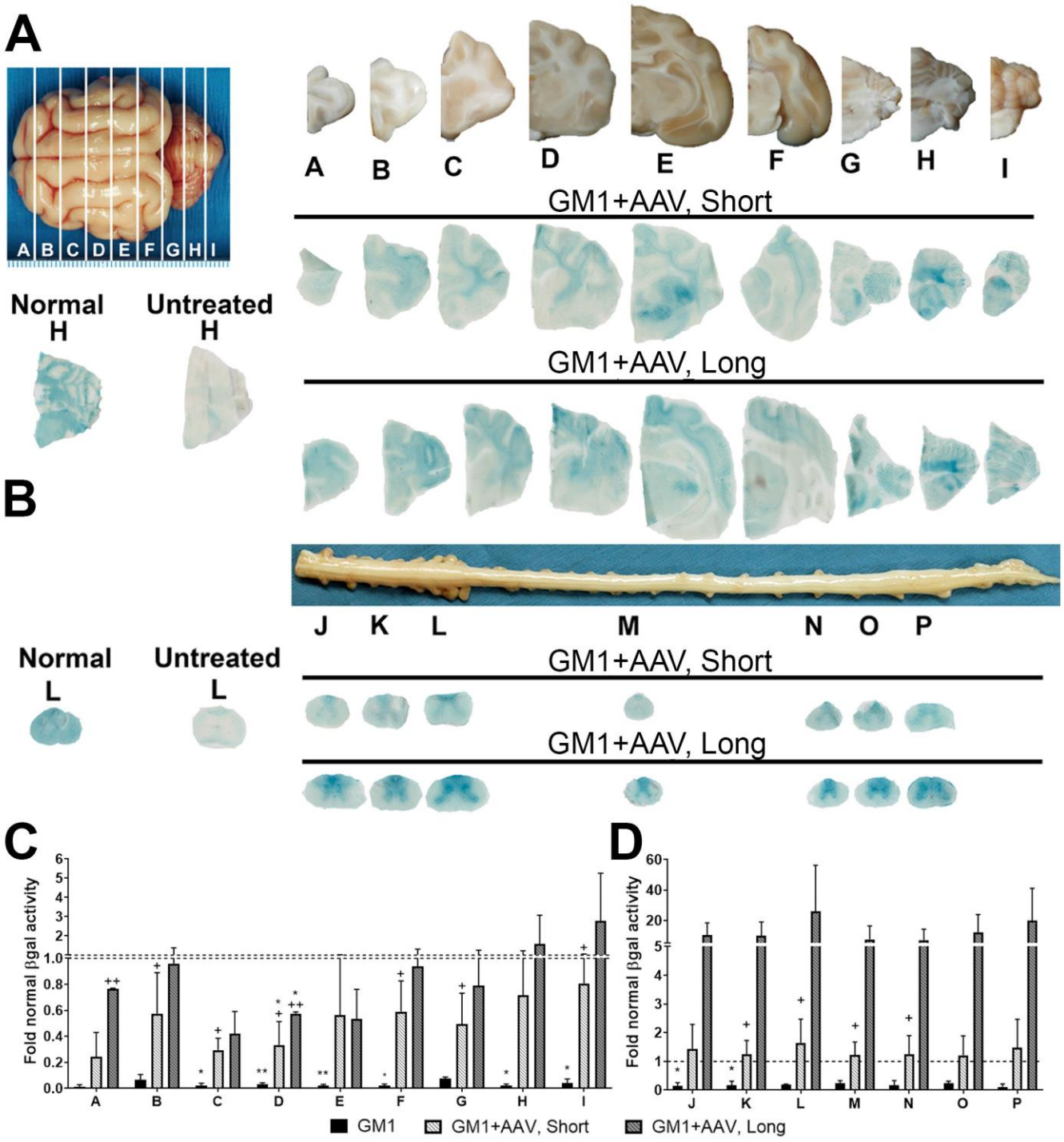

Figure 3. Activity and biodistribution of βgal in GM1+AAV animals. A. Top left, gross image of the feline brain with letters indicating the 6mm blocks used in analysis; Top right, gross images of the right hemisphere of each brain block, which was used for measuring βgal activity

and distribution in treated cats (blue stain). Also shown are untreated normal and GM1 controls. B. Regions of the spinal cord tested for βgal activity. βgal activity in homogenate from each brain block (C) and spinal cord segment (D) expressed as fold of normal activity. Error bars represent standard deviation. Graphs show activity from untreated GM1 animals at humane endpoint (GM1), the short-term cohort (GM1+AAV, Short), and the long-term cohort (GM1+AAV, Long). Dashed horizontal line represents normal activity. *$p<0.05$ versus normal cats and +$p<0.05$ versus untreated GM1 cats.

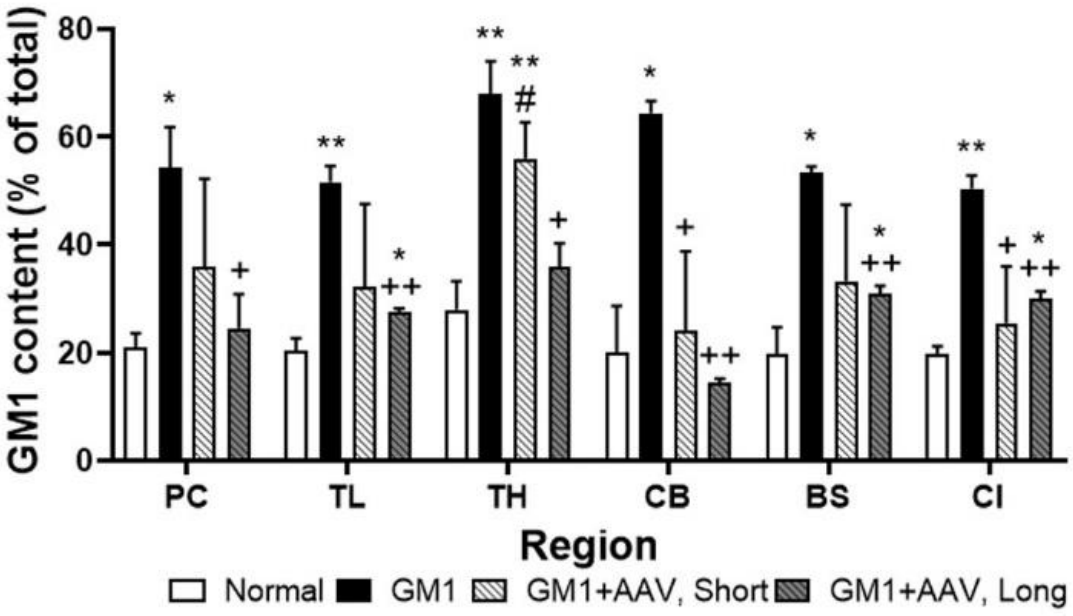

Figure 4. GM1 ganglioside content. GM1 ganglioside content in the CNS of normal, treated and untreated GM1 animals. Data was determined from densitometric scanning of HPTLC plates and is shown as a percentage of total ganglioside content. Data is represented as mean ± S.D. (error bars). PC, parietal cortex; TL, temporal lobe; TH, thalamus; CB, cerebellum; BS, brainstem; CI, cervical intumescence of spinal cord. *$p<0.05$, **<0.005 versus normal; +$p<0.05$, ++ $p<0.005$ versus untreated GM1; and #$p<0.05$ versus GM1+AAV, Long.

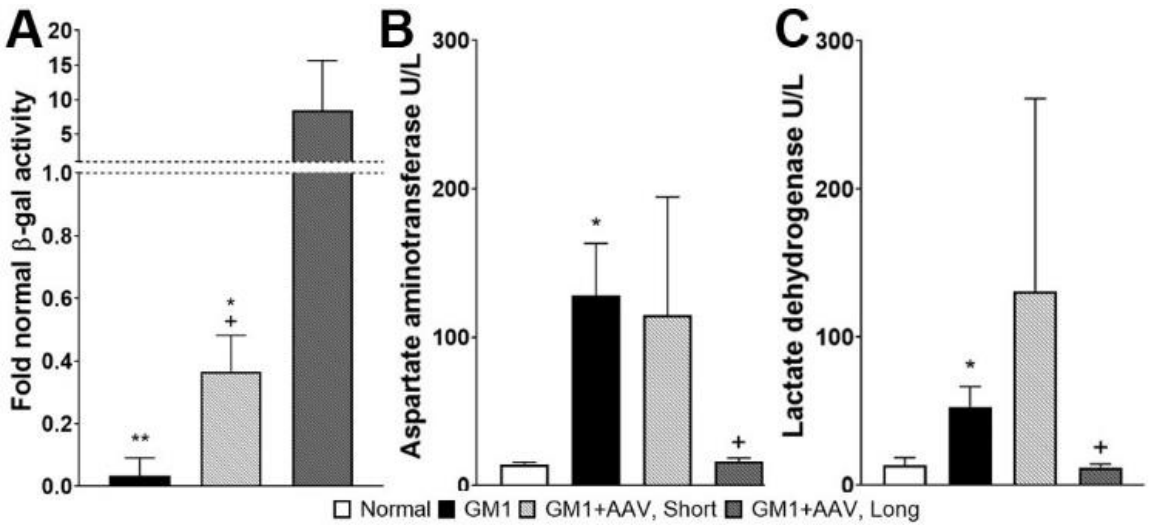

Figure 5. CSF biomarkers. A. βgal activity in CSF of untreated animals (GM1), the short-term cohort (GM1+AAV, Short) and the long-term cohort (GM1+AAV, Long). Data is represented as mean fold normal activity and the dotted line at 1 indicates normal activity. Mean CSF biomarker levels for aspartate aminotransferase (AST, B) and lactate dehydrogenase (LDH, C) in normal, untreated GM1, and treated GM1 animals. Error bars represent standard deviation. *p<0.05 and **p<0.005 versus normal; +p<0.05 versus untreated GM1 animals.

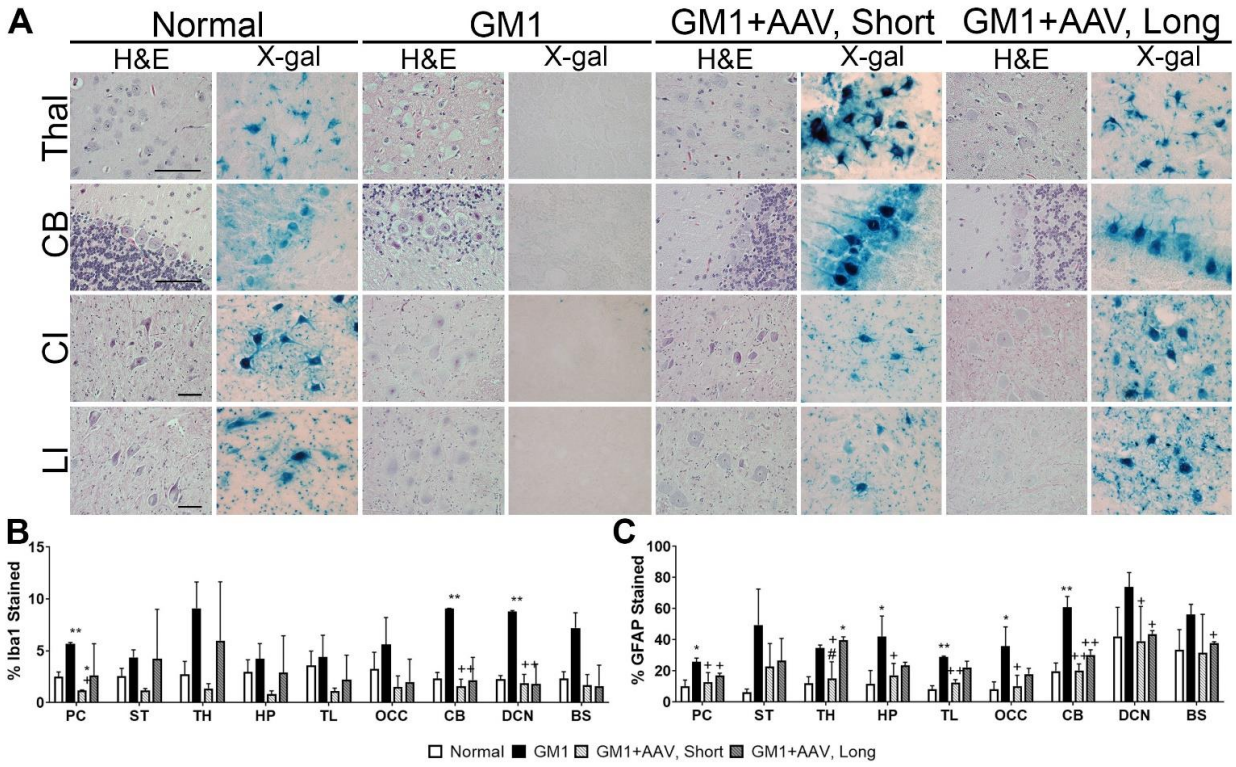

Figure 6. Normalization of histopathology. A. GM1 cats had pronounced neuronal pathology in the thalamus (Thal), cerebellar folia (CB), cervical intumescence (CI) and lumbar intumescence (LI) of the spinal cord. Neuronal morphology was normalized in both the short-term (GM1+AAV, Short) and long-term (GM1+AAV, Long) cohorts. After staining with X-gal, βgal activity (blue) was seen in similar cell populations of the treated animals and normal animals. For Thal and CB, images were taken at 20X magnification and scale bars represent 100um. CI and LI images were taken at 40x magnification and scale bars are 50um. Slides stained with IBA-1 (B) and GFAP (C) were quantified for % area stained in the parietal cortex (PC), striatum (ST), thalamus (TH), hippocampus (HP), temporal lobe (TL), occipital cortex (OCC), cerebellum (CB), deep cerebellar nuclei (DCN), and brainstem (BS). See also Figure S3 for representative images. Data are represented as mean ± S.D. *$p<0.05$ versus normal and +$p<0.05$ versus untreated GM1.

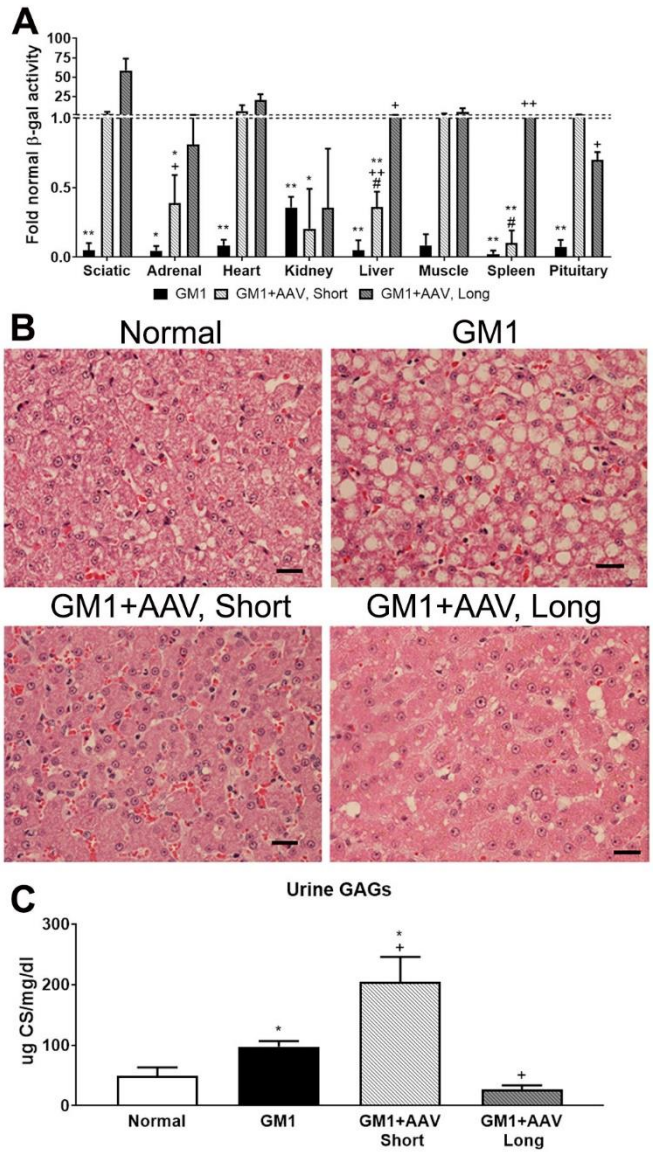

Figure 7. Evaluation of peripheral disease. A. βgal activity was measured in various peripheral organs in untreated (GM1), short-term treated (GM1+AAV, Short), and long-term treated (GM1+AAV, Long) animals. Data is represented as mean fold normal activity ± S.D. and the dotted line at 1 indicates normal activity. B. Representative images of livers stained with H&E, showing accumulation of lipid storage in the cytoplasm of untreated GM1 animals. After treatment, the livers appear normalized. C. Concentration of urinary glycosaminoglycans (GAGs) were determined using a colorimetric assay. Results are represented as mean ± S.D. and

μg of GAG per mg of creatinine /dL of urine. *$p<0.05$ versus normal and +$p<0.05$ versus untreated GM1.

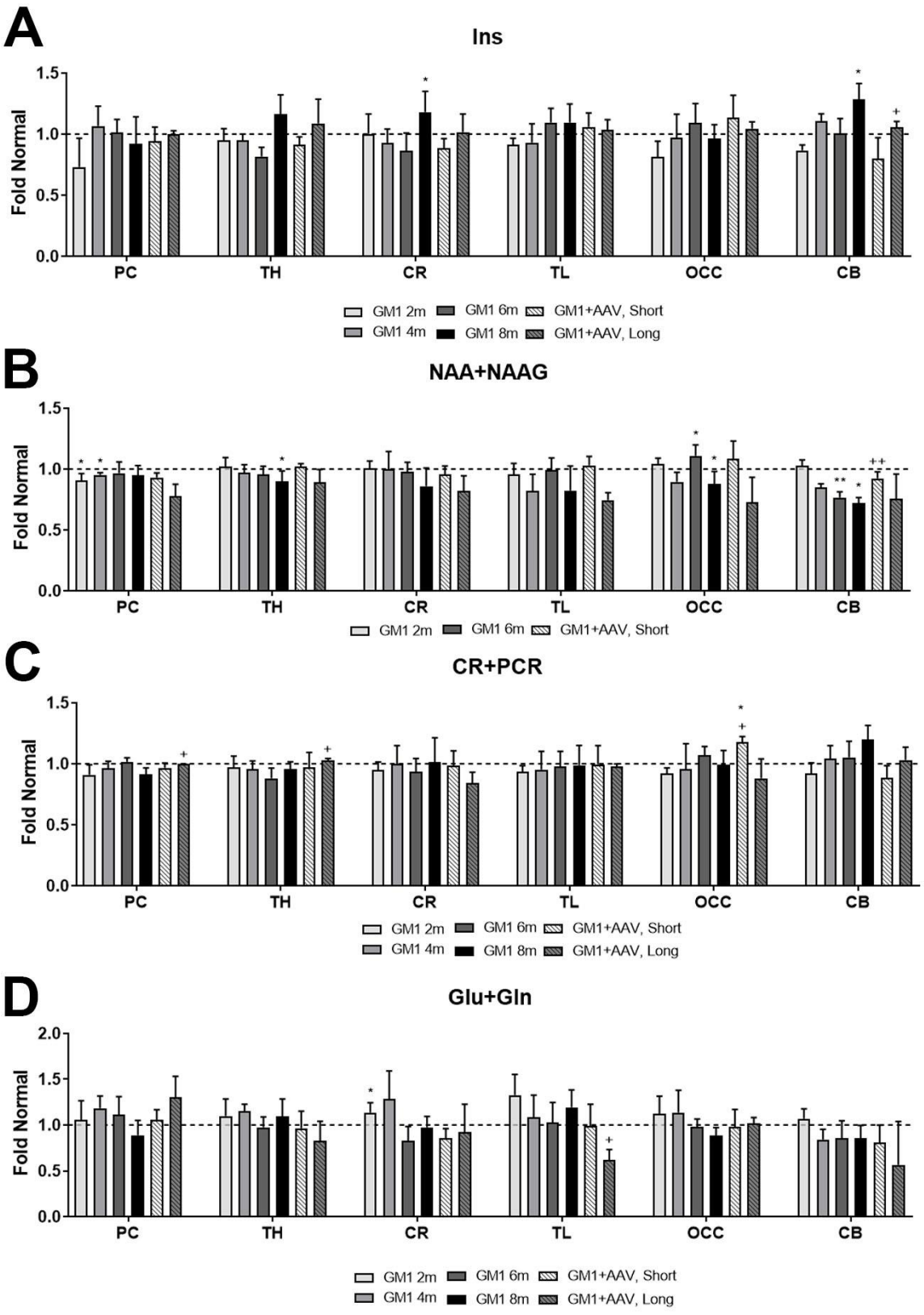
A
Ins
Fold Normal
1.5
1.0
0.5
0.0
PC
TH
CR
TL
OCC
CB
GM1 2m
GM1 4m
GM1 6m
GM1 8m
GM1+AAV, Short
GM1+AAV, Long
B
NAA+NAAG
Fold Normal
1.5
1.0
0.5
0.0
PC
TH
CR
TL
OCC
CB
GM1 2m
GM1 6m
GM1+AAV, Short
C
CR+PCR
Fold Normal
1.5
1.0
0.5
0.0
PC
TH
CR
TL
OCC
CB
GM1 2m
GM1 4m
GM1 6m
GM1 8m
GM1+AAV, Short
GM1+AAV, Long
D
Glu+Gln
Fold Normal
2.0
1.5
1.0
0.5
0.0
PC
TH
CR
TL
OCC
CB
GM1 2m
GM1 4m
GM1 6m
GM1 8m
GM1+AAV, Short
GM1+AAV, Long

Supplemental Figure 1. Additional MRS metabolites. Myoinositol (Ins, A), N-acetyl aspartate and N-acetyl aspartyl glutamate (NAA+NAAG, B), Creatine and phosphocreatine (CR+PCR, C), and Glutamate and Glutamine (Glu+Gln, D) were measured via MRS in 6 voxels: parietal cortex (PC), thalamus (TH), corona radiata (CR), temporal lobe (TL), occipital cortex (OCC), and cerebellum (CB). Scans were performed at 2, 4, 6 and 8 months of age in untreated GM1 cats, 5 months in the short-term cohort (GM1+AAV, Short), and 2 years in the long-term group (GM1+AAV, Long). Measurements are standardized to the appropriate age-matched normal controls and are represented as fold normal ± S.D. *$p<0.05$ and **$p<0.005$ versus age-matched normal and ++ $p<0.005$ versus age-matched untreated GM1.

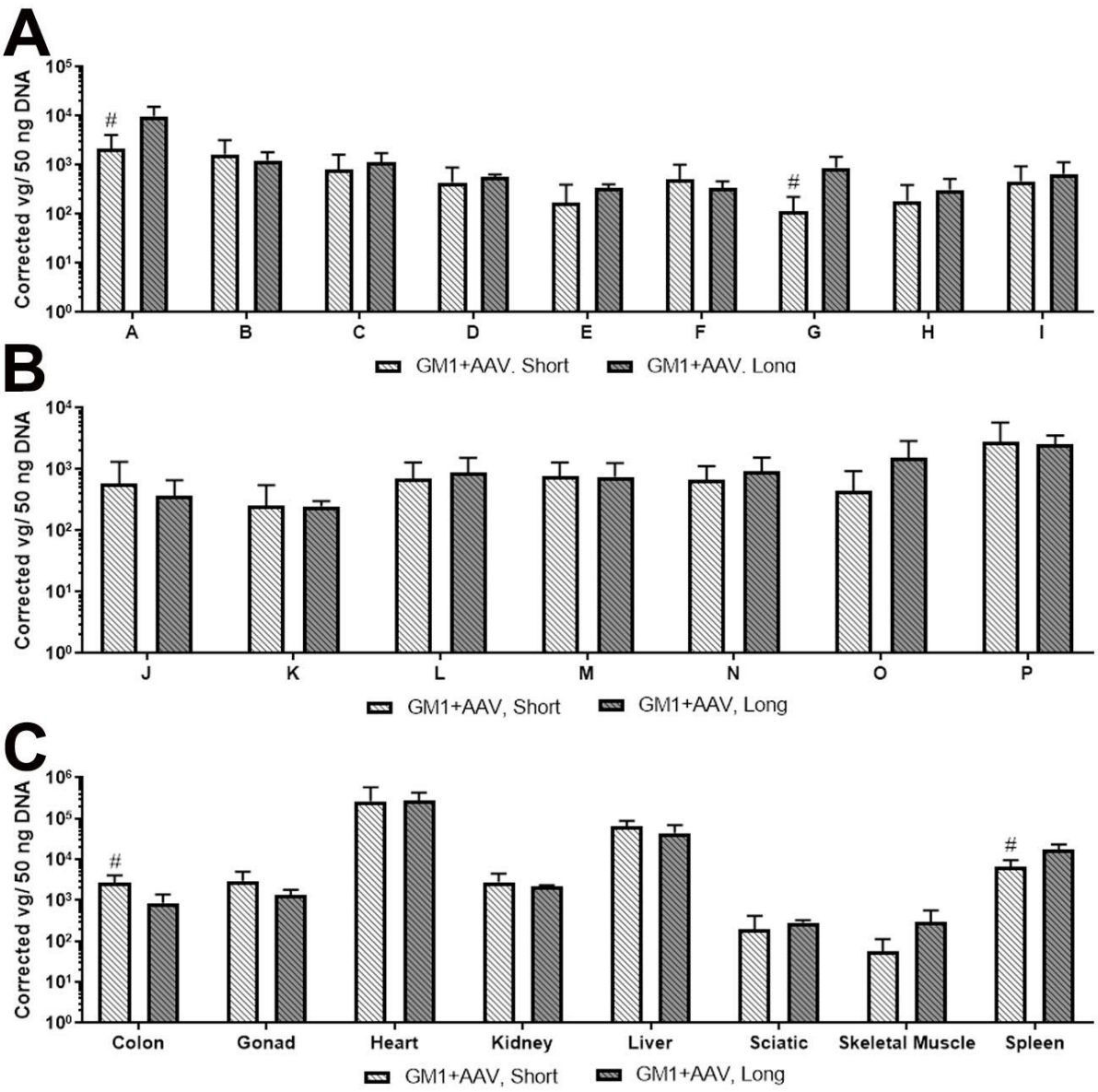

Supplemental Figure 2. Vector biodistribution. The biodistribution of AAV throughout the brain (A), spinal cord (B), and select peripheral tissues (C) was determined via qPCR for both treatment cohorts. Values are represented as a mean ± S.D. of vg/ 50 ng genomic DNA, with the background (untreated animal value) subtracted from each value. # $p<0.05$ versus GM1+AAV, Long.

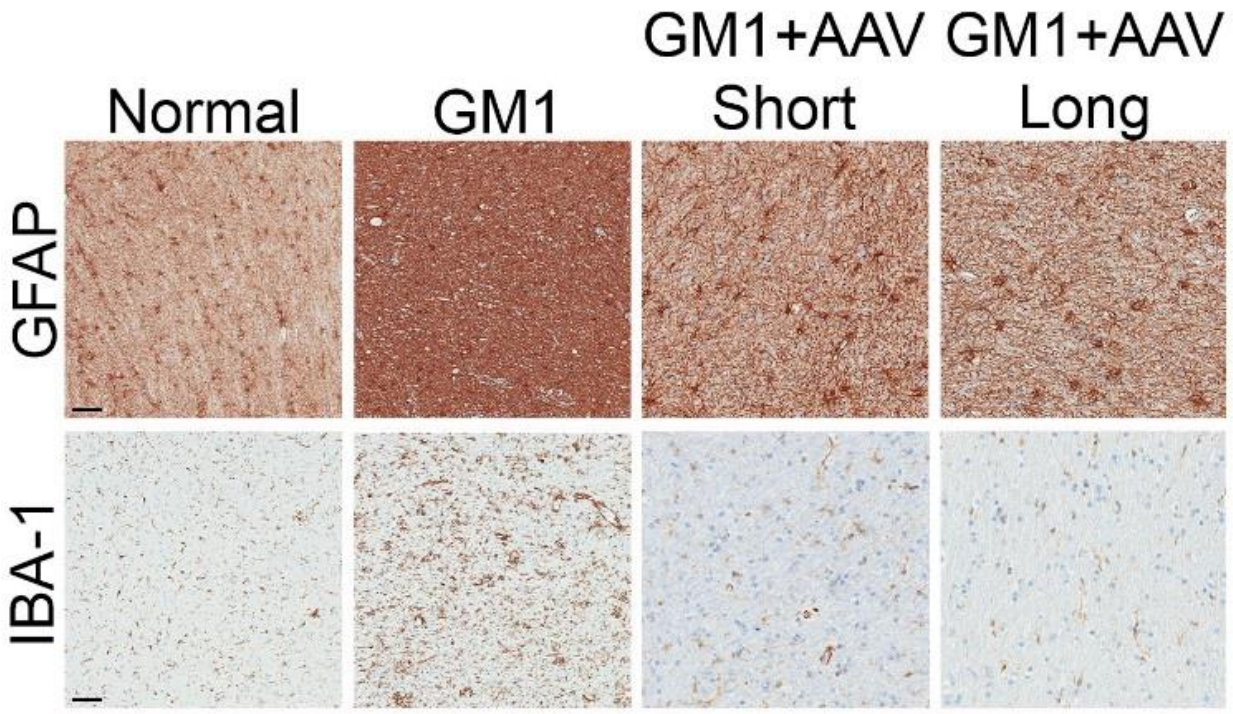

Supplemental Figure 3. Astrocytes and microglia in GM1 cats. Representative images of the cerebellum after staining for astrocytes (GFAP) and microglia (IBA-1).

Chapter 4

Summary and future directions

With several AAV therapies available for clinical use in the U.S. and in Europe[66-68], there is great potential for additional successful AAV gene therapies. The goals and outcomes for this project were two-fold. First, evaluate alternative routes of AAV administration for the treatment of GM1 gangliosidosis. Second, directly compare common variables in AAV production and treatment to elucidate any potential benefits or pitfalls. A comparison of the various studies can be found in Table 1.

For neurodegenerative diseases, invasive intracranial injections pose a substantial risk to patients. Though intraparenchymal injections have shown great efficacy for treating both the murine and feline models of GM1[114, 116], a less invasive treatment than the previously studied bilateral injection of the thalamus and deep cerebellar nuclei is needed for young children with active neurological symptoms. In Chapter one, GM1 animals were injected bilaterally in the thalamus and in the left lateral ventricle. This treatment removes the direct injection of the cerebellum, rather relying on the CSF to deliver AAV throughout the central nervous system. Overall, there was a significant increase in lifespan and quality of life in the treated animals in comparison to untreated animals; however the results were not as robust as with the thalamus and deep cerebellar nuclei injections[114]. As expected, the CSF delivery enabled βgal recovery throughout the spinal cord, showing the potential for further utilization of CSF delivery.

In Chapter two, an alternative CSF delivery location was used. Due to its location beneath the cerebellum, a spinal puncture of the cerebromedullary cistern (or cisterna magna, CM) is significantly less invasive than intracranial injection. Furthermore, the lateral ventricle injection still requires a craniotomy. The AAV CM injections were well tolerated and once again

delayed disease progression and stabilized various biomarkers, but not to the extent of the intracranial injection[114]. There was widespread βgal activity throughout the CNS, but it did not penetrate necessary deep brain structures, such as the thalamus and deep cerebellar nuclei.

It became clear that another delivery method would need to be evaluated for a minimally invasive treatment of GM1. Since it is reported that every brain neuron is closely located to a capillary[175] and certain AAV capsids can penetrate the blood-brain barrier (such as AAV9[176-178]), intravenous (IV) delivery for GM1 was investigated in Chapter three. The IV delivery of AAV was far superior to that of the Thal+ICV or CM results and comparable to the Thal+DCN results[114]. In addition to significant improvements in longevity and quality of life, there was an unprecedented recovery of βgal within neurons. Taken with the considerable improvement in biomarkers, brain architecture, and metabolites, this data demonstrates that intravenous delivery of AAV9 is an effective treatment of feline GM1 gangliosidosis.

The second goal of this work was to directly compare various AAV preparations for known variables. Initially, the method of AAV purification was directly evaluated due to anecdotal evidence from our laboratory. Cesium chloride (CsCl) and iodixanol are commonly used to purify AAV preparations and there is limited data directly comparing these methods. After Thal+ICV treatment in GM1 cats, a significant difference in efficacy of preparations purified with iodixanol and CsCl was clear. Through mechanisms that need further evaluation, iodixanol produces a more beneficial effect than CsCl preparations. Additionally, a direct comparison of AAV serotypes was performed for efficacy in treating GM1 after CSF delivery. Though less clear than the iodixanol results, the AAV9 serotype showed a marginally better result than the AAVrh10 serotype. These two studies, in addition with the efficacy of other treatments, led to the evaluation of an iodixanol purified AAV9 for treatment of GM1.

While there is great enthusiasm for gene therapy, as indicated by the numerous clinical and pre-clinical trials, there are still very real challenges to AAV gene therapy. A very large subset of disorders cannot utilize AAV due to its 5 kb carrying capacity. Therapeutic cDNAs for diseases such as cystic fibrosis and muscular dystrophy are unable to be packaged in their entirety due to their large sizes of 4,450 bp[208] and 14,000 bp[209], respectively. GM2 gangliosidosis is one such disease. GM2 is caused by a deficiency in the lysosomal enzyme β-N-acetylhexosaminidase (Hex, EC 3.1.2.52), which consists of two subunits whose cDNAs push the limit of the AAV packaging capacity. There have been numerous studies optimizing AAV treatment for GM2; however, they require modification or truncation of the coding region[128, 151, 210]. To overcome the size barrier, hybrid gene therapies, which combine the advantages of AAV with the larger capacity of other delivery platforms, should be investigated.

Combining portions of eukaryotic viruses, particularly AAV, with bacterial viruses, such as lambda bacteriophage (commonly referred to as phage), has the potential to overcome the carrying capacity barrier of AAV gene therapy. Cis-elements from AAV, such as inverted terminal repeats (ITRs), could be incorporated into the phage genomes to increase post-targeting transgene expression. The initial AAV and phage chimera, or AAVP, inserted a eukaryotic gene cassette with AAV ITRs on either end into an intergenomic region of filamentous phage[211]. These AAV-phage hybrids have been used to deliver reporter constructs, such as green fluorescent protein (GFP) or luciferase[211, 212], and cytotoxic or suicide genes, such as *Herpes simplex virus* thymidine kinase (HSVtk)[211-214] or tumor necrosis factor α (TNF-α)[215-219], for cancer therapy. However, this technology could be utilized for delivery of therapeutic genes for genetic disorders. There is also potential to combine synthetic particles, such as liposomes or polymersomes, with portions of AAV to make a synthetic gene therapy.

In summation, there is great potential for AAV gene therapy as the treatment of GM1 gangliosidosis. The work shown here contributed to the initiation of one clinical trial for GM1 (https://clinicaltrials.gov/ Identifier NCT03952637) and an application for a second (https://clinicaltrials.gov/ Identifier NCT04273269). Furthermore, utilizing portions of AAV in conjunction with other molecules may open the door to options for debilitating diseases.

Figures and Tables

Table 1. Summary and comparison of studies

		GM1	Thal+ICV		CM		IV
	Capsid	-	AAVrh8	AAVrh8	AAVrh10	AAV9	AAV9
	Purification method	-	CsCl	Iodixanol	Iodixanol	Iodixanol	Iodixanol
	Dose (vg/kg)	-	7.40E+11	7.25E+11	1.50E+13	1.50E+13	1.50E+13
	Survival (m)	7.9 ± 0.3	14.8 ± 3.6	31.4 ± 8.4	11.3 ± 0.6	13.9 ± 1.9	42.1 ± 1.8
	CRS	0.2 ± 0.4	0.7 ± 0.2	1.5 ± 0.4	0.5 ± 0.5	3.7 ± 2.1	8.5 ± 0.0
	MRI	-	+	+	++	++	+++
	MRS	-	-	-	-	+	+++
CSF	AST	-	+	++	+	++	+++
	LDH	-	+	+	-	+	+++
ßgal activity	Brain	-	+	+	+	+	++
	SC	-	+	+	+	+	++
	Periphery	-	N/A	N/A	+	+	++
	Ganglioside Storage	-	N/A	N/A	N/A	N/A	+++

References

1. Hastie, E, and Samulski, RJ (2015). Adeno-associated virus at 50: a golden anniversary of discovery, research, and gene therapy success--a personal perspective. *Hum Gene Ther* **26**: 257-265.

2. Rose, JA, Hoggan, MD, and Shatkin, AJ (1966). Nucleic acid from an adeno-associated virus: chemical and physical studies. *Proceedings of the National Academy of Sciences of the United States of America* **56**: 86-92.

3. Naso, MF, Tomkowicz, B, Perry, WL, and Strohl, WR (2017). Adeno-Associated Virus (AAV) as a Vector for Gene Therapy. *Biodrugs* **31**: 317-334.

4. Mendelson, E, Trempe, JP, and Carter, BJ (1986). Identification of the trans-acting Rep proteins of adeno-associated virus by antibodies to a synthetic oligopeptide. *Journal of virology* **60**: 823-832.

5. Srivastava, A, Lusby, EW, and Berns, KI (1983). Nucleotide sequence and organization of the adeno-associated virus 2 genome. *Journal of virology* **45**: 555-564.

6. Kohlbrenner, E, Aslanidi, G, Nash, K, Shklyaev, S, Campbell-Thompson, M, Byrne, BJ, *et al.* (2005). Successful Production of Pseudotyped rAAV Vectors Using a Modified Baculovirus Expression System. *Mol Ther* **12**: 1217-1225.

7. Wu, Z, Asokan, A, and Samulski, RJ (2006). Adeno-associated virus serotypes: vector toolkit for human gene therapy. *Mol Ther* **14**: 316-327.

8. Samulski, RJ, and Muzyczka, N (2014). AAV-Mediated Gene Therapy for Research and Therapeutic Purposes. *Annu Rev Virol* **1**: 427-451.

9. Naumer, M, Sonntag, F, Schmidt, K, Nieto, K, Panke, C, Davey, NE, *et al.* (2012). Properties of the Adeno-Associated Virus Assembly-Activating Protein. *Journal of virology* **86**: 13038-13048.

10. Grosse, S, Penaud-Budloo, M, Herrmann, AK, Borner, K, Fakhiri, J, Laketa, V, *et al.* (2017). Relevance of Assembly-Activating Protein for Adeno-associated Virus Vector Production and Capsid Protein Stability in Mammalian and Insect Cells. *Journal of virology* **91**: e0.1198-1117.

11. Goncalves, MA (2005). Adeno-associated virus: from defective virus to effective vector. *Virol J* **2**: 43.

12. McCarty, DM, Young, SM, Jr., and Samulski, RJ (2004). Integration of adeno-associated virus (AAV) and recombinant AAV vectors. *Annu Rev Genet* **38**: 819-845.

13. Surosky, RT, Urabe, M, Godwin, SG, McQuiston, SA, Kurtzman, GJ, Ozawa, K, *et al.* (1997). Adeno-associated virus Rep proteins target DNA sequences to a unique locus in the human genome.

14. Li, C, Hirsch, M, Asokan, A, Zeithaml, B, Ma, H, Kafri, T, *et al.* (2007). Adeno-associated virus type 2 (AAV2) capsid-specific cytotoxic T lymphocytes eliminate only

vector-transduced cells coexpressing the AAV2 capsid in vivo. *Journal of virology* **81**: 7540-7547.

15. Kronenberg, S, Bottcher, B, von der Lieth, CW, Bleker, S, and Kleinschmidt, JA (2005). A conformational change in the adeno-associated virus type 2 capsid leads to the exposure of hidden VP1 N termini. *Journal of virology* **79**: 5296-5303.

16. Li, C, and Samulski, RJ (2020). Engineering adeno-associated virus vectors for gene therapy. *Nature reviews Genetics*.

17. Xie, Q, Bu, W, Bhatia, S, Hare, J, Somasundaram, T, Azzi, A, *et al.* (2002). The atomic structure of adeno-associated virus (AAV-2), a vector for human gene therapy. *Proceedings of the National Academy of Sciences of the United States of America* **99**: 10405-10410.

18. Earley, LF, Powers, JM, Adachi, K, Baumgart, JT, Meyer, NL, Xie, Q, *et al.* (2017). Adeno-associated Virus (AAV) Assembly-Activating Protein Is Not an Essential Requirement for Capsid Assembly of AAV Serotypes 4, 5, and 11. *Journal of virology* **91**.

19. Pillay, S, Zou, W, Cheng, F, Puschnik, AS, Meyer, NL, Ganaie, SS, *et al.* (2017). Adeno-associated Virus (AAV) Serotypes Have Distinctive Interactions with Domains of the Cellular AAV Receptor. *Journal of virology* **91**.

20. Huang, LY, Halder, S, and Agbandje-McKenna, M (2014). Parvovirus Glycan Interactions. *Curr Opin Virol* **0**: 108-118.

21. Wu, Z, Miller, E, Agbandje-McKenna, M, and Samulski, RJ (2006). Alpha2,3 and alpha2,6 N-linked sialic acids facilitate efficient binding and transduction by adeno-associated virus types 1 and 6. *Journal of virology* **80**: 9093-9103.

22. Seiler, MP, Miller, AD, Zabner, J, and Halbert, CL (2006). Adeno-associated virus types 5 and 6 use distinct receptors for cell entry. *Hum Gene Ther* **17**: 10-19.

23. Summerford, C, and Samulski, RJ (1998). Membrane-associated heparan sulfate proteoglycan is a receptor for adeno-associated virus type 2 virions. *Journal of virology* **72**: 1438-1445.

24. Bell, CL, Vandenberghe, LH, Bell, P, Limberis, MP, Gao, GP, Van Vliet, K, *et al.* (2011). The AAV9 receptor and its modification to improve in vivo lung gene transfer in mice. *The Journal of clinical investigation* **121**: 2427-2435.

25. Shen, S, Bryant, KD, Brown, SM, Randell, SH, and Asokan, A (2011). Terminal N-linked galactose is the primary receptor for adeno-associated virus 9. *The Journal of biological chemistry* **286**: 13532-13540.

26. Davidson, BL, Stein, CS, Heth, JA, Martins, I, Kotin, RM, Derksen, TA, *et al.* (2000). Recombinant adeno-associated virus type 2, 4, and 5 vectors: transduction of variant cell types and regions in the mammalian central nervous system. *Proceedings of the National Academy of Sciences of the United States of America* **97**: 3428-3432.

27. Nguyen, JB, Sanchez-Pernaute, R, Cunningham, J, and Bankiewicz, KS (2001). Convection-enhanced delivery of AAV-2 combined with heparin increases TK gene transfer in the rat brain. *Neuroreport* **12**: 1961-1964.

28. Smith-Arica, JR, Thomson, AJ, Ansell, R, Chiorini, J, Davidson, B, and McWhir, J (2003). Infection efficiency of human and mouse embryonic stem cells using adenoviral and adeno-associated viral vectors. *Cloning Stem Cells* **5**: 51-62.

29. Hughes, SM, Moussavi-Harami, F, Sauter, SL, and Davidson, BL (2002). Viral-mediated gene transfer to mouse primary neural progenitor cells. *Mol Ther* **5**: 16-24.

30. Dong, JY, Fan, PD, and Frizzell, RA (1996). Quantitative analysis of the packaging capacity of recombinant adeno-associated virus. *Hum Gene Ther* **7**: 2101-2112.

31. Kwon, I, and Schaffer, DV (2008). Designer gene delivery vectors: molecular engineering and evolution of adeno-associated viral vectors for enhanced gene transfer. *Pharm Res* **25**: 489-499.

32. Wobus, CE, Hugle-Dorr, B, Girod, A, Petersen, G, Hallek, M, and Kleinschmidt, JA (2000). Monoclonal antibodies against the adeno-associated virus type 2 (AAV-2) capsid: epitope mapping and identification of capsid domains involved in AAV-2-cell interaction and neutralization of AAV-2 infection. *Journal of virology* **74**: 9281-9293.

33. Sun, JY, Anand-Jawa, V, Chatterjee, S, and Wong, KK (2003). Immune responses to adeno-associated virus and its recombinant vectors. *Gene Ther* **10**: 964-976.

34. Wang, D, Tai, PWL, and Gao, G (2019). Adeno-associated virus vector as a platform for gene therapy delivery. *Nat Rev Drug Discov* **18**: 358-378.

35. McCown, TJ, Xiao, X, Li, J, Breese, GR, and Samulski, RJ (1996). Differential and persistent expression patterns of CNS gene transfer by an adeno-associated virus (AAV) vector. *Brain Res* **713**: 99-107.

36. Paterna, JC, Moccetti, T, Mura, A, Feldon, J, and Bueler, H (2000). Influence of promoter and WHV post-transcriptional regulatory element on AAV-mediated transgene expression in the rat brain. *Gene Ther* **7**: 1304-1311.

37. Gray, SJ, Foti, SB, Schwartz, JW, Bachaboina, L, Taylor-Blake, B, Coleman, J, *et al.* (2011). Optimizing Promoters for Recombinant Adeno-Associated Virus-Mediated Gene Expression in the Peripheral and Central Nervous System Using Self-Complementary Vectors. *Hum Gene Ther* **22**: 1143-1153.

38. Kugler, S, Lingor, P, Scholl, U, Zolotukhin, S, and Bahr, M (2003). Differential transgene expression in brain cells in vivo and in vitro from AAV-2 vectors with small transcriptional control units. *Virology* **311**: 89-95.

39. Xu, R, Janson, CG, Mastakov, M, Lawlor, P, Young, D, Mouravlev, A, *et al.* (2001). Quantitative comparison of expression with adeno-associated virus (AAV-2) brain-specific gene cassettes. *Gene Ther* **8**: 1323-1332.

40. Lawlor, PA, Bland, RJ, Mouravlev, A, Young, D, and During, MJ (2009). Efficient gene delivery and selective transduction of glial cells in the mammalian brain by AAV serotypes isolated from nonhuman primates. *Mol Ther* **17**: 1692-1702.

41. Saraiva, J, Nobre, RJ, and Pereira de Almeida, L (2016). Gene therapy for the CNS using AAVs: The impact of systemic delivery by AAV9. *Journal of controlled release : official journal of the Controlled Release Society* **241**: 94-109.

42. Satkunanathan, S, Wheeler, J, Thorpe, R, and Zhao, Y (2014). Establishment of a Novel Cell Line for the Enhanced Production of Recombinant Adeno-Associated Virus Vectors for Gene Therapy. *Hum Gene Ther* **25**: 929-941.

43. Nicolas, A, Jolinon, N, Alazard-Dany, N, Barateau, V, Epstein, AL, Greco, A, *et al.* (2012). Factors influencing helper-independent adeno-associated virus replication. *Virology* **432**: 1-9.

44. Collaco, RF, Cao, X, and Trempe, JP (1999). A helper virus-free packaging system for recombinant adeno-associated virus vectors. *Gene* **238**: 397-405.

45. Allay, JA, Sleep, S, Long, S, Tillman, DM, Clark, R, Carney, G, *et al.* (2011). Good manufacturing practice production of self-complementary serotype 8 adeno-associated viral vector for a hemophilia B clinical trial. *Hum Gene Ther* **22**: 595-604.

46. Blessing, D, Deglon, N, and Schneider, BL (2018). Scalable Production and Purification of Adeno-Associated Viral Vectors (AAV). *Methods in molecular biology* **1850**: 259-274.

47. Grieger, JC, Soltys, SM, and Samulski, RJ (2016). Production of Recombinant Adeno-associated Virus Vectors Using Suspension HEK293 Cells and Continuous Harvest of Vector From the Culture Media for GMP FIX and FLT1 Clinical Vector. *Mol Ther* **24**: 287-297.

48. Clément, N, and Grieger, JC (2016). Manufacturing of recombinant adeno-associated viral vectors for clinical trials. *Mol Ther Methods Clin Dev* **3**: 16002-.

49. Mietzsch, M, Grasse, S, Zurawski, C, Weger, S, Bennett, A, Agbandje-McKenna, M, *et al.* (2014). OneBac: platform for scalable and high-titer production of adeno-associated virus serotype 1-12 vectors for gene therapy. *Hum Gene Ther* **25**: 212-222.

50. Sandro, Q, Relizani, K, and Benchaouir, R (2019). AAV Production Using Baculovirus Expression Vector System. *Methods in molecular biology* **1937**: 91-99.

51. Aslanidi, G, Lamb, K, and Zolotukhin, S (2009). An inducible system for highly efficient production of recombinant adeno-associated virus (rAAV) vectors in insect Sf9 cells. *Proceedings of the National Academy of Sciences of the United States of America* **106**: 5059-5064.

52. Wu, Y, Jiang, L, Geng, H, Yang, T, Han, Z, He, X, *et al.* (2018). A Recombinant Baculovirus Efficiently Generates Recombinant Adeno-Associated Virus Vectors in Cultured Insect Cells and Larvae. *Mol Ther Methods Clin Dev*, vol. 10. pp 38-47.

53. Burova, E, and Ioffe, E (2005). Chromatographic purification of recombinant adenoviral and adeno-associated viral vectors: methods and implications. *Gene Ther* **12 Suppl 1**: S5-17.

54. Drittanti, L, Jenny, C, Poulard, K, Samba, A, Manceau, P, Soria, N, *et al.* (2001). Optimised helper virus-free production of high-quality adeno-associated virus vectors. *J Gene Med* **3**: 59-71.

55. Strobel, B, Miller, FD, Rist, W, and Lamla, T (2015). Comparative Analysis of Cesium Chloride- and Iodixanol-Based Purification of Recombinant Adeno-Associated Viral Vectors for Preclinical Applications. *Hum Gene Ther Methods* **26**: 147-157.

56. Qu, G, Bahr-Davidson, J, Prado, J, Tai, A, Cataniag, F, McDonnell, J, *et al.* (2007). Separation of adeno-associated virus type 2 empty particles from genome containing vectors by anion-exchange column chromatography. *J Virol Methods* **140**: 183-192.

57. Davidoff, AM, Ng, CY, Sleep, S, Gray, J, Azam, S, Zhao, Y, *et al.* (2004). Purification of recombinant adeno-associated virus type 8 vectors by ion exchange chromatography generates clinical grade vector stock. *J Virol Methods* **121**: 209-215.

58. Auricchio, A, O'Connor, E, Hildinger, M, and Wilson, JM (2001). A single-step affinity column for purification of serotype-5 based adeno-associated viral vectors. *Mol Ther* **4**: 372-374.

59. Grimm, D, Pandey, K, and Kay, MA (2005). Adeno-associated virus vectors for short hairpin RNA expression. *Methods Enzymol* **392**: 381-405.

60. Zolotukhin, S, Byrne, BJ, Mason, E, Zolotukhin, I, Potter, M, Chesnut, K, *et al.* (1999). Recombinant adeno-associated virus purification using novel methods improves infectious titer and yield. *Gene Therapy* **6**: 973-985.

61. Gao, G, Qu, G, Burnham, MS, Huang, J, Chirmule, N, Joshi, B, *et al.* (2000). Purification of recombinant adeno-associated virus vectors by column chromatography and its performance in vivo. *Hum Gene Ther* **11**: 2079-2091.

62. Smith, RH, Ding, C, and Kotin, RM (2003). Serum-free production and column purification of adeno-associated virus type 5. *J Virol Methods* **114**: 115-124.

63. Kaludov, N, Handelman, B, and Chiorini, JA (2002). Scalable purification of adeno-associated virus type 2, 4, or 5 using ion-exchange chromatography. *Hum Gene Ther* **13**: 1235-1243.

64. Brument, N, Morenweiser, R, Blouin, V, Toublanc, E, Raimbaud, I, Cherel, Y, *et al.* (2002). A versatile and scalable two-step ion-exchange chromatography process for the purification of recombinant adeno-associated virus serotypes-2 and -5. *Mol Ther* **6**: 678-686.

65. Clark, KR, Liu, X, McGrath, JP, and Johnson, PR (1999). Highly purified recombinant adeno-associated virus vectors are biologically active and free of detectable helper and wild-type viruses. *Hum Gene Ther* **10**: 1031-1039.

66. Maguire, AM, Russell, S, Wellman, JA, Chung, DC, Yu, ZF, Tillman, A, *et al.* (2019). Efficacy, Safety, and Durability of Voretigene Neparvovec-rzyl in RPE65 Mutation-Associated Inherited Retinal Dystrophy: Results of Phase 1 and 3 Trials. *Ophthalmology* **126**: 1273-1285.

67. Mendell, JR, Al-Zaidy, S, Shell, R, Arnold, WD, Rodino-Klapac, LR, Prior, TW, *et al.* (2017). Single-Dose Gene-Replacement Therapy for Spinal Muscular Atrophy. *The New England journal of medicine* **377**: 1713-1722.

68. Wierzbicki, AS, and Viljoen, A (2013). Alipogene tiparvovec: gene therapy for lipoprotein lipase deficiency. *Expert Opin Biol Ther* **13**: 7-10.

69. (2020). Search of: AAV - List Results - ClinicalTrials.gov https://clinicaltrials.gov/ct2/results?cond=&term=AAV&cntry=&state=&city=&dist=.

70. Salabarria, SM, Nair, J, Clement, N, Smith, BK, Raben, N, Fuller, DD, *et al.* (2020). Advancements in AAV-mediated Gene Therapy for Pompe Disease. *J Neuromuscul Dis* **7**: 15-31.

71. Han, SO, Li, S, McCall, A, Arnson, B, Everitt, JI, Zhang, H, *et al.* (2020). Comparisons of Infant and Adult Mice Reveal Age Effects for Liver Depot Gene Therapy in Pompe Disease. *Mol Ther Methods Clin Dev* **17**: 133-142.

72. Hudry, E, and Vandenberghe, LH (2019). Therapeutic AAV Gene Transfer to the Nervous System: A Clinical Reality. *Neuron* **102**: 263.

73. D'Azzo, A, Hoogeveen, A, Reuser, AJ, Robinson, D, and Galjaard, H (1982). Molecular defect in combined beta-galactosidase and neuraminidase deficiency in man. *Proceedings of the National Academy of Sciences of the United States of America* **79**: 4535-4539.

74. Okada, S, and O'Brien, JS (1968). Generalized gangliosidosis: beta-galactosidase deficiency. *Science* **160**: 1002-1004.

75. Fuller, M, Meikle, PJ, and Hopwood, JJ (2006). Epidemiology of lysosomal storage diseases: an overview.

76. Sinigerska, I, Chandler, D, Vaghjiani, V, Hassanova, I, Gooding, R, Morrone, A, *et al.* (2006). Founder mutation causing infantile GM1-gangliosidosis in the Gypsy population. *Mol Genet Metab* **88**: 93-95.

77. Brunetti-Pierri, N, and Scaglia, F (2008). GM1 gangliosidosis: review of clinical, molecular, and therapeutic aspects. *Mol Genet Metab* **94**: 391-396.

78. Oshima, A, Tsuji, A, Nagao, Y, Sakuraba, H, and Suzuki, Y (1988). Cloning, sequencing, and expression of cDNA for human beta-galactosidase. *Biochem Biophys Res Commun* **157**: 238-244.

79. Morreau, H, Galjart, NJ, Gillemans, N, Willemsen, R, van der Horst, GT, and d'Azzo, A (1989). Alternative splicing of beta-galactosidase mRNA generates the classic lysosomal enzyme and a beta-galactosidase-related protein. *The Journal of biological chemistry* **264**: 20655-20663.

80. Arash-Kaps, L, Komlosi, K, Seegraber, M, Diederich, S, Paschke, E, Amraoui, Y, *et al.* (2019). The Clinical and Molecular Spectrum of GM1 Gangliosidosis. *J Pediatr* **215**: 152-157.e153.

81. Regier, DS, and Tifft, CJ (1993). GLB1-Related Disorders. In: Adam, MP, *et al.* (eds). *GeneReviews((R))*: Seattle (WA).

82. Suzuki, Y, Nakamura, N, and Fukuoka, K (1978). GM1-gangliosidosis: accumulation of ganglioside GM1 in cultured skin fibroblasts and correlation with clinical types. *Hum Genet* **43**: 127-131.

83. Tessitore, A, del, PMM, Sano, R, Ma, Y, Mann, L, Ingrassia, A, *et al.* (2004). GM1-ganglioside-mediated activation of the unfolded protein response causes neuronal death in a neurodegenerative gangliosidosis. *Molecular cell* **15**: 753-766.

84. d'Azzo, A, Tessitore, A, and Sano, R (2006). Gangliosides as apoptotic signals in ER stress response. *Cell Death Differ* **13**: 404-414.

85. Folkerth, RD (1999). Abnormalities of developing white matter in lysosomal storage diseases. *J Neuropathol Exp Neurol* **58**: 887-902.

86. Hahn, CN, del Pilar Martin, M, Schroder, M, Vanier, MT, Hara, Y, Suzuki, K, *et al.* (1997). Generalized CNS disease and massive GM1-ganglioside accumulation in mice defective in lysosomal acid beta-galactosidase. *Hum Mol Genet* **6**: 205-211.

87. Matsuda, J, Suzuki, O, Oshima, A, Ogura, A, Noguchi, Y, Yamamoto, Y, *et al.* (1997). Beta-galactosidase-deficient mouse as an animal model for GM1-gangliosidosis. *Glycoconj J* **14**: 729-736.

88. Przybilla, MJ, Ou, L, Tabaran, AF, Jiang, X, Sidhu, R, Kell, PJ, *et al.* (2019). Comprehensive behavioral and biochemical outcomes of novel murine models of GM1-gangliosidosis and Morquio syndrome type B. *Mol Genet Metab* **126**: 139-150.

89. Casal, M, and Haskins, M (2006). Large animal models and gene therapy. *Eur J Hum Genet* **14**: 266-272.

90. Martin, DR, Rigat, BA, Foureman, P, Varadarajan, GS, Hwang, M, Krum, BK, *et al.* (2008). Molecular consequences of the pathogenic mutation in feline GM1 gangliosidosis. *Mol Genet Metab* **94**: 212-221.

91. Georgiou, T, Stylianidou, G, Anastasiadou, V, Caciotti, A, Campos, Y, Zammarchi, E, *et al.* (2005). The Arg482His mutation in the beta-galactosidase gene is responsible for a high frequency of GM1 gangliosidosis carriers in a Cypriot village. *Genet Test* **9**: 126-132.

92. Suzuki, Y, and Oshima, A (1993). A beta-galactosidase gene mutation identified in both Morquio B disease and infantile GM1 gangliosidosis. *Hum Genet* **91**: 407.

93. Caciotti, A, Donati, MA, Boneh, A, d'Azzo, A, Federico, A, Parini, R, *et al.* (2005). Role of beta-galactosidase and elastin binding protein in lysosomal and nonlysosomal complexes of patients with GM1-gangliosidosis. *Hum Mutat* **25**: 285-292.

94. Mosna, G, Fattore, S, Tubiello, G, Brocca, S, Trubia, M, Gianazza, E, *et al.* (1992). A homozygous missense arginine to histidine substitution at position 482 of the beta-galactosidase in an Italian infantile GM1-gangliosidosis patient. *Hum Genet* **90**: 247-250.

95. Baker, HJ, Jr., Lindsey, JR, McKhann, GM, and Farrell, DF (1971). Neuronal GM1 gangliosidosis in a Siamese cat with beta-galactosidase deficiency. *Science* **174**: 838-839.

96. Baker, HJ, and Lindsey, JR (1974). Animal model: feline GM1 gangliosidosis. *Am J Pathol* **74**: 649-652.

97. Farrell, DF, Baker, HJ, Herndon, RM, Lindsey, JR, and McKhann, GM (1973). Feline GM 1 gangliosidosis: biochemical and ultrastructural comparisons with the disease in man. *J Neuropathol Exp Neurol* **32**: 1-18.

98. Vite, CH, Passini, MA, Haskins, ME, and Wolfe, JH (2003). Adeno-associated virus vector-mediated transduction in the cat brain. *Gene Ther* **10**: 1874-1881.

99. Parenti, G, Moracci, M, Fecarotta, S, and Andria, G (2014). Pharmacological chaperone therapy for lysosomal storage diseases. *Future Med Chem* **6**: 1031-1045.

100. Matsuda, J, Suzuki, O, Oshima, A, Yamamoto, Y, Noguchi, A, Takimoto, K, *et al.* (2003). Chemical chaperone therapy for brain pathology in GM1-gangliosidosis. *Proceedings of the National Academy of Sciences of the United States of America* **100**: 15912-15917.

101. Suzuki, Y, Ichinomiya, S, Kurosawa, M, Matsuda, J, Ogawa, S, Iida, M, *et al.* (2012). Therapeutic chaperone effect of N-octyl 4-epi-beta-valienamine on murine G(M1)-gangliosidosis. *Mol Genet Metab* **106**: 92-98.

102. Suzuki, Y, Ichinomiya, S, Kurosawa, M, Ohkubo, M, Watanabe, H, Iwasaki, H, *et al.* (2007). Chemical chaperone therapy: clinical effect in murine G(M1)-gangliosidosis. *Ann Neurol* **62**: 671-675.

103. Aguilar-Moncayo, M, Takai, T, Higaki, K, Mena-Barragan, T, Hirano, Y, Yura, K, *et al.* (2012). Tuning glycosidase inhibition through aglycone interactions: pharmacological chaperones for Fabry disease and GM1 gangliosidosis. *Chem Commun (Camb)* **48**: 6514-6516.

104. Suzuki, Y (2013). Chaperone therapy update: Fabry disease, GM1-gangliosidosis and Gaucher disease. *Brain Dev* **35**: 515-523.

105. Chen, JC, Luu, AR, Wise, N, Angelis, RD, Agrawal, V, Mangini, L, *et al.* (2019). Intracerebroventricular enzyme replacement therapy with Beta-Galactosidase reverses brain pathologies due to GM1 gangliosidosis in mice.

106. Slavc, I, Cohen-Pfeffer, JL, Gururangan, S, Krauser, J, Lim, DA, Maldaun, M, *et al.* (2018). Best practices for the use of intracerebroventricular drug delivery devices. *Mol Genet Metab* **124**: 184-188.

107. Kelly, JM, Gross, AL, Martin, DR, and Byrne, ME (2017). Polyethylene glycol-b-poly(lactic acid) polymersomes as vehicles for enzyme replacement therapy. *Nanomedicine (Lond)* **12**: 2591-2606.

108. Bellettato, CM, and Scarpa, M (2018). Possible strategies to cross the blood-brain barrier. *Ital J Pediatr* **44**: 131.

109. Platt, FM, and Jeyakumar, M (2008). Substrate reduction therapy. *Acta Paediatr* **97**: 88-93.

110. Elliot-Smith, E, Speak, AO, Lloyd-Evans, E, Smith, DA, van der Spoel, AC, Jeyakumar, M, *et al.* (2008). Beneficial effects of substrate reduction therapy in a mouse model of GM1 gangliosidosis. *Mol Genet Metab* **94**: 204-211.

111. Deodato, F, Procopio, E, Rampazzo, A, Taurisano, R, Donati, MA, Dionisi-Vici, C, *et al.* (2017). The treatment of juvenile/adult GM1-gangliosidosis with Miglustat may reverse disease progression. *Metab Brain Dis* **32**: 1529-1536.

112. O'Brien, JS, Storb, R, Raff, RF, Harding, J, Appelbaum, F, Morimoto, S, *et al.* (1990). Bone marrow transplantation in canine GM1 gangliosidosis. *Clin Genet* **38**: 274-280.

113. Shield, JP, Stone, J, and Steward, CG (2005). Bone marrow transplantation correcting beta-galactosidase activity does not influence neurological outcome in juvenile GM1-gangliosidosis. *J Inherit Metab Dis* **28**: 797-798.

114. McCurdy, VJ, Johnson, AK, Gray-Edwards, HL, Randle, AN, Brunson, BL, Morrison, NE, *et al.* (2014). Sustained Normalization of Neurological Disease After Intracranial Gene Therapy in a Feline Model. *Sci Transl Med* **6**: 11.

115. Baek, RC, Broekman, ML, Leroy, SG, Tierney, LA, Sandberg, MA, d'Azzo, A, *et al.* (2010). AAV-mediated gene delivery in adult GM1-gangliosidosis mice corrects lysosomal storage in CNS and improves survival. *PloS one* **5**: e13468.

116. Broekman, ML, Baek, RC, Comer, LA, Fernandez, JL, Seyfried, TN, and Sena-Esteves, M (2007). Complete correction of enzymatic deficiency and neurochemistry in the GM1-gangliosidosis mouse brain by neonatal adeno-associated virus-mediated gene delivery. *Mol Ther* **15**: 30-37.

117. (2020). ALD-101 Adjuvant Therapy of Unrelated Umbilical Cord Blood Transfusion (UCBT) in Patients With Inherited Metabolic Diseases - Full Text View - ClinicalTrials.gov https://clinicaltrials.gov/ct2/show/NCT00654433.

118. Bennett, A, Keravala, A, Makal, V, Kurian, J, Belbellaa, B, Aeran, R, *et al.* (2020). Structure comparison of the chimeric AAV2.7m8 vector with parental AAV2. *J Struct Biol* **209**: 107433.

119. Liguore, WA, Domire, JS, Button, D, Wang, Y, Dufour, BD, Srinivasan, S, *et al.* (2019). AAV-PHP.B Administration Results in a Differential Pattern of CNS Biodistribution in Non-human Primates Compared with Mice. *Mol Ther* **27**: 2018-2037.

120. Qu, W, Wang, M, Wu, Y, and Xu, R (2015). Scalable downstream strategies for purification of recombinant adeno- associated virus vectors in light of the properties. *Curr Pharm Biotechnol* **16**: 684-695.

121. Ferreira, CR, and Gahl, WA (2017). Lysosomal storage diseases. *Transl Sci Rare Dis* **2**: 1-71.

122. Yoshida, K, and Yanagisawa, N (1995). [beta-galactosidosis--GM1 gangliosidosis and Morquio B disease]. *Nihon Rinsho* **53**: 2960-2966.

123. Rama Rao, KV, and Kielian, T (2016). Astrocytes and lysosomal storage diseases. *Neuroscience* **323**: 195-206.

124. Gurda, BL, and Vite, CH (2019). Large animal models contribute to the development of therapies for central and peripheral nervous system dysfunction in patients with lysosomal storage diseases. *Hum Mol Genet* **28**: R119-R131.

125. Gray-Edwards, HL, Regier, DS, Shirley, JL, Randle, AN, Salibi, N, Thomas, SE, *et al.* (2017). Novel Biomarkers of Human GM1 Gangliosidosis Reflect the Clinical Efficacy of Gene Therapy in a Feline Model. *Mol Ther* **25**: 892-903.

126. Gray-Edwards, HL, Maguire, AS, Salibi, N, Ellis, LE, Voss, TL, Diffie, EB, *et al.* (2019). 7T MRI predicts amelioration of neurodegeneration in the brain after AAV gene therapy. *Molecular Therapy - Methods & Clinical Development* **0**.

127. Kaplitt, MG, Feigin, A, Tang, C, Fitzsimons, HL, Mattis, P, Lawlor, PA, *et al.* (2007). Safety and tolerability of gene therapy with an adeno-associated virus (AAV) borne GAD gene for Parkinson's disease: an open label, phase I trial. *Lancet* **369**: 2097-2105.

128. Bradbury, AM, Cochran, JN, McCurdy, VJ, Johnson, AK, Brunson, BL, Gray-Edwards, H, *et al.* (2013). Therapeutic response in feline sandhoff disease despite immunity to intracranial gene therapy. *Mol Ther* **21**: 1306-1315.

129. Swain, GP, Prociuk, M, Bagel, JH, O'Donnell, P, Berger, K, Drobatz, K, *et al.* (2014). Adeno-associated virus serotypes 9 and rh10 mediate strong neuronal transduction of the dog brain. *Gene Ther* **21**: 28-36.

130. de Lange, EC (2013). Utility of CSF in translational neuroscience. *J Pharmacokinet Pharmacodyn* **40**: 315-326.

131. Knopf, PM, Cserr, HF, Nolan, SC, Wu, TY, and Harling-Berg, CJ (1995). Physiology and immunology of lymphatic drainage of interstitial and cerebrospinal fluid from the brain. *Neuropathol Appl Neurobiol* **21**: 175-180.

132. Ohno, K, Samaranch, L, Hadaczek, P, Bringas, JR, Allen, PC, Sudhakar, V, *et al.* (2019). Kinetics and MR-Based Monitoring of AAV9 Vector Delivery into Cerebrospinal Fluid of Nonhuman Primates. *Mol Ther Methods Clin Dev* **13**: 47-54.

133. Klein, RL, Dayton, RD, Tatom, JB, Henderson, KM, and Henning, PP (2008). AAV8, 9, Rh10, Rh43 vector gene transfer in the rat brain: effects of serotype, promoter and purification method. *Mol Ther* **16**: 89-96.

134. Zhu, H, and Barker, PB (2011). MR spectroscopy and spectroscopic imaging of the brain. *Methods in molecular biology* **711**: 203-226.

135. Ross, B, and Bluml, S (2001). Magnetic resonance spectroscopy of the human brain. *Anat Rec* **265**: 54-84.

136. Ford, TC, and Crewther, DP (2016). A Comprehensive Review of the 1H-MRS Metabolite Spectrum in Autism Spectrum Disorder. *Front Mol Neurosci* **9**.

137. Rae, CD (2014). A guide to the metabolic pathways and function of metabolites observed in human brain 1H magnetic resonance spectra. *Neurochem Res* **39**: 1-36.

138. Bak, LK, Schousboe, A, and Waagepetersen, HS (2006). The glutamate/GABA-glutamine cycle: aspects of transport, neurotransmitter homeostasis and ammonia transfer. *J Neurochem* **98**: 641-653.

139. Panteghini, M (1990). Aspartate aminotransferase isoenzymes. *Clin Biochem* **23**: 311-319.

140. Markert, CL (1984). Lactate dehydrogenase. Biochemistry and function of lactate dehydrogenase. *Cell Biochem Funct* **2**: 131-134.

141. Clogston, JD, and Patri, AK (2011). Zeta potential measurement. *Methods in molecular biology* **697**: 63-70.

142. Baker, HJ, Reynolds, GD, Walkley, SU, Cox, NR, and Baker, GH (1979). The gangliosidoses: comparative features and research applications. *Vet Pathol* **16**: 635-649.

143. De Grandis, E, Di Rocco, M, Pessagno, A, Veneselli, E, and Rossi, A (2009). MR imaging findings in 2 cases of late infantile GM1 gangliosidosis. *AJNR Am J Neuroradiol* **30**: 1325-1327.

144. Chen, CY, Zimmerman, RA, Lee, CC, Chen, FH, Yuh, YS, and Hsiao, HS (1998). Neuroimaging findings in late infantile GM1 gangliosidosis. *AJNR Am J Neuroradiol* **19**: 1628-1630.

145. O'Brien, JS, Ho, MW, Veath, ML, Wilson, JF, Myers, G, Opitz, JM, *et al.* (1972). Juvenile GM 1 gangliosidosis: clinical, pathological, chemical and enzymatic studies. *Clin Genet* **3**: 411-434.

146. Whittaker, DE, Drees, R, and Beltran, E (2018). MRI and clinical characteristics of suspected cerebrovascular accident in nine cats. *J Feline Med Surg* **20**: 674-684.

147. Castellano, G, Dias, CS, Foerster, B, Li, LM, and Covolan, RJ (2012). NAA and NAAG variation in neuronal activation during visual stimulation. *Braz J Med Biol Res* **45**: 1031-1036.

148. Gray, SJ, Nagabhushan Kalburgi, S, McCown, TJ, and Jude Samulski, R (2013). Global CNS gene delivery and evasion of anti-AAV-neutralizing antibodies by intrathecal AAV administration in non-human primates. *Gene Ther* **20**: 450-459.

149. Hordeaux, J, Hinderer, C, Buza, EL, Louboutin, JP, Jahan, T, Bell, P, *et al.* (2019). Safe and Sustained Expression of Human Iduronidase After Intrathecal Administration of Adeno-Associated Virus Serotype 9 in Infant Rhesus Monkeys. *Hum Gene Ther* **30**: 957-966.

150. Borel, F, Adams, E, and Mueller, C (2019). Intrathecal Delivery of AAV Vectors in Cynomolgus Macaques for CNS Gene Therapy and Gene Expression Analysis in Microdissected Motor Neurons. *Methods in molecular biology* **1937**: 295-303.

151. McCurdy, VJ, Rockwell, HE, Arthur, JR, Bradbury, AM, Johnson, AK, Randle, AN, *et al.* (2015). Widespread correction of central nervous system disease after intracranial gene therapy in a feline model of Sandhoff disease. *Gene Ther* **22**: 181-189.

152. Rockwell, HE, McCurdy, VJ, Eaton, SC, Wilson, DU, Johnson, AK, Randle, AN, *et al.* (2015). AAV-mediated gene delivery in a feline model of Sandhoff disease corrects lysosomal storage in the central nervous system. *ASN Neuro* **7**.

153. Golebiowski, D, van der Bom, IMJ, Kwon, CS, Miller, AD, Petrosky, K, Bradbury, AM, *et al.* (2017). Direct Intracranial Injection of AAVrh8 Encoding Monkey beta-N-Acetylhexosaminidase Causes Neurotoxicity in the Primate Brain. *Hum Gene Ther* **28**: 510-522.

154. Mingozzi, F, Anguela, XM, Pavani, G, Chen, Y, Davidson, RJ, Hui, DJ, *et al.* (2013). Overcoming Preexisting Humoral Immunity to AAV Using Capsid Decoys. *Sci Transl Med* **5**: 194ra192.

155. Hoffman, BE, and Herzog, RW (2013). Covert warfare against the immune system: decoy capsids, stealth genomes, and suppressors. *Mol Ther* **21**: 1648-1650.

156. Wright, JF (2014). AAV Empty Capsids: For Better or for Worse? *Mol Ther* **22**: 1-2.

157. Oh, N, and Park, JH (2014). Endocytosis and exocytosis of nanoparticles in mammalian cells. *International journal of nanomedicine* **9 Suppl 1**: 51-63.

158. Broekman, ML, Comer, LA, Hyman, BT, and Sena-Esteves, M (2006). Adeno-associated virus vectors serotyped with AAV8 capsid are more efficient than AAV-1 or -2 serotypes for widespread gene delivery to the neonatal mouse brain. *Neuroscience* **138**: 501-510.

159. Gray-Edwards, HL, Maguire, AS, Salibi, N, Ellis, LE, Voss, TL, Diffie, EB, *et al.* (2020). 7T MRI Predicts Amelioration of Neurodegeneration in the Brain after AAV Gene Therapy. *Mol Ther Methods Clin Dev* **17**: 258-270.

160. Grieger, JC, Choi, VW, and Samulski, RJ (2006). Production and characterization of adeno-associated viral vectors. *Nat Protoc* **1**: 1412-1428.

161. Chow, BW, and Gu, C (2015). The molecular constituents of the blood-brain barrier. *Trends Neurosci* **38**: 598-608.

162. Schuster, DJ, Dykstra, JA, Riedl, MS, Kitto, KF, Belur, LR, McIvor, RS, *et al.* (2014). Biodistribution of adeno-associated virus serotype 9 (AAV9) vector after intrathecal and intravenous delivery in mouse. *Front Neuroanat* **8**: 42.

163. Park, SH, Eber, MR, Tsuzuki, S, Booker, ME, Sunil, AG, Widner, DB, *et al.* (2017). Adeno-associated virus serotype rh10 is a useful gene transfer vector for sensory nerves that innervate bone in immunodeficient mice. *Scientific reports* **7**: 17428.

164. Vallender, EJ, and Miller, GM (2013). Nonhuman primate models in the genomic era: a paradigm shift. *Ilar j* **54**: 154-165.

165. Matsuda, J, Suzuki, O, Oshima, A, Ogura, A, Naiki, M, and Suzuki, Y (1997). Neurological manifestations of knockout mice with beta-galactosidase deficiency. *Brain Dev* **19**: 19-20.

166. Gray, SJ, Matagne, V, Bachaboina, L, Yadav, S, Ojeda, SR, and Samulski, RJ (2011). Preclinical differences of intravascular AAV9 delivery to neurons and glia: a comparative study of adult mice and nonhuman primates. *Mol Ther* **19**: 1058-1069.

167. Federici, T, Taub, JS, Baum, GR, Gray, SJ, Grieger, JC, Matthews, KA, *et al.* (2012). Robust spinal motor neuron transduction following intrathecal delivery of AAV9 in pigs. *Gene Ther* **19**: 852-859.

168. Hoshino, Y, Nishide, K, Nagoshi, N, Shibata, S, Moritoki, N, Kojima, K, *et al.* (2019). The adeno-associated virus rh10 vector is an effective gene transfer system for chronic spinal cord injury. *Scientific reports* **9**: 1-12.

169. Jessen, F, Fingerhut, N, Sprinkart, AM, Kuhn, KU, Petrovsky, N, Maier, W, *et al.* (2013). N-acetylaspartylglutamate (NAAG) and N-acetylaspartate (NAA) in patients with schizophrenia. *Schizophr Bull* **39**: 197-205.

170. Pardridge, WM (2016). CSF, blood-brain barrier, and brain drug delivery. *Expert opinion on drug delivery* **13**: 963-975.

171. Chang, KJ, Dillon, LL, Deverell, L, Boon, MY, and Keay, L (2019). Orientation and mobility outcome measures. *Clin Exp Optom*.

172. Dodge, JC, Clarke, J, Song, A, Bu, J, Yang, W, Taksir, TV, *et al.* (2005). Gene transfer of human acid sphingomyelinase corrects neuropathology and motor deficits in a mouse model of Niemann-Pick type A disease. *Proceedings of the National Academy of Sciences of the United States of America* **102**: 17822-17827.

173. Bosch, A, Perret, E, Desmaris, N, and Heard, JM (2000). Long-term and significant correction of brain lesions in adult mucopolysaccharidosis type VII mice using recombinant AAV vectors. *Mol Ther* **1**: 63-70.

174. Skorupa, AF, Fisher, KJ, Wilson, JM, Parente, MK, and Wolfe, JH (1999). Sustained production of beta-glucuronidase from localized sites after AAV vector gene transfer results in widespread distribution of enzyme and reversal of lysosomal storage lesions in a large volume of brain in mucopolysaccharidosis VII mice. *Exp Neurol* **160**: 17-27.

175. Pardridge, WM (2002). Drug and gene delivery to the brain: the vascular route. *Neuron* **36**: 555-558.

176. Zhang, H, Yang, B, Mu, X, Ahmed, SS, Su, Q, He, R, *et al.* (2011). Several rAAV vectors efficiently cross the blood-brain barrier and transduce neurons and astrocytes in the neonatal mouse central nervous system. *Mol Ther* **19**: 1440-1448.

177. Foust, KD, Nurre, E, Montgomery, CL, Hernandez, A, Chan, CM, and Kaspar, BK (2009). Intravascular AAV9 preferentially targets neonatal neurons and adult astrocytes. *Nature biotechnology* **27**: 59-65.

178. Mondo, E, Moser, R, Gao, G, Mueller, C, Sena-Esteves, M, Sapp, E, *et al.* (2018). Selective Neuronal Uptake and Distribution of AAVrh8, AAV9, and AAVrh10 in Sheep After Intra-Striatal Administration. *J Huntingtons Dis* **7**: 309-319.

179. Martin, DR, Cox, NR, Morrison, NE, Kennamer, DM, Peck, SL, Dodson, AN, *et al.* (2005). Mutation of the GM2 activator protein in a feline model of GM2 gangliosidosis. *Acta Neuropathol* **110**: 443-450.

180. Meikle, PJ, Fietz, MJ, and Hopwood, JJ (2004). Diagnosis of lysosomal storage disorders: current techniques and future directions. *Expert Rev Mol Diagn* **4**: 677-691.

181. Hahn, CN, del Pilar Martin, M, Schroder, M, Vanier, MT, Hara, Y, Suzuki, K, *et al.* (1997). Generalized CNS disease and massive GM1-ganglioside accumulation in mice defective in lysosomal acid beta-galactosidase. *Hum Mol Genet* **6**: 205-211.

182. McCurdy, VJ, Johnson, AK, Gray-Edwards, HL, Randle, AN, Brunson, BL, Morrison, NE, *et al.* (2014). Sustained normalization of neurological disease after intracranial gene therapy in a feline model. *Sci Transl Med* **6**: 231ra248.

183. Yang, B, Li, S, Wang, H, Guo, Y, Gessler, DJ, Cao, C, *et al.* (2014). Global CNS transduction of adult mice by intravenously delivered rAAVrh.8 and rAAVrh.10 and nonhuman primates by rAAVrh.10. *Mol Ther* **22**: 1299-1309.

184. Weismann, CM, Ferreira, J, Keeler, AM, Su, Q, Qui, L, Shaffer, SA, *et al.* (2015). Systemic AAV9 gene transfer in adult GM1 gangliosidosis mice reduces lysosomal storage in CNS and extends lifespan. *Hum Mol Genet* **24**: 4353-4364.

185. Bevan, AK, Duque, S, Foust, KD, Morales, PR, Braun, L, Schmelzer, L, *et al.* (2011). Systemic gene delivery in large species for targeting spinal cord, brain, and peripheral tissues for pediatric disorders. *Mol Ther* **19**: 1971-1980.

186. Samaranch, L, Salegio, EA, San Sebastian, W, Kells, AP, Foust, KD, Bringas, JR, *et al.* (2012). Adeno-associated virus serotype 9 transduction in the central nervous system of nonhuman primates. *Hum Gene Ther* **23**: 382-389.

187. Bluml, S, Seymour, KJ, and Ross, BD (1999). Developmental changes in choline- and ethanolamine-containing compounds measured with proton-decoupled (31)P MRS in in vivo human brain. *Magn Reson Med* **42**: 643-654.

188. Regier, DS, Kwon, HJ, Johnston, J, Golas, G, Yang, S, Wiggs, E, *et al.* (2016). MRI/MRS as a surrogate marker for clinical progression in GM1 gangliosidosis. *Am J Med Genet A* **170**: 634-644.

189. Erol, I, Alehan, F, Pourbagher, MA, Canan, O, and Vefa Yildirim, S (2006). Neuroimaging findings in infantile GM1 gangliosidosis. *Eur J Paediatr Neurol* **10**: 245-248.

190. Blyth, BJ, Farhavar, A, Gee, C, Hawthorn, B, He, H, Nayak, A, *et al.* (2009). Validation of serum markers for blood-brain barrier disruption in traumatic brain injury. *J Neurotrauma* **26**: 1497-1507.

191. Cunha-Vaz, JG, Shakib, M, and Ashton, N (1966). Studies on the permeability of the blood-retinal barrier. I. On the existence, development, and site of a blood-retinal barrier. *Br J Ophthalmol* **50**: 441-453.

192. Gurda, BL, De Guilhem De Lataillade, A, Bell, P, Zhu, Y, Yu, H, Wang, P, *et al.* (2016). Evaluation of AAV-mediated Gene Therapy for Central Nervous System Disease in Canine Mucopolysaccharidosis VII. *Mol Ther* **24**: 206-216.

193. Iwamori, M, Iwamori, Y, Adachi, S, and Nomura, T (2011). Excretion into feces of asialo GM1 in the murine digestive tract and Lactobacillus johnsonii exhibiting binding ability toward asialo GM1. A possible role of epithelial glycolipids in the discharge of intestinal bacteria. *Glycoconj J* **28**: 21-30.

194. Lawrence, R, Van Vleet, JL, Mangini, L, Harris, A, Martin, N, Clark, W, *et al.* (2019). Characterization of glycan substrates accumulating in GM1 Gangliosidosis. *Mol Genet Metab Rep* **21**: 100524.

195. Popoff, MR, and Poulain, B (2010). Bacterial toxins and the nervous system: neurotoxins and multipotential toxins interacting with neuronal cells. *Toxins (Basel)* **2**: 683-737.

196. Hansson, HA, Holmgren, J, and Svennerholm, L (1977). Ultrastructural localization of cell membrane GM1 ganglioside by cholera toxin. *Proceedings of the National Academy of Sciences of the United States of America* **74**: 3782-3786.

197. Remely, M, Tesar, I, Hippe, B, Gnauer, S, Rust, P, and Haslberger, AG (2015). Gut microbiota composition correlates with changes in body fat content due to weight loss. *Benef Microbes* **6**: 431-439.

198. Matalon, R, Surendran, S, Rady, PL, Quast, MJ, Campbell, GA, Matalon, KM, *et al.* (2003). Adeno-associated virus-mediated aspartoacylase gene transfer to the brain of knockout mouse for canavan disease. *Mol Ther* **7**: 580-587.

199. Choudhury, SR, Harris, AF, Cabral, DJ, Keeler, AM, Sapp, E, Ferreira, JS, *et al.* (2016). Widespread Central Nervous System Gene Transfer and Silencing After Systemic Delivery of Novel AAV-AS Vector. *Mol Ther* **24**: 726-735.

200. Baek, RC, Martin, DR, Cox, NR, and Seyfried, TN (2009). Comparative analysis of brain lipids in mice, cats, and humans with Sandhoff disease. *Lipids* **44**: 197-205.

201. Baek, RC, Kasperzyk, JL, Platt, FM, and Seyfried, TN (2008). N-butyldeoxygalactonojirimycin reduces brain ganglioside and GM2 content in neonatal Sandhoff disease mice. *Neurochem Int* **52**: 1125-1133.

202. Seyfried, TN, Yu, RK, and Miyazawa, N (1982). Differential cellular enrichment of gangliosides in the mouse cerebellum: analysis using neurological mutants. *J Neurochem* **38**: 551-559.

203. Kasperzyk, JL, El-Abbadi, MM, Hauser, EC, D'Azzo, A, Platt, FM, and Seyfried, TN (2004). N-butyldeoxygalactonojirimycin reduces neonatal brain ganglioside content in a mouse model of GM1 gangliosidosis. *J Neurochem* **89**: 645-653.

204. Macala, LJ, Yu, RK, and Ando, S (1983). Analysis of brain lipids by high performance thin-layer chromatography and densitometry. *J Lipid Res* **24**: 1243-1250.

205. Seyfried, TN, Glaser, GH, and Yu, RK (1978). Cerebral, cerebellar, and brain stem gangliosides in mice susceptible to audiogenic seizures. *J Neurochem* **31**: 21-27.

206. Folch, J, Lees, M, and Sloane Stanley, GH (1957). A simple method for the isolation and purification of total lipides from animal tissues. *The Journal of biological chemistry* **226**: 497-509.

207. Kasperzyk, JL, d'Azzo, A, Platt, FM, Alroy, J, and Seyfried, TN (2005). Substrate reduction reduces gangliosides in postnatal cerebrum-brainstem and cerebellum in GM1 gangliosidosis mice. *J Lipid Res* **46**: 744-751.

208. Riordan, JR, Rommens, JM, Kerem, B, Alon, N, Rozmahel, R, Grzelczak, Z, *et al.* (1989). Identification of the cystic fibrosis gene: cloning and characterization of complementary DNA. *Science* **245**: 1066-1073.

209. Koenig, M, Hoffman, EP, Bertelson, CJ, Monaco, AP, Feener, C, and Kunkel, LM (1987). Complete cloning of the Duchenne muscular dystrophy (DMD) cDNA and preliminary genomic organization of the DMD gene in normal and affected individuals. *Cell* **50**: 509-517.

210. Bradbury, AM, Peterson, TA, Gross, AL, Wells, SZ, McCurdy, VJ, Wolfe, KG, *et al.* (2017). AAV-mediated gene delivery attenuates neuroinflammation in feline Sandhoff disease. *Neuroscience* **340**: 117-125.

211. Hajitou, A, Trepel, M, Lilley, CE, Soghomonyan, S, Alauddin, MM, Marini, FC, 3rd, *et al.* (2006). A hybrid vector for ligand-directed tumor targeting and molecular imaging. *Cell* **125**: 385-398.

212. Hajitou, A, Lev, DC, Hannay, JAF, Korchin, B, Staquicini, FI, Soghomonyan, S, *et al.* (2008). A preclinical model for predicting drug response in soft-tissue sarcoma with targeted AAVP molecular imaging.

213. Przystal, JM, Waramit, S, Pranjol, MZI, Yan, W, Chu, G, Chongchai, A, *et al.* (2019). Efficacy of systemic temozolomide-activated phage-targeted gene therapy in human glioblastoma. *EMBO Mol Med* **11**.

214. Staquicini, FI, Smith, TL, Tang, FHF, Gelovani, JG, Giordano, RJ, Libutti, SK, *et al.* (2019). Targeted AAVP-based therapy in a mouse model of human glioblastoma: a comparison of cytotoxic versus suicide gene delivery strategies. *Cancer gene therapy*: 1-10.

215. Tandle, A, Hanna, E, Lorang, D, Hajitou, A, Moya, CA, Pasqualini, R, *et al.* (2009). Tumor vasculature-targeted delivery of tumor necrosis factor-alpha. *Cancer* **115**: 128-139.

216. Paoloni, MC, Tandle, A, Mazcko, C, Hanna, E, Kachala, S, Leblanc, A, *et al.* (2009). Launching a novel preclinical infrastructure: comparative oncology trials consortium directed therapeutic targeting of TNFalpha to cancer vasculature. *PloS one* **4**: e4972.

217. Yuan, Z, Syrkin, G, Adem, A, Geha, R, Pastoriza, J, Vrikshajanani, C, *et al.* (2013). Blockade of inhibitors of apoptosis (IAPs) in combination with tumor-targeted delivery of tumor necrosis factor-alpha leads to synergistic antitumor activity. *Cancer gene therapy* **20**: 46-56.

218. Smith, TL, Yuan, Z, Cardo-Vila, M, Sanchez Claros, C, Adem, A, Cui, MH, *et al.* (2016). AAVP displaying octreotide for ligand-directed therapeutic transgene delivery in neuroendocrine tumors of the pancreas. *Proceedings of the National Academy of Sciences of the United States of America* **113**: 2466-2471.

219. Quinn, TJ, Healy, N, Sara, A, Maggi, E, Claros, CS, Kabarriti, R, *et al.* (2017). Preclinical evaluation of radiation and systemic, RGD-targeted, adeno-associated virus phage-TNF gene therapy in a mouse model of spontaneously metastatic melanoma. *Cancer gene therapy* **24**: 13-19.